RESEARCH ARTICLE

Brachionus paranguensis sp. nov. (Rotifera, Monogononta), a member of the L group of the *Brachionus plicatilis* complex

Gerardo Guerrero-Jiménez[1], Patrizia Elena Vannucchi[2], Marcelo Silva-Briano[3], Araceli Adabache-Ortiz[3], Roberto Rico-Martínez[4], David Roberts[5], Roy Neilson[5], Manuel Elías-Gutiérrez[6]

1 *Instituto del Agua, Universidad de Granada, Ramón y Cajal 4, 18071, Granada, España. Departamento de Ecología, Facultad de ciencias, Universidad de Granada, Fuentenueva s/n, 18071Granada, Spain* **2** *Centro de Investigación en Ciencias del Mar y Limnología (CIMAR), Universidad de Costa Rica, San Pedro, San José, 11501, Costa Rica* **3** *Universidad Autónoma de Aguascalientes, Centro de Ciencias Básicas, Departamento de Biología. Avenida Universidad 940, C.P. 20131, Aguascalientes, Ags. México* **4** *Universidad Autónoma de Aguascalientes, Centro de Ciencias Básicas, Departamento de Química. Avenida Universidad 940, C.P. 20131, Aguascalientes, Ags., México* **5** *The James Hutton Institute, Craigiebuckler, Dundee DD2 5DA, Scotland, UK* **6** *El Colegio de la Frontera Sur, Unidad Chetumal. Av. Centenario Km 5.5, C.P. 77014, Chetumal, Quintana Roo, México*

Corresponding author: *Gerardo Guerrero-Jiménez* (gerardogj@correo.ugr.es)

Abstract

The *Brachionus plicatilis* complex represents the most studied group of rotifers, although the systematics of the species complex has not been completely clarified. Many studies have been conducted trying to explore the diversity within the complex, leading to the recognition of three major morphotypes: large (L), small-medium (SM), and small (SS). Currently six species have been described and classified under these types and another nine taxa have been identified but not formally described. Within the L group, three species have been officially described [*B. plicatilis* s.s. (L1), *B. manjavacas* (L2), and *B. asplanchnoidis* (L3)], while a formal description of L4, unofficially known as *B.* 'Nevada', is still lacking. In the present study, a new species, *Brachionus paranguensis* **sp. nov.**, is formally described and presented as a repre-

sentative of the L4 clade. The species has been named after a high altitude saline crater lake from Central Mexico, where the specimens were collected. An integrated approach using DNA taxonomy through COI and ITS1 markers, morphology, and ecology was used to confirm the identity of the new species.

Introduction

The presence of multiple cryptic species that have been classified as a single species due to their morphological similarity still represents a major challenge for biologists (Bickford et al. 2007; Pfenninger and Schwenk 2007). The first approach used when trying to identify and classify an organism is the detection of morphological characters able to distinguish a species. Nevertheless, the exclusive use of morphology-based identification may be problematic when dealing with taxa that lack clear diagnostic characters. To deal with these difficulties, the use of DNA taxonomy represents a valid tool to help reveal the presence of cryptic diversity within taxa whose systematics is still uncertain (Hebert et al. 2004; Hajibabaei et al. 2007). Additionally, complexes of cryptic species may present differences in their ecology, whose characterization might help unravel the identity of such species (Miller 2007).

In rotifers high levels of cryptic speciation occur (Fontaneto et al. 2009; García-Morales and Elías-Gutiérrez 2013) and, in this sense, the *Brachionus plicatilis* complex represents are good example and one of the best studied groups. The *Brachionus plicatilis* species complex is composed of three major morphotypes: the large (L), the small-medium (SM) and the small size (SS) types (Ciros-Pérez et al. 2001). The species currently described are:

1. *B. asplanchnoidis* Charin, 1947 (L)
2. *B. plicatilis* sensu stricto Müller, 1786 (L)
3. *B. manjavacas* Fontaneto et al., 2007 (L)
4. *B. ibericus* Ciros-Pérez et al., 2001 (SM)
5. *B. koreanus* Hwang et al., 2013 (SM)
6. *B. rotundiformis* Tschugunoff, 1921 (SS)

However, Mills et al. (2017) provided a conservative estimate of nine additional species within the *B. plicatilis* complex, with 11 more likely when applying the automatic barcode gap discovery method to the COI gene.

In the present work, *Brachionus paranguensis* sp. nov., collected in the hypersaline and highly alkaline volcanic maar Rincón de Parangueo, Guanajuato, Mexico (Cerca et al. 2014; Rocha-Treviño 2015) is described. It represents the unofficially known and undescribed *B.* 'Nevada' of the L4 clade (Gómez et al. 2002; Mills et al. 2017). The formal description of *Brachionus paranguensis* sp. nov. includes *B.* 'Nevada' which does not represent a formal taxonomic identity, and L4 could therefore be officially named *B. paranguensis* sp. nov.

To support the identity of the new species an integrated approach using DNA taxonomy, ecology and morphology was applied. The DNA taxonomy was based on two genes, the mitochondrial gene COI (cytochrome c oxidase I), sometimes referred to as the DNA barcoding gene, and the nuclear ribosomal ITS1 (internal transcribed spacer I). Sequences of *B. paranguensis* sp. nov. were compared with published sequences belonging to the L group of the *B. plicatilis* species complex and phylogenetic analyses were performed to infer the relationship among sequences.

In order to provide further evidence to support the recognition of *B. paranguensis* sp. nov., a morphological description of parthenogenetic females and resting eggs is provided, as well as lifespan analysis. Furthermore, a formal description of the species is given along with potential diagnostic features specific to *B. paranguensis* sp. nov. that could discriminate this species from other members of the L group.

Material and methods

Water samples were collected with a zooplankton net of 50 μm from the three water bodies located in the Rincón de Parangueo volcano, Guanajuato, Mexico (WGS84 coordinates 20°25'46"N; 101°14'48"W, altitude 1686 m above the sea level). Samples used for taxonomic identification were fixed with 4% formalin, while those intended for DNA analysis were fixed with 96% ethanol. An additional *in vivo* sample was kept for culturing under laboratory conditions. This latter sample was kept in a cooler at 4 °C for no more than 4 hours until cultures were set up in the laboratory.

Physical and chemical parameters were measured in situ using the Yellow Spring Instruments Model 556 MPS probe. Environmental variables included: pH, temperature, dissolved oxygen (DO), conductivity and salinity [calculated with the conductivity to salinity conversion table by Bodelón et al. (1994)].

DNA taxonomy

From field samples ten specimens were selected for DNA analysis. DNA was extracted from each individual using a mixture of proteinase K with lysis buffer for invertebrates and digested overnight at 56 °C. Genomic DNA was subsequently extracted using the glass fiber membrane method in 2 μm Pall plates (Hajibabaei et al. 2005). Both COI and ITS1 were amplified from the same specimens. For COI the PCR (polymerase chain reaction) reactions were prepared using 6.25 μl of 10% trehalose, 1.63 μl of deionized water, 1.25 μl of 10X Buffer, 0.625 μl of $MgCl_2$ (50 mM), 0.31 μl of both primers (0.01 mM), 0.0625 μl of dNTPs (10 mM), 0.0625 μl of Taq polymerase (Invitrogen) and 2 μl of DNA template. The universal COI primers for animals, LCO1490 and HCO2198 (Folmer et al. 1994) were used. The PCR program used included an initial polymerase activation step at 94 °C for 1 min, five cycles of denaturation at 94 °C for 40 s, annealing at 45 °C for 40 s and an extension at 72 °C for 1 min, fol-

lowed by 35 cycles of 94 °C during 40 s, 51 °C for 40 s and 72 °C for 1 min, with a final extension at 72 °C for 5 min.

For ITS1 the PCR reactions were prepared using 8.85 µl of deionized water, 1.5 µl of 10X Buffer, 1 µl of BSA, 0.6 of µl MgCl2 (50mM), 0.3 µl of both primers (20 µM), 0.3 µl of dNTPs (10 mM) and 0.15 µl Taq polymerase (Platinum). The ITS1 primers used were III (5'-CACACCGCCCGTCGCTACTACCGATTG-3') and VIII (5'-GT-GCGTTCGAAGTGTCGATGATCAA-3') of Palumbi (1996). The PCR program used included an initial step at 95 °C for 5 min, 36 cycles of 95 °C for 50 s, 54 °C for 50 s, 72 °C for 1 min and one cycle at 72 °C for 5 min.

All amplified products were screened with an agarose E-gel (Invitrogen) and pictures of the positives were taken. The products were labeled with the BigDye Terminator v. 3.1 (Applied Biosystems, Inc.) and sequenced bidirectionally. The DNA sequencing process was conducted at the James Hutton Institute of Dundee (Scotland, UK). All sequences were quality checked with Geneious 4.8 (http://www.geneious. com, Kearse et al. 2012) and with the quality tools provided by the Barcode of Life Database (BOLD, www.boldsystems.org) (Ratnasingham and Hebert 2007). Alignment of COI and ITS1 sequences was performed with Topali v2.5 (Milne et al. 2008) using a F84+Gamma model. All new COI sequences after this work were uploaded in BOLD within the Dataset DS-BPAR01 under the accession numbers BPMX010-19 to BPMX017-19 and GenBank (www.ncbi.nlm.nih.gov) accession numbers MK434153–MK435160. All new ITS1 sequences were deposited in BOLD with accession numbers from BPMX001-18 to BPMX008-18 and GenBank MH708047–MH708053.

Both COI and ITS1 sequences of *B. paranguensis* sp. nov. were aligned against all *B. plicatilis* complex L clade COI and ITS1 sequences available in the NCBI (National Center for Biotechnology Information) public database. Sequences were trimmed to a sequence length of 550 bp for COI and to 350 bp for ITS1, and those that did not cluster with the members of the L group were discarded. A total of 665 COI and 148 ITS1 sequences belonging to the whole L group of the *B. plicatilis* complex were retained for this study. One COI sequence, KU299077 (Mills et al. 2017), was not used for analyses as it was poor with too much missing information. Likewise, two ITS1 sequences, AY772137 and AY772159 (Suatoni et al. 2006) identified as *B. plicatilis* s.s. and *B.* 'Nevada' respectively, were excluded from the analyses. A BLAST search in the NCBI database showed the former sequence to be 100% similar to another sequence, KU299536, belonging to the SM group (Mills et al. 2017); while AY772159 was placed outside the four L groups presenting a 22% genetic distance from the other *B.* 'Nevada' clones.

Sequence alignments were reduced to haplotypes by collapsing all identical sequences, using the online toolbox users-birc.au.dk/biopv/php/fabox/dnacollapser. php# (Villesen 2007). In order to infer the relationship among *B. paranguensis* sp. nov. and the other species of the L group of the *B. plicatilis* complex, a maximum likelihood tree (ML) was constructed for the COI and ITS1 datasets with PhyML 3.0 (Guindon and Gascuel 2003). Two sequences of the congeneric species *Brachionus rotundiformis*,

AF387287 and AF387239 for COI and ITS1 respectively, were used as outgroups as this species represents the closest one to the L group (Mills et al. 2017). The best model was identified as TN93+G for COI, and GTR+G for ITS1 dataset. In order to set an appropriate threshold value able to define species belonging to the L group of the *Brachionus* complex, mean uncorrected p-distances were calculated within and between members of the group, with Mega 7.0.21 (Kumar et al. 2016).

Morphology

A Light Microscope (LM) (Nikon Eclipse Ni) and a Scanning Electron Microscope (SEM) were used to analyze the morphology of *B. paranguensis* sp. nov. females, males, trophi, and eggs. Specifically, the presence of gastric glands, the shape of the dorsal sinus and the anterior spines of the female were analyzed by LM. Whereas, the lorica surface structure, the presence of lateral antennae, the foot aperture in the female, the male, the three different type of eggs, and the trophi, were analyzed by SEM. All samples were taken directly from the same field samples as the material for DNA analyses with the exception of the males, which were taken from laboratory cultures.

Preparation of organisms for SEM

One hundred females, fifty males, twenty parthenogenetic eggs, twenty mictic eggs and twenty unfertilized eggs were extracted from the field samples and fixed in 4% formalin. Specimens were dehydrated using a graded ethanol series, starting with 60% and finishing with 100% ethanol; after which critical drying point was performed. Samples were then mounted in a SEM stub (1 cm high x 1.2 cm in diameter) and covered with gold. For the preparation of trophi a sample of 20 female organisms was used. Trophi were removed according to the methodology of Segers et al. (1993). The organisms and trophi were mounted on glass slides and observed under SEM JEOL 5900 LV; pictures were taken according to Silva-Briano et al. (2015).

Morphometric analysis

New-born females were isolated from cultures and placed in a well of a 24-well polystyrene plate for 48 hours. In order to compare morphometric data of *B. paranguensis* sp. nov. against the other members of the L group, females were fixed with 4 % formaldehyde and placed all in the same position under the optical microscope where twenty digital pictures were taken. Organisms were placed and measured according to Fu et al. (1991) and Ciros-Pérez et al. (2001), see Figure 1, using the program provided by the microscope Nikon Eclipse Ni with digital camera D5-Fi2.
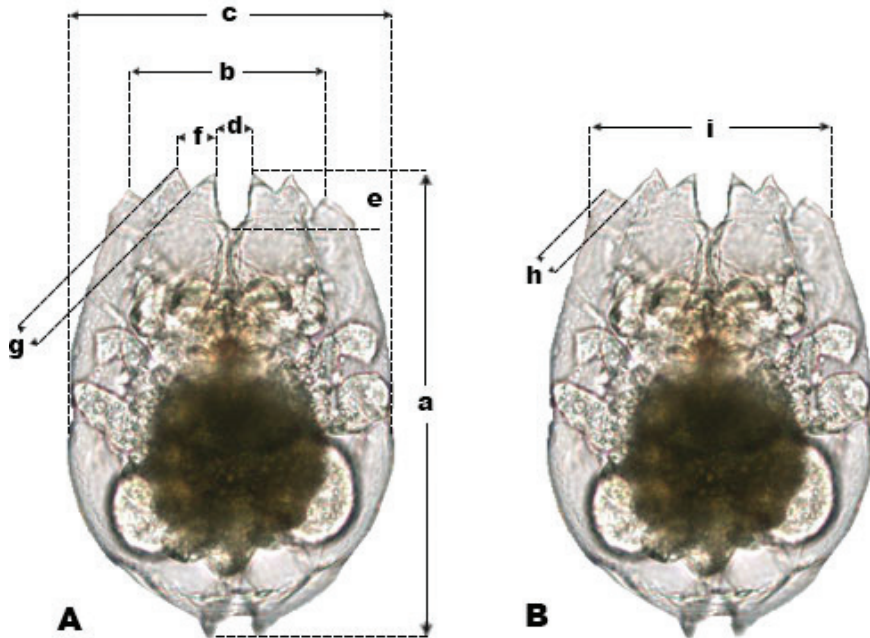
Figure 1. Different types of measurements. Dorsal view with the strokes of how anterior spines were measured according to **A** Fu et al. (1991) and **B** Ciros-Pérez et al. (2001).

Ecological analysis
Culture conditions

Cultures were set up from several wild individuals collected in the volcanic maar Rincón de Parangueo, using the same salinity recorded in situ, 25 g L^{-1}. Cultures were maintained in a bioclimatic chamber with a photoperiod of 16: 8 light: dark, a temperature of 25 °C and a medium with 25 g L^{-1} of RED-SEA SALT (Ca 410 ppm, Mg 1230 ppm, and AlK / KH Meq / l / 7.7 dKH) dissolved in distilled water (pH = 8.5). Rotifers were fed with 10^6 cells/ml concentration of the algae *Nannochloropsis oculata*.

Lifespan of parthenogenetic female and males

Lifespan analysis of males and females was conducted under laboratory conditions in order to provide ecological information of the species. In 1 mL of medium, 10 neonates of parthenogenetic females were isolated in individual wells of a 24-well polystyrene plate until they died. Every 24 hours neonates of each female were collected from the wells. Rotifers were fed with 10^6 cells/ml of *Nannochloropsis oculata* and placed into a new well with fresh medium in a total volume of 1 ml, every day during the experiment. The mean lifespan, the number of eggs per rotifer, and the maximum intrinsic growth rate were calculated for parthenogenetic females according to Krebs (1985) and Begon et al. (1996). Mean lifespan was calculated from twenty males collected within six hours of hatching.

Results

DNA taxonomy

From the 10 processed individuals of *Brachionus paranguensis* sp. nov., eight sequences were obtained for each marker, COI and ITS1, from the same individuals. For both markers, sequences belonged to a single haplotype (MK434153 and MH708047, respectively). The COI alignment that included 665 sequences belonging to members of the L group, collapsed into 146 haplotypes; while ITS1 alignment contained 148 sequences and collapsed into 12 haplotypes. The ML trees for both COI and ITS1, formed four well-defined clusters representing the four L clades of the *B. plicatilis* complex (Mills et al. 2017) (Suppl. material 1: Figs S1, S2). For COI, mean uncorrected genetic distances within groups ranged from 2.8% to 8.5% (mean = 4%, media = 4%), while distances between groups ranged from 15% to 19.8% (mean = 16%, median = 16%) (Table 1). *Brachionus paranguensis* sp. nov. haplotype was included in the L4 clade unofficially known as 'Nevada'. The L4 clade presented 17 haplotypes; besides *B. paranguensis* sp. nov., these were represented by clones of *B. plicatilis* collected from Chile (Aránguiz-Acuña et al. 2018), UK (Lowe et al. 2007), Australia (Mills et al. 2017), Japan (Suatoni et al. 2006), and clonal cultures belonging to the undescribed *B.* 'Nevada' (Gómez et al. 2002; Papakostas et al. 2006; Michaloudi et al. 2017) (Fig. 2). The mean uncorrected p-distance within the L4 clade was 8.5%, ranging from 0 to 15%. For ITS1, mean uncorrected genetic distances within groups ranged from 0.001% to 0.7% (mean = 0.4%, median = 0.3%), while distances between groups ranged from 2.8% to 9.3% (mean = 6.6%, median = 6%) (Table 2). Congruently with the results obtained for COI, *B. paranguensis* sp. nov. haplotype was included in the L4 clade, together with another haplotype belonging to a clone of *B. plicatilis* collected from Chile (Aránguiz-Acuña et al. 2018) (Fig. 2). The haplotype was sourced from

Table 1. COI genetic distances among and within the members of the L group. COI uncorrected p-distances generated within and among members of the L group. In black are within distances, while lower left are between mean p-distances.

	L1	L2	L3	L4
L1	3.6%			
L2	19.8%	2.8%		
L3	18%	19.7%	4%	
L4	18.9%	17.7%	15%	8.5%

Table 2. ITS1 genetic distances among and within the members of the L group. ITS1 uncorrected p-distances generated within and among members of the L group. In black are within distances, while lower left are between mean p-distances. Within distance for L2 has N/A as only one haplotype is present.

	L1	L2	L3	L4
L1	0.7%			
L2	8.9%	N/A		
L3	6.3%	9.3%	0.6%	
L4	2.8%	7.6%	5%	0.001%

COI gene

ITS1 gene

99 *B. plicatilis s. s.* (L1)

96 *B. asplanchnoidis* (L3)

74

50

B. asplanchnoidis (L3) 93

B. plicatilis s. s. (L1) 90

100

76

94

86

B. 'Nevada'[1]
B. plicatilis (Australia)[2]
B. plicatilis (Uk)[3]
B. plicatilis (Japan)[4]
B. 'Nevada'[5]
B. 'Nevada'[6]
B. plicatilis (Unknown origin)[7]

99

75 **B. paranguensis** n. sp. (L4)

B. paranguensis n. sp. (L4)

MH708047
MH720974

70

96

28

98

B. plicatilis 'Nevada'[8]
B. Paranguensis n. sp. (Mexico)
B. plicatilis (Chile)[9]
B. plicatilis (Chile)
B. plicatilis (Chile)
B. plicatilis (Chile)
B. plicatilis (Chile)
B. plicatilis (Chile)
B. plicatilis (Chile)
B. plicatilis (Chile)

B. manjavacas (L2) 90

52 *B. manjavacas* (L2)

B. rotundiformis

B. rotundiformis

0.20

0.050

[1] AF387246 Gomez et al., 2012
[2] KU299363 Mills et al., 2016
[3] DQ140386 Lowe et al., 2007
[4] AY785198 Suatoni et al., 2006
[5,6] DQ314558 , DQ314559 Papakostas et al., 2006
[7] KU299274 Mills et al., 2016
[8] KU189744 Michaloudi et al., 2016
[9] MH710538- 42-52-59-60-62-63-64 Aranguiz-Acuña et al., 2018

Figure 2. Comparison of COI and ITS1 LM trees focusing on the L4 group. COI and ITS1 Maximum Likelihood trees representing the four L groups of the *Brachionus plicatilis* complex and one outgroup species *Brachionus rotundiformis*. Focus is placed upon *B. paranguensis* sp. nov. L4 clade (grey shading) where details of the origin of each haplotype are given; all the other species are collapsed. Dotted lines between haplotypes indicate COI and ITS1 sequences that were sourced from the same individuals. Numbers at nodes represent support values (bootstrap = 1000). A list of references for each haplotype within the L4 group is provided.

the same individual as one of the haplotypes present in the L4 clade of the COI ML tree. No variability in the ITS1 fragment was found between *B. paranguensis* n. sp and three clones named *B.* 'Nevada' (LC339820, FR729715 and AF387207) available in GenBank. The mean uncorrected p-distance within the L4 clade was 0.001%.

Taxonomy

Class Eurotatoria De Ridder, 1957
Subclass Monogononta Plate, 1889
Superorder Pseudotrocha Kutikova, 1970
Order Ploima Hudson & Gosse, 1886
Family Brachionidae Ehrenberg, 1838

Brachionus paranguensis **sp. nov.**
http://zoobank.org/2BE62C89-4A13-40EE-B395-08E8B13B3971
Figs 4A–H, 5A–C, 6A–F

Type locality. The volcano Rincón de Parangueo, Guanajuato, Mexico, has two or three water bodies inside the crater, depending on the season, and *B. paranguensis*
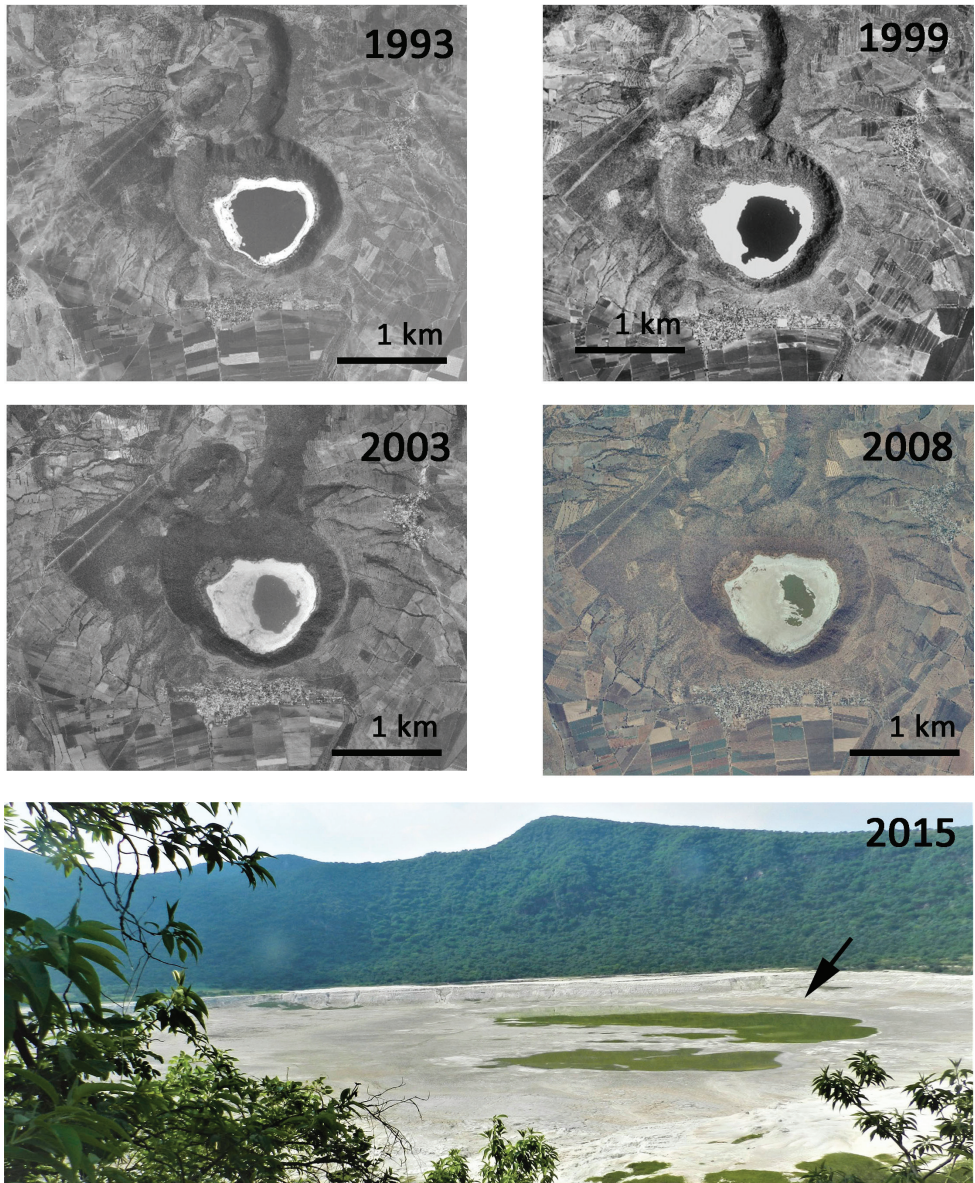
Figure 3. Map of the studied area. Sequence of pictures of the volcanic maar Rincón de Parangueo from 1993 to 2015, showing how the lake gradually desiccated. The arrow indicates the water pond where *B. paranguensis* sp. nov., was found (digital pictures downloaded from INEGI 2019).

sp. nov. was present in one of them, 20°25'46"N; 101°14'48"W, at the altitude of 1686 m above sea level (Fig. 3).

Material examined. In order to confirm the identity of *B. paranguensis* sp. nov., hundreds of individuals from field and culture samples representing all stages (amictic females, males, resting eggs, parthenogenetic eggs, and unfertilized sexual eggs), and

around 30 trophi, were examined by LM and SEM. Specifically, hundreds of females were used to take morphometric measurements, and dozens of males were observed to analyze their morphological features. Moreover, diapausing eggs, parthenogenetic eggs and unfertilized eggs were examined and pictures of each egg were taken. Finally, approximately 30 trophi were analyzed in order to compare their morphological features with those of the other eggs belonging to the L group.

Holotype. A parthenogenetic female mounted on a slide with a mix of formaldehyde-glycerol sealed with DePex medium, deposited in the Zooplankton Reference Collection of El Colegio de la Frontera Sur with accession number ECO-CH-Z-10331. *Paratypes.* Two slides with a parthenogenetic female, deposited in the Zooplankton Reference Collection of El Colegio de la Frontera Sur with accession numbers ECO-CH-Z-10332, 10333.

Differential diagnosis. *Parthenogenetic female***:** No clear morphological differences were observed between *B. paranguensis* sp. nov. and the other species belonging to the L group of the *B. plicatilis* complex with respect to the anterior dorsal spine, the U-shape sinus, the orange peel like surface of the lorica, and the presence of gastric glands. An exception is *B. asplanchnoidis*, whose lorica presents an elongated and wider shape, and the antero-ventral U-shape sinus is wider compared to that of the other members.

Trophi: In *B. paranguensis* sp. nov. satellites are robust and there are sharp projections in the inner upper margin; basifenestras with similar size and shape, ramus with two posterior projections, the left one smaller and thinner than the right one. In *B. plicatilis* s.s. the shape of the satellites is triangular with no projection; ramus with two posterior projections, the left one bigger and wider than the right one; basifenestras asymmetrical with different sizes. In *B. manjavacas* the shape of the satellites is triangular and sharper compared to *B. plicatilis* s.s.; ramus with two posterior projections, the left one bigger and wider than the right one; basifenestras with same shape but different size, the left one bigger than the right one. In *B. asplanchnoidis* satellites are robust and the projections in the inner upper margin is rounded; ramus with two posterior projections, the left one smaller and thinner than the right one, the right one with cylindrical shape; basifenestras with different shape and size, the left one smaller than the right one.

Resting eggs: Oval shape in *B. paranguensis* sp. nov., *B. plicatilis* s.s. and *B. manjavacas*, although the two latter species also present small holes on the surface of the eggs (Ciros-Pérez et al. 2001; Guerrero-Jiménez et al. in prep.).

Ecology: B. paranguensis sp. nov. grows preferentially in salinities higher than 25 g L^{-1}. *B. plicatilis* s.s. grows better in salinities from 5 to 15 g L^{-1} (Yin and Zhao 2008), while *B. manjavacas* is usually cultured in a salinity of 12 g L^{-1}. Finally, *B. asplanchnoidis* can be observed in salinities from 8 to 44 g L^{-1}, although Michaloudi et al. (2017) for their study cultured the species in a salinity of 16 g L-1.

Description. The population of *B. paranguensis* sp. nov. from Rincón de Parangueo volcano was used to formally describe all individuals belonging to the L4 group of the *B. plicatilis* complex. Parthenogenetic females (Fig. 4F, G) had a soft lorica with an orange peel like surface (Fig. 4C), two gastric glands (gg) (see arrows, Fig. 4A) and
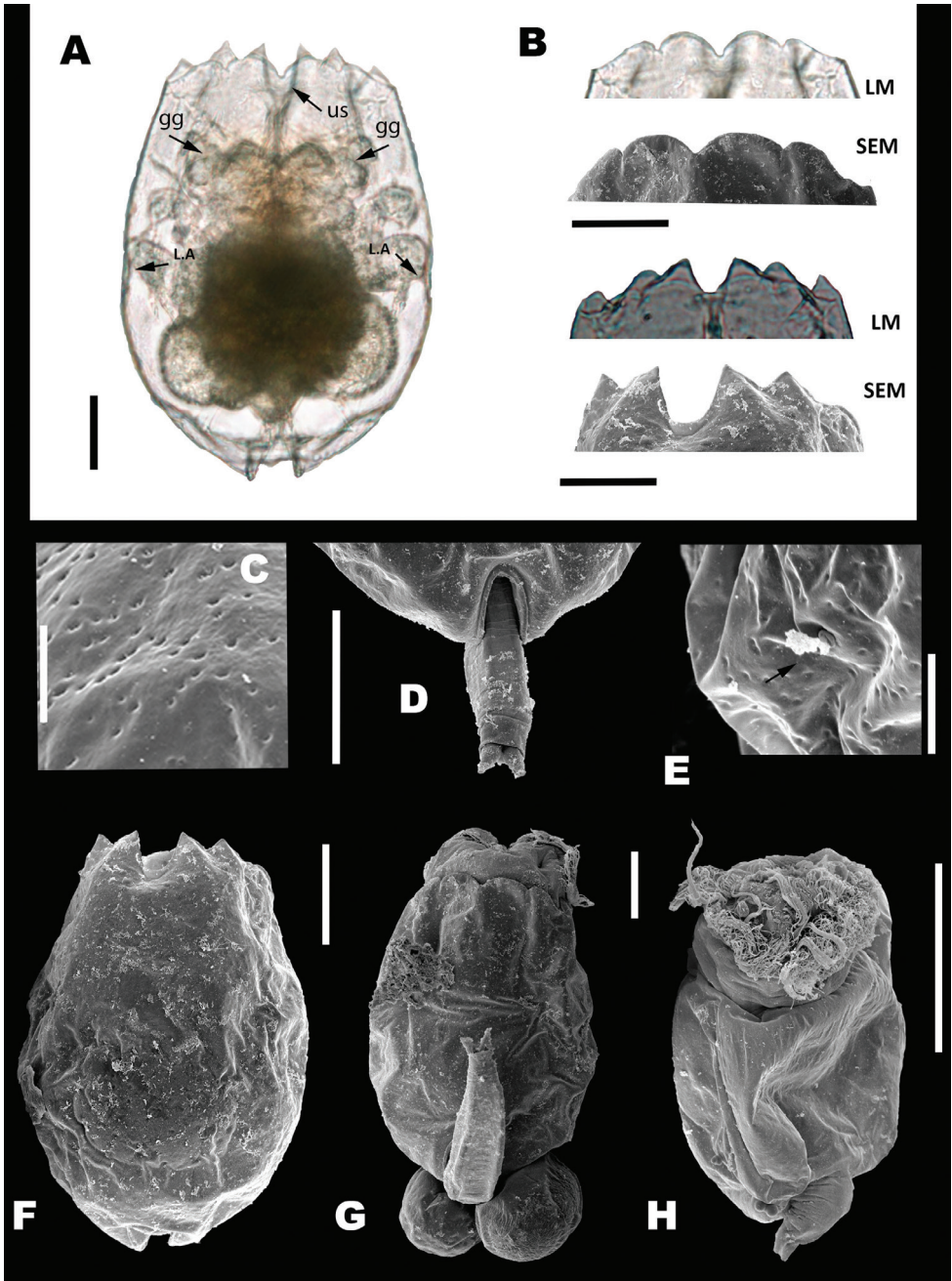
Figure 4. Taxonomic features of *B. paranguensis* sp. nov. **A** parthenogenetic female with lateral antennae (LA), gastric glands (gg), an U-shape sinus (us) **B** anterior dorsal and ventral spines taken by LM and SEM **C** lorica with an orange peel like surface **D** foot aperture **E** lateral antenna (see arrow) **F** SEM microphotographs of the female, ventral plate and **G** dorsal plate and **H** male. Scale bars: 50 μm (**A, B, D, F, G, H**), 10 μm (**C, E**). All females from sample collected in June 27, 2015. Males from cultures obtained from females collected in the volcanic maar Rincón de Parangueo.

two lateral antennae (LA) in the middle of the body (see arrows, Fig. 4A, E). Anterior dorsal margin with six spines, three on each side of a U-shape sinus like the other members of the L group. All spines are triangular (Fig. 4A, B). Anterior ventral margin with bilateral symmetry, four well-defined lobes with a medial sinus, both internal lobes were more pronounced than the external lobes (Fig. 4A, B). Foot aperture well defined (Fig. 4D). Adult females had a length of 216.97 ± SD 13.78 μm (N = 20), width 159.93 ± SD 10.93 μm (N = 20), and 126.21 ± SD 7.7 μm of head aperture, dorsal view (N = 20), see Table 3.

Male (Fig. 4H): Twenty individuals were analyzed. Anterior ventral margin had two lobes with a medial sinus and five to six pellets, the life cycle without food was of four days and its length was 78.48 ± SD 2.8 μm and width 72.7 ± SD 2.3 μm.

Egg types: The outer membrane of the resting eggs presented a slightly rough ornamentation (Fig. 5A.a, A.b) and the length was 112.6 ± SD 4.8 μm and 91.2 ± SD 4.7 μm width (N = 7), see Figure 5A. The parthenogenetic eggs had a smooth surface and was 127.4 ± 9.5 long and 110.7 ± SD 6.1 μm wide (N = 9), see Figure 5B. Finally, the unfertilized sexual eggs that produced males were 73.03 ± SD 3.2 μm long and 59.8 ± SD 2.18 μm wide (N = 9), see Figure 5C.

Trophi: Malleate type with all the characters of the genus (Fig. 6A, B). Manubria were triangular in shape with sharp claw-shaped tips at their distal end (Fig. 6D). The junction that holds the manubrium with the uncus was wide in both dorsal and ventral view (Fig. 6A, B). Unci presented four teeth decreasing in size from the ventral one and the subuncus is present underneath each tooth (Fig. 6F). The membrane that joins the uncus with the satellites was thick and the protrusion that innervates them was also clearly denoted on the back of the uncus (see Fig. 6A). The satellites were robust, irregularly shaped but arranged symmetrically, also sharp projections were observed on the anterior section of the satellites with the tip pointing inwards towards the central axis of the trophi (Fig. 6E). Ramus asymmetrical with two posterior projections, the left one smaller and thinner than the right one and basifenestras with similar shape and size (Fig. 6C). Fulcrum short, with triangular shape (Fig. 6C, see arrow and F).

Etymology. The specific name refers to the type locality, the volcanic maar Rincón de Parangueo.

Table 3. Measurements of all species belonging to the L group. Measurements of adult females between all species belonging to the L group, according to Fu et al. (1991) and Ciros-Pérez et al. (2001). All measurements not belonging to *B. paranguensis* sp. nov. were taken from Michaloudi et al. (2017).

Group L	Measurements								
	a	b	c	d	e	f	g	h	i
B. plicatilis s. s. (L1)	283.63 ± 6.38	122. 36 ± 1.72	203.62 ± 5.49		27.33 ± 0.42		13.74 ± 0.31		132.44 ± 2.13
B. manjavacas (L2)	256.28 ± 3.9	109.37 ± 1.75	177.67 ± 2.62		21.74 ± 0.52		10.04 ± 0.28		125.09 ± 1.91
B. asplanchnoidis (L3)	295.12 ± 8.1	126.12 ± 1.85	204.58 ± 4.8		26.64 ± 0.75		14.42 ± 0.45		130.88 ± 2.12
B. paranguensis sp. nov. (L4) N = 20	216.97 ± 13.78	106.43 ± 8.13	159.93 ± 10.93	25.43 ± 2.88	23.82 ± 2.23	20.13 ± 2.06	9.75 ± 0.81	12.93 ± 1.09	126.21 ± 7.72
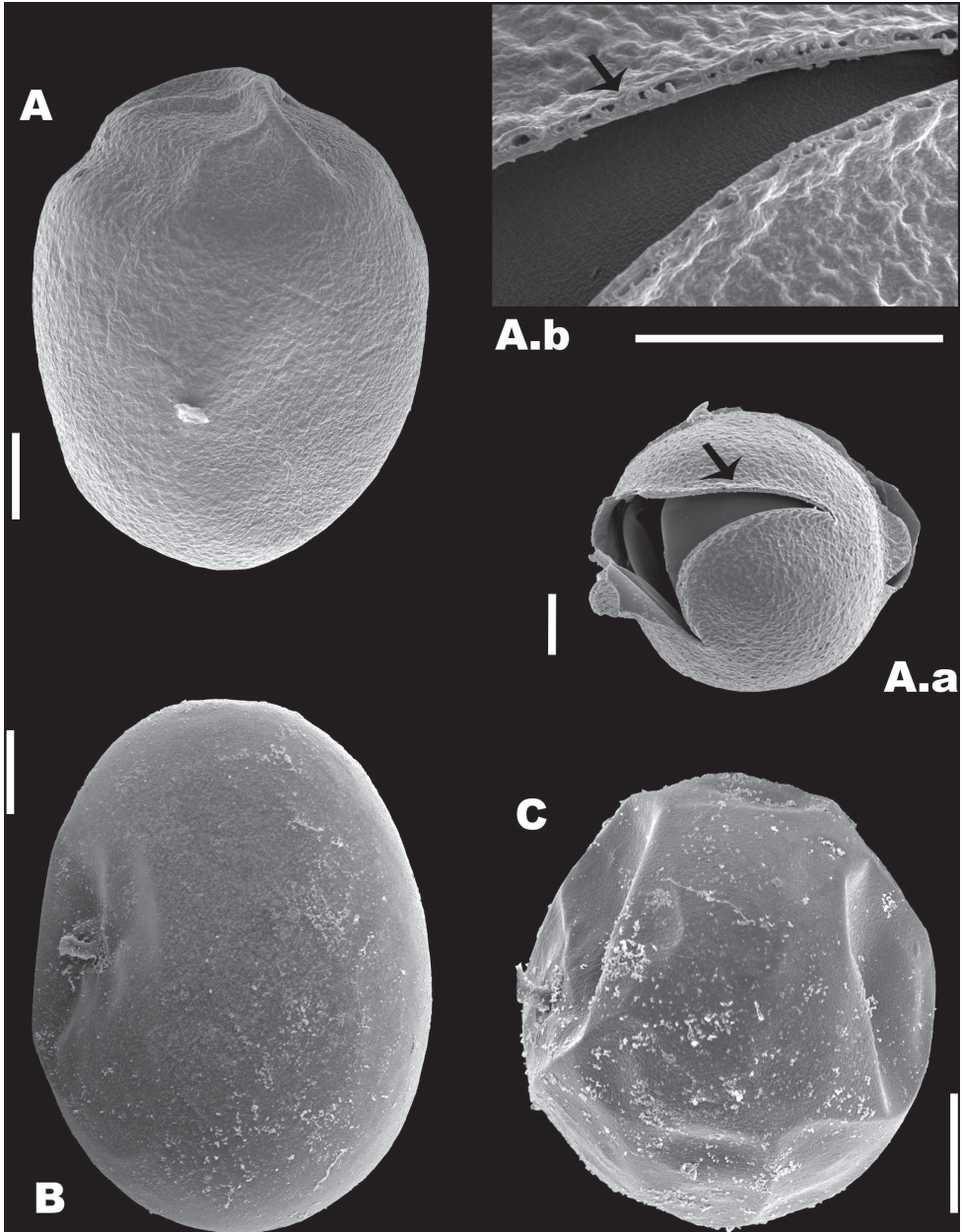
Figure 5. Types of eggs in *B. paranguensis* sp. nov. SEM micrographs of the different types of eggs of *B. paranguensis* sp. nov. **A** resting egg from field samples and its special ornamentation and zoom of its membrane, see arrows (A.a, A.b) **B** parthenogenetic egg and **C** unfertilized sexual egg, both from cultured samples. Scale bars: 20 μm

Distribution-habitat. According to the DNA sequences available in NCBI, *B. paranguensis* sp. nov. individuals were reported in Mexico, USA, Chile, Europe, Australia, and Japan. The habitat of *B. paranguensis* n. sp is represented by high salinity environ-
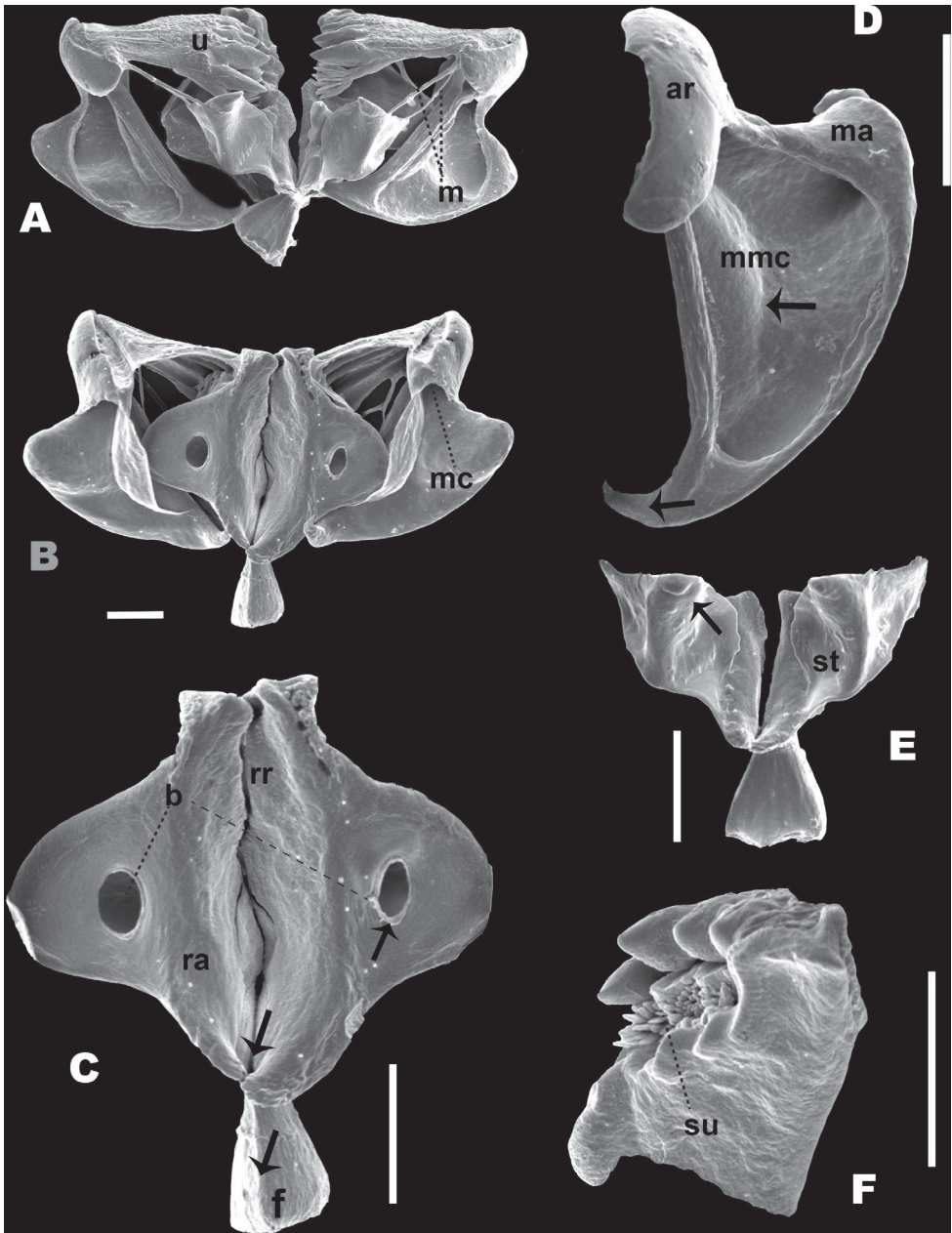
Figure 6. Trophi components of *B. paranguensis* sp. nov. SEM pictures of the trophi components of *B. paranguensis* sp. nov., collected in June 27, 2015 **A** ventral view **B** dorsal view **C** rami and fulcrum **D** manubrium **E** satellites **F** unco and sub uncus ar: articulation of manubrium, m: membrane; ma: manubrium with posterior claw, see arrow (**D**); mmc: manubrium middle crest, see arrow (**D**); rr: reinforced ridge; st: satellites, see arrow (**E**); su: sub uncus; u: uncus.: b: basifenestras, see arrow (**C**); f: fulcrum, see arrow (**C**); mc: manubrium cavities; ra: rami, and projections of the posterior portion of the rami, see arrow (**C**)). Scale bars: 10 μm.

ments (>25 g L^{-1}). Physical and chemical parameters of the maar where specimens were collected: Temperature= 28 °C; Conductivity= 43.2 mS/cm^{-1}; Dissolved Oxygen = 5.5 mg L^{-1}; pH= 11.07.

Ecology. Under laboratory conditions (25 °C, 25 g L^{-1} salinity, 10^6 cells/ml of *Nannochloropsis oculata* provided as food) amictic females had a maximum lifespan of 10.8 days. Eggs per rotifer were 15.4 ± SD 5.8, and the maximum intrinsic growth rate was 0.49 (N = 10).

Discussion

DNA taxonomy

Due to the morphological stasis of the external characters that characterizes the *B. plicatilis* species complex (Gómez et al. 2002; Campillo et al. 2005; Mills et al. 2017) the use of genetic analysis represented a fundamental aid to help unravel the cryptic species diversity within this group, in combination with other diagnostic characters. Additionally, its discrimination power among species is reliable, as was demonstrated in previous studies (García-Morales and Elías-Gutiérrez 2013; Mills et al. 2017).

The current taxonomy of the L group has not been resolved yet, leading to an underestimation of the true diversity present within the complex (Gómez et al. 2002; Mills et al. 2017). An enormous confusion is currently present due to sequencing only resting eggs from localities not accurately described, for example, Little Fish Pond (Gómez et al. 2002; Suatoni et al. 2006, Mills et al. 2017) or even China (Mills et al. 2017). Moreover, some members of the group lack a formal taxonomic description, therefore unofficial names are used to identify taxa, which may create problems when communicating about the group or comparing results between studies (Serra and Fontaneto 2017). Thus, a common effort is required to provide unambiguous names that allow a link between the name and the taxonomic identity (Segers et al. 2012). In the present study, DNA taxonomy through the use of the two markers COI and ITS1, represented an important tool that helped confer an identity to the yet undescribed *B.* 'Nevada', named here as *B. paranguensis* sp. nov.

Phylogenetic analyses using both markers clustered *B. paranguensis* sp. nov. and *B.* 'Nevada' together as a single species, although a higher genetic variability in COI was observed within haplotypes (8.5%, ranging from 0 to 15%). Sequences of *B. paranguensis* sp. nov. revealed no variability in ITS1 with three clones of *B.* 'Nevada' available in GenBank, representing therefore a single haplotype, with only a single base-pair difference with the other haplotype belonging to a clone of *B. plicatilis* collected from Chile, included in the L4 clade.

Previous genetic analysis with the COI gene reported high genetic divergences within the *B. plicatilis* species complex up to about 20% (Fontaneto 2014), and a similar maximum intraspecific divergence of 15% was found in this study within hap-

lotypes included in L4. This value represents a much higher threshold than the 0.03 cut off commonly used in animal studies for delimiting species using COI (Hebert et al. 2003). Studies conducted on other animal groups, such as the springtail *Friesea grisea* (Torricelli et al. 2010) or the copepod *Tigriopus californicus* (Edmands 2001), also reported the presence of higher genetic divergences in COI sequences, demonstrating the impracticability of applying a 0.03 to all animal taxa. The mitonuclear discordance between COI and ITS1 in rotifers has already been observed in previous studies (Papakostas et al. 2016) as the mitochondrial gene COI was shown to evolve more rapidly than the nuclear ribosomal internal transcribed spacer ITS1 (Tang et al. 2012). The high mutational rate of COI might explain the high genetic variation found for this gene within *Brachionus* species and, therefore, the 8.5% mean genetic divergence existing within haplotypes in L4. To avoid the over-splitting of *Brachionus* species, which occurs when using COI marker, ITS1 has been suggested as a more reliable predictor of the species in the *B. plicatilis* complex (Papakostas et al. 2016; Mills et al. 2017). In view of the above, it is possible to affirm that, according to DNA taxonomy analysis, *B. paranguensis* n. sp and *B.* 'Nevada' represent the same taxonomic identity.

Morphology

Morphological differentiation among parthenogenetic females belonging to the L group species of the *B. plicatilis* complex is poor. The high variability in size and the lack of differentiation between the anterior dorsal and ventral margins, already reported for *B. asplanchnoidis* by Michaloudi et al. (2017), may also occur in other species. However, it is worth mentioning that Michaloudi et al. (2017, 2018) observed that the ventral margin represented a helpful diagnostic character in females of *B. asplanchnoidis* and *B. calyciflorus*. Other morphological similarities were found among the members of the L group, i.e., the presence of gastric glands, the lorica with an orange peel like surface, and the U-shape sinus. Therefore, so far, no reliable morphological features that could allow distinguishing among species have been observed in females. However, for *B. paranguensis* sp. nov. some differences were observed in the trophi, in the resting eggs ornamentation, and in the salinity preference.

Trophi are indeed relatively consistent features in rotifers (Segers et al. 1993; Fontaneto and Melone 2005) and are already used as valid diagnostic features for identification in some bdelloids (Melone and Fontaneto 2005). Although there is no evidence of species specificity in the ultrastructure of the trophi, small differences were observed in some components, especially in the satellites, among the species of the L group. These could be used for a preliminary identification of the species as an alternative to DNA taxonomy.

The study of resting eggs morphology could represent another alternative for species differentiation. Indeed, in rotifers, evidence of species specificity in resting eggs was already documented by Nipkow (1961), Beauchamp (1952), Bogoslovsky (1967), and Gilbert and Wurdak (1978). When comparing the ultrastructure of resting eggs

in the members of the L group, differences were observed. *Brachionus plicatilis* s.s. eggs have a quite smooth surface (Ciros-Pérez et al. 2001), while in *B. manjavacas* the surface presents wrinkles (Guerrero-Jiménez et. al., in prep). Moreover, small holes were observed on the surface of the eggs belonging to these two species, unlike *B. paranguensis* sp. nov. Although the analyses of *B. asplanchnoidis* eggs is not yet available, so far data seem to support the presence of species specificity among the members of the L group of the *B.plicatilis* complex.

Ecology

Differences in salinity preference among the species belonging to the L group may represent another factor that allows discriminating between species. Nevertheless, no studies have been carried out on specific salinity preferences of the L group species. Available data reveal that in *B. plicatilis* s.s, a peak in the population growth rate was obtained at a salinity of 10 to 15 g/L^{-1}, and then declined when salinity increased (Yin and Zhao 2008). Montero-Pau et al. (2011) presented similar results for *B. manjavacas*, demonstrating that when *B. manjavacas* and *B. plicatilis* s.s. coexist, both in the field and under laboratory conditions, the former species tolerates higher salinity better than *B. plicatilis* s.s. As regards *B. asplanchnoidis*, a study of Papakostas et al. (2013) carried out in Koronia Lake showed a salinity tolerance range of the species of 3.8–8.5 g L^{-1}, although Michaloudi et al. (2017) conducted experiments at 16 g/L^{-1} salinity. *Brachionus paranguensis* sp. nov., represents the species better adapted to high salinity concentrations (>25 g L^{-1}) as documented by Kostopoulou et al. (2006, 2007, 2009), who cultured individuals of *B.* Nevada at salinities above 30 g L^{-1}. Although *B. paranguensis* sp. nov. can be cultured using lower salinities, according to the results obtained in the present study from preliminary tests performed at 15 g/L^{-1} salinity, the lifespan, the number of eggs per rotifer, and the maximum intrinsic growth rate, drastically decreased. These results are also confirmed by Aránguiz-Acuña et al. (2018) who looked at the different response to salinity (from 2.5 to 10 g L^{-1}) in two *Brachionus* species, namely *B. quadridentatus* and *B. paranguensis* sp. nov.. While the former species did not survive at the highest salinity, *B. paranguensis* n. sp was positively affected by higher salinity which led to an increased growth rate. This high tolerance to salinity allowed the species to colonize the volcanic maar, representing the only active species found in the water column; resting eggs of two other species, *B. dimidiatus* and *Hexarthra* sp., were also found in the sediment of the water body. Before the 1980s the volcanic maar Rincón de Parangueo was a big lake, with a much lower salinity concentration, until a fracture inside the crater occurred, and the lake started to gradually desiccate (Aranda-Gómez et al. 2013). As the lake dried out, water became hypersaline and highly alkaline as reported by Cerca et al. (2014). Unfortunately, there is no evidence of the presence of *B. paranguensis* sp. nov. in the lake in the past when salinity was much lower, as no studies of the zooplankton community have been previously conducted in this area.

Conclusion

A formal taxonomic description has been provided for *B. paranguensis* sp. nov. combining DNA taxonomy, morphology and ecology, and results confirmed the identity of the species within the L group.

Based on DNA taxonomy, both COI and ITS1 markers placed *B. paranguensis* sp. nov. within the L4 clade of the *B. plicatilis* complex, confirming that *B. paranguensis* sp. nov. and *B.* 'Nevada' represent the same taxonomic identity. Results of genetic variability within the L4 clade were different among markers, with a higher COI intraspecific variability (8.5%) compared to the low 0.001% divergence in the ITS1. High genetic divergence in the COI marker is not unusual and its reliability for predicting species in the *B. plicatilis* complex has already been questioned due to its high mutational rate that leads to an over-splitting of the species. ITS1 has been therefore suggested as a more reliable marker for DNA taxonomy.

Comparison of SEM images among the trophi of *B. paranguensis* sp. nov., *B. plicatilis* s.s., *B. manjavacas*, and *B. asplanchnoidis*, indicate clear differences, including basifenestras, ramus posterior projections and satellites. Resting eggs morphotypes seemed to be species specific, although a comparison with *B. asplanchnoidis* resting eggs is also necessary. A differentiation of parthenogenetic females is only possible between *B. asplanchnoidis* and the other members of the L group, as no clear diagnostic characters are observed between females of the other L clades.

Ecological results on salinity preferences showed that *B. paranguensis* sp. nov. is the species better adapted to hypersaline water bodies. Indeed, results demonstrated that high salinity (>25 g L^{-1}) positively affected individuals of *B. paranguensis* sp. nov., while the other members of the L group presented an optimum growth rate at salinities lower than 15–16 g L^{-1}.

Acknowledgment

References

Aranda-Gómez JJ, Levresse G, Pacheco-Martínez J, Ramos-Leal JA, Carrasco-Nuñez G, Chacón-Baca E, González-Naranjo G, Chávez-Cabello G, Vega-González M, Origel G, Noyola-Medrano C (2013) Active sinking at the bottom of the Rincón de Parangueo Maar (Guanajuato, México) and its probable relation with subsidence faults at Salaman-

ca and Celaya. Boletín de la Sociedad Geológica Mexicana 65 (1): 169–188. https://doi.org/10.18268/BSGM2013v65n1a13

Aránguiz-Acuña A, Perez-Portilla P, De la Fuente A, Fontaneto D (2018) Life-history strategies in zooplankton promote coexistence of competitors in extreme environments with high metal content. Scientific Reports: 8: 11060 https://doi.org/10.1038/s41598-018-29487-3

Beauchamp PM (1952) Un facteur de la variabilite chez les rotiferes du genre *Brachionus*. Comptes Redus de I´Académie des Science 234: 573–575.

Begon M, Harper JL, Townsend CP (1996) Ecology: Individuals, Populations, and Communities (3rd eds). Blackwell Scientific, Malden, 1068 pp.

Bickford D, Lohman DJ, Sohdi NSPKL, Ng Meier R, Winker K, Ingram KK, Das I (2007) Cryptic species as a window on diversity and conservation. Trends in Ecology and Evolution 22: 148–155. https://doi.org/10.1016/j.tree.2006.11.004

Bodelón OG, Bernués M, Baltanás A, Montes C (1994) Conductividad y salinidad en los ecosistemas acuáticos del Parque Nacional de Doñana (SO, España). [Conductivity and salinity in the aquatic ecosystems of the Doñana National Park (SW Spain)]. Limnética 10: 27–31.

Bogoslovsky AS (1967) Materials to the study of the resting eggs of rotifers. Communication 2. Bjulleten Moscovskogo obscestva ispytatelej prirody. Otdel Biologiceskij 72:46–67 [in Russian with English summary]

Campillo S, García-Roger EM, Martínez-Torres D, Serra M (2005) Morphological stasis of two species belonging to the L-morphotype in the *Brachionus plicatilis* species complex. In: Herzig A, Gulati RD, Jersabek CD, May L (Eds) Rotifera X. Developments in Hydrobiology vol 181. Springer, Dordrecht. https://doi.org/10.1007/1-4020-4408-9_17

Charin NN (1947) O novom vide kolovratki is roda *Brachionus*. Doklady Akademii Nauk SSSR 56: 107–108.

Cerca M, Carreón-Freyre D, Aranda-Gómez JJ, Rocha-Treviño L (2014) GPR profiles for characterizing subsidence deformation in lake sediments within a maar crater. Proceedings of the 2014 15Th International Conference on Ground Penetrating Radar: 274–278. https://doi.org/10.1109/ICGPR.2014.6970428

Ciros-Pérez J, Gómez A, Serra M (2001) On the taxonomy of three sympatric sibling species of the *Brachionus plicatilis* (Rotifera) complex from Spain, with the description of *B. ibericus* n. sp. Journal of Plankton Research 23 (12): 1311–1328. https://doi.org/10.1093/plankt/23.12.1311

Edmands S (2001) Phylogeography of the intertidal copepod *Tigriopus californicus* reveals substantially reduced population differentiation at northern latitudes. Molecular Ecology 10: 1743–1750. https://doi.org/10.1046/j.0962-1083.2001.01306.x

Folmer O, Black M, Hoeh W, Lutz R, Vrijenhoek R (1994) DNA primers for amplification of mitochondrial cytochrome c oxidase subunit I from diverse metazoan invertebrates. Molecular Marine Biology and Biotechnology 3: 294–299.

Fontaneto D, Melone G (2005) Do Rotifer Jaws Grow after Hatching? Hydrobiologia 181: 213–221. https://doi.org/10.1007/1-4020-4408-9_21

Fontaneto D, Giordani I, Melone G, Serra M (2007) Disentangling the morphological stasis in two rotifer species of the *Brachionus plicatilis* species complex. Hydrobiologia 583: 297–307. https://doi.org/10.1007/s10750-007-0573-1

Fontaneto D, Kaya M, Herniou EA, Barraclough TG (2009) Extreme levels of hidden diversity in microscopic animals (Rotifera) revealed by DNA taxonomy. Molecular Phylogenetics and Evolution 53: 182–189. https://doi.org/10.1016/j.ympev.2009.04.011

Fontaneto D (2014) Molecular phylogenies as a tool to understand diversity in rotifers. International Review of Hydrobiology 99: 178–187. https://doi.org/10.1002/iroh.201301719

Fu Y, Hirayama K, Natsukari Y (1991) Morphological differences between two types of the rotifer *Brachionus plicatilis* O.F. Müller. Journal of Experimental Marine Biology and Ecology 151: 29–41. https://doi.org/10.1016/0022-0981(91)90013-M

García-Morales AE, Elías-Gutiérrez M (2013) DNA barcoding of freshwater Rotifera in Mexico: Evidence of cryptic speciation in common rotifers. Molecular Ecology Resources 13: 1097–1107. https://doi.org/10.1111/1755-0998.12080

Gilbert JJ, Wurdak ES (1978) Species-specific morphology of resting eggs in the Rotifer Asplanchna. Transactions of the American Microscopical Society 97: 330–339. https://doi.org/10.2307/3225986

Gómez A, Serra M, Carvalho GR, Lunt DH (2002) Speciation in ancient cryptic species complexes: Evidence from the molecular phylogeny of *Brachionus plicatilis* (Rotifera). Evolution 56: 1431–1444. https://doi.org/10.1111/j.0014-3820.2002.tb01455.x

Guindon S, Gascuel O (2003) A simple, fast, and accurate algorithm to estimate large phylogenies by maximum likelihood. Systematic Biology 52: 696–704. https://doi.org/10.1080/10635150390235520

Hajibabaei M, De Waard JR, Ivanova NV, Ratnasingham S, Dooh R, Kirk SL, Mackie PM, Hebert PDN (2005) Critical factors for assembling a high volume of DNA barcodes. Philosophical Transactions of the Royal Society of London Series B-Biological Sciences 360: 1959–1967. https://doi.org/10.1098/rstb.2005.1727

Hajibabaei M, Singer GC, Hebert PDN, Hickey D (2007) DNA barcoding: how it complements taxonomy, molecular phylogenetics and population genetics. Trends in Genetics 23: 167–172. https://doi.org/10.1016/j.tig.2007.02.001

Hebert PDN, Ratnasingham S, de Waard JR (2003) Barcoding animal life: cytochrome c oxidase subunit 1 divergences among closely related species. Proceedings of the Royal Society of London B: Biological Sciences 270: 596–599. https://doi.org/10.1098/rsbl.2003.0025

Hebert PDN, Stoeckle MY, Zemlak TS, Francis CM (2004) Identification of Birds through DNA Barcodes. PLoS Biology 2(10): e312. https://doi.org/10.1371/journal.pbio.0020312

Hwang DS, Dahms HU, Park HG, Lee JS (2013) A new intertidal *Brachionus* and intrageneric phylogenetic relationships among *Brachionus* as revealed by allometry and CO1-ITS1 gene analysis. Zoological Studies 52 789: 1–10. https://doi.org/10.1186/1810-522X-52-13

Kearse M, Moir R, Wilson A, Stones-Havas S, Cheung M, Sturrock S, Buxton S, Cooper A, Markowitz S, Duran C, Thierer T, Ashton B, Mentjies P, Drummond A (2012) Geneious Basic: an integrated and extendable desktop software platform for the organization and analysis of sequence data. Bioinformatic 28: 1647–1649. https://doi.org/10.1093/bioinformatics/bts199

Kostopoulou V, Miliou H, Katis G, Verriopoulos G (2006) Changes in the population structure of the lineage 'Nevada' belonging to the *Brachionus plicatilis* species complex, batch-cultured under different feeding regimes. Aquaculture International 14(5):451–466. https://doi.org/10.1007/s10499-006-9048-z

Kostopoulou V, Miliou H, Krontira Y, Verriopoulos G (2007) Mixis in rotifers of the lineage 'Nevada', belonging to the Brachionus plicatilis species complex, under different feeding regimes. Acuaculture Researches 38: 1093–1115. https://doi.org/10.1111/j.1365-2109.2007.01783.x

Kostopoulou V, Miliou H, Verriopoulos G (2009) Morphometric changes in a strain of the lineage 'Nevada', belonging to the *Brachionus plicatilis* (Rotifera) complex. Aquaculture Research 40: 938–949. https://doi.org/10.1111/j.1365-2109.2009.02188.x

Kumar S, Stecher G, Tamura K (2016) MEGA7: Molecular Evolutionary Genetics Analysis Version 7.0 for Bigger Datasets. Molecular Biology and Evolution 33: 1870–1874.https://doi.org/10.1093/molbev/msw054

Krebs CJ (1985) Ecología: Estudio de la distribución y la abundancia (2nd eds), Editorial Harla, Mexico City, 753 pp.

Lowe CD, Kemp SJ, Diaz-Avalos C, Montagnes DJS (2007) How does salinity tolerance influence the distributions of *Brachionus plicatilis* sibling species? Marine Biology 150(3): 377–386. https://doi.org/10.1007/s00227-006-0366-5

Melone G, Fontaneto D (2005) Trophi structure in bdelloid rotifers. Hydrobiologia 546: 197–202. https://doi.org/10.1007/s10750-005-4197-z

Michaloudi E, Mills S, Papakostas S, Stelzer CP, Triantafyllidis A, Kappas I, Abatzopoulos TJ (2017) Morphological and taxonomic demarcation of *Brachionus asplanchnoidis* Charin within the *Brachionus plicatilis* cryptic species complex (Rotifera, Monogononta). Hydrobiologia 796: 19. https://doi.org/10.1007/s10750-016-2924-2

Michaloudi E, Papakostas S, Stamou G, Neděla V, Tihlaříková E, Zhang W, Declerck SAJ (2018) Reverse taxonomy applied to the Brachionus calyciflorus cryptic species complex: Morphometric analysis confirms species delimitations revealed by molecular phylogenetic analysis and allows the (re)description of four species. PLOS ONE 13(9): e0203168. https://doi.org/10.1371/journal.pone.0203168

Miller SE (2007) DNA barcoding and the renaissance of taxonomy. Proceedings of the National Academy of Sciences USA 104: 4775–4776. https://doi.org/10.1073/pnas.0700466104

Mills S, Alcantara-Rodriguez JA, Ciros-Pérez J, Gómez A, Hagiwara A, Galindo KH, Jersabek CD, Malekzadeh-Viayeh R, Leasi F, Lee JS, Welch DBM, Papakostas S, Riss S, Segers H, Serra M, Shiel R, Smolak R, Snell T, Stelzer CP, Tang CQ, Wallace R, Fontaneto D, Walsh EJ (2017) Fifteen species in one: deciphering the *Brachionus plicatilis* species complex (Rotifera, Monogononta) through DNA taxonomy. Hydrobiologia 1–20. https://doi.org/10.1007/s10750-016-2725-7

Milne I, Lindner D, Bayer M, Husmeier D, McGuire G, Marshal DF, Wright F (2008) TOPALi v2: a rich graphical interface for evolutionary analyses of multiple alignments on HPC clusters and multi-core desktops. Bioinformatics 25: 126–127. https://doi.org/10.1093/bioinformatics/btn575

Montero-Pau J, Ramos-Rodríguez E, Serra M, Gómez A (2011) Long-Term Coexistence of Rotifer Cryptic Species. PLOS ONE 6: e21530. https://doi.org/10.1371/journal.pone.0021530

Müller OF (1786) Anintalcula infusoria ,fluviatilia et marina, quae detexit, syitematice descripsit et ad vevum delineari curavit.Copenhagen, 367 pp. https://doi.org/10.5962/bhl.title.47041

Nipkow, F (1961) Die Rädertiere im Plankton des Zürichsees und ihre Entwicklungsphasen. Schweiz. Z. Hydrologie 23: 398–461. https://doi.org/10.1007/BF02505448

Palumbi SR (1996) Nucleic acids II. The polymerase chain reaction. In: HillisD, Moritz C, Mable BK (Eds) Molecular systematics: Sinauer, Sunderland, Massachusetts, 321–383.

Papakostas S, Dooms S, Christodoulou M, Triantafyllidis A, Kappas I, Dierckens K, Bossier P, Sorgeloos P, Abatzopoulos TJ (2006) Identification of cultured Brachionus rotifers based on RFLP and SSCP screening. Marine Biotechnology 8(5):547–559. https://doi.org/10.1007/s10126-005-6181-z

Papakostas S, Michaloudi E, Triantafyllidis A, Kappas I, Abatzopoulos TJ (2013) Allochronic divergence and clonal succession: two microevolutionary processes sculpturing population structure of Brachionus rotifers. Hydrobiologia 700: 33–45. https://doi.org/10.1007/s10750-012-1217-7

Papakostas S, Michaloudi E, Proios K, Brehm M, Verhage L, Rota J, Pena C, Stamou G, Pritchard VL, Fontaneto D, Declerck SAJ (2016) Integrative taxonomy recognizes evolutionary units despite widespread mitonuclear discordance: evidence from a rotifer cryptic species complex. Systematic Biology 65: 508–524. https://doi.org/10.1093/sysbio/syw016

Pfenninger M, Schwenk K (2007) Cryptic animal species are homogeneously distributed among taxa and biogeographical regions. BMC Evolutionary Biology 7 (121): 6. https://doi.org/10.1186/1471-2148-7-121

Ratnasingham S, Hebert PDN (2007) BOLD: The Barcode of Life Data System (www.barcodinglife.org). Molecular Ecology Notes 7: 355–364. https://doi.org/10.1111/j.1471-8286.2007.01678.x

Rocha-Treviño L (2015) Análisis de la deformación y hundimiento activo causado por la desecación del lago del mar Rincón de Parangueo (Guanajuato, México) mediante modelos análogos y perfiles de Radar dePenetración Terrestre (RPT). Tesis de Maestría: Ciudad de México, México: UNAM, Porgrama de Posgrado en Ciencias de la Tierra, Centro de Geociencias.

Segers H, Murugan G, Dumont H (1993) On the Taxonomy of the Brachionidae: Description of *Plationus* n. gen. (Rotifera, Monogononta). Hydrobiologia 268: 1–8. https://doi.org/10.1007/BF00005736

Segers H, De Smet W, Fischer C, Fontaneto D, Michaloudi E, Wallace RL, Jersabek CD (2012) Towards a list of available names in zoology, partim Phylum Rotifera. Zootaxa 3179: 61–68. https://doi.org/10.11646/zootaxa.3179.1.3

Serra M, Fontaneto D (2017) Speciation in the *Brachionus plicatilis* species complex. In: Hagiwara A, Yoshinaga T (Eds) Rotifers. Fisheries Science Series. Springer, Singapore. https://doi.org/10.1007/978-981-10-5635-2_2

Silva-Briano M, Adabache-Ortiz A, Guerrero-Jiménez G, Rico-Martínez R, Zavala-Padilla G (2015) Ultrastructural and Morphological Description of the Three Major Groups of Freshwater Zooplankton (Rotifera, Cladocera, and Copepoda) from the State of Aguascalientes, Mexico. INTECH open science/ open minds, 307–325. https://doi.org/10.5772/60659

Suatoni E, Vicario S, Rice S, Snell T, Caccone A (2006) An analysis of species boundaries and biogeographic patterns in a cryptic species complex: The rotifer-*Brachionus plicatilis*. Molecular Phylogenetics and Evolution 41: 86–98. https://doi.org/10.1016/j.ympev.2006.04.025

Tang CQ, Leasi F, Obertegger U, Kieneke A, Barradough TG, Fontaneto D (2012) The widely used small subunit 18S rDNA molecule greatly underestimates true diversity in biodiversity surveys of the meiofauna. Proceedings of the National Academy of Sciences 109: 16208–16212. https://doi.org/10.1073/pnas.1209160109

Torricelli G, Carapelli A, Convey P, Nardi F, Boore JL, Frati F (2010) High divergence across the whole mitochondrial genome in the "pan-Antarctic" springtail *Friesea grisea*: Evidence for cryptic species? Gene 449: 30–40. https://doi.org/10.1016/j.gene.2009.09.006

Tschugunoff NL (1921) Über das Plankton des nördlichen Teiles des Kaspisees. Raboty Volzhskoj Biologicheskoj Stancii, Saratov 6: 159–162.

Villesen P (2007) FaBox: an online toolbox for fasta sequences. Molecular Ecology Notes 7: 965–968. https://doi.org/10.1111/j.1471-8286.2007.01821.x

Yin XW, Zhao W (2008) Studies on life history characteristics of *Brachionus plicatilis* O. F. Mueller (Rotifera) in relation to temperature, salinity and food algae. Aquatic Ecology 42: 165–176. https://doi.org/10.1007/s10452-007-9092-4

Supplementary material 1

Figures S1–S2
Authors: Gerardo Guerrero-Jiménez, Patrizia Elena Vannucchi, Marcelo Silva-Briano, Araceli Adabache-Ortiz, Roberto Rico-Martínez, David Roberts, Roy Neilson, Manuel Elías-Gutiérrez
Data type: molecular data
Explanation note: **Figure 1.** COI (TN93+G) Maximum Likelihood tree obtained with PhyML 3.0 of 146 haplotypes belonging to the four L clades of Brachionus plicatilis complex and one outgroup species Brachionus rotundiformis (AF387287). **Figure 2.** ITS1 (GTR+G) Maximum Likelihood tree obtained with PhyML 3.0 of 12 haplotypes belonging to the four L clades of Brachionus plicatilis complex and one outgroup species Brachionus rotundiformis (AF387239).

Link: https://doi.org/10.3897/zookeys.880.28992.suppl1

RESEARCH ARTICLE

A new species of *Claviramus* (Annelida, Sabellida, Sabellidae) from the Ariake Inland Sea, Kyushu, Japan

Eijiroh Nishi[1], Katsuhiko Tanaka[2], María Ana Tovar-Hernández[3]

1 *College of Education, Yokohama National University, Hodogaya, Yokohama 240-8501, Japan* **2** *Department of Marine Biology, School of Marine Science and Technology, Tokai University, 3-20-1, Orido, Shimizu-ku, Shizuoka-shi, Shizuoka 424-8610, Japan* **3** *Universidad Autónoma de Nuevo León, Facultad de Ciencias Biológicas, Laboratorio de Biosistemática, San Nicolás de los Garza, Nuevo León, México*

Corresponding author: *Eijiroh Nishi* (nishi-eijiroh-nr@ynu.ac.jp)

Citation: Nishi E, Tanaka K, Tovar-Hernández MA (2019) A new species of *Claviramus* (Annelida, Sabellida, Sabellidae) from the Ariake Inland Sea, Kyushu, Japan. ZooKeys 880: 25–32. https://doi.org/10.3897/zookeys.880.36281

Abstract

A new species of the sabellid polychaete genus *Claviramus* Fitzhugh, 2002, is described from Ariake Inland Sea, Kyushu, Japan. *Claviramus* is a small genus, composed of three species worldwide. Its distinctive feature is the presence of foliaceous flanges at the distal ends of the radioles. *Claviramus kyushuensis* **sp. nov.** here described is characterized by the presence of a glandular ridge on chaetiger 2, glandular shields on the abdomen, thoracic uncini bidentate, and the presence of a short, distal filament in some radioles. A key and a comparative table of diagnostic characters for species of *Claviramus* are provided.

Keywords

Introduction

Japanese waters are represented by approximately 40 species of sabellid polychaetes (Nishi et al. 2017). Among them, eight species from soft bottoms belonging to plesiomorphic genera *Chone* Krøyer, 1856, *Dialychone* Claparède, 1870, *Jasmineira* Langerhans, 1880 and *Paradialychone* Tovar-Hernández, 2008, have been reported (Nishi et al. 2009). In this study, a new species of *Claviramus* Fitzhugh, 2002 is described

from Ariake Inland Sea, Kyushu, Japan. It was found co-occurring with *Jasmineira kikuchii* Nishi, Tanaka, Tovar-Hernández & Giangrande, 2009.

The sabellid genus *Claviramus* is currently composed of three species worldwide. *Claviramus candelus* (Grube, 1863), the type species of the genus, was originally described as *Sabella candela* Grube, 1863, from the northern Adriatic Sea, but Langerhans (1884) transferred it to the genus *Jasmineira*. *Claviramus oculatus* (Langerhans, 1884) was described as *Jasmineira oculata* Langerhans, 1884, from Madeira. Cochrane (2000) redescribed both species within *Jasmineira* in detail based on type and additional specimens. Fitzhugh (2002) established the genus *Claviramus* based on the presence of prominent foliaceous flanges at the distal ends of the radioles, and transferred *J. candelus* and *J. oculatus* to *Claviramus*. The third known species, *Claviramus grubei* Fitzhugh, 2002, was described from Thailand, Andaman Sea. A thorough revision and synthesis of these three species was provided by Cochrane (2000) and Fitzhugh (2002).

Materials and methods

Specimens were measured to record width of the middle of the thorax, trunk length (chaetiger 1 or collar to pygidium), radiolar crown length, number of radiolar pairs, number of thoracic and abdominal segments, and presence of gametes. The diagnosis and a full description of the new species were based on the holotype, with variation in the paratypes indicated in parentheses. The thoracic and abdominal glandular pattern was revealed by staining the worms with methyl green. Parts of thorax and abdomen of one paratype CBM-ZW 1124 were observed on the scanning electron microscope JSM-6500 at the Yokohama National University. Digital photographs were taken with an attached Canon EOS Rebel T7i digital camera. Type materials were deposited at the Natural History Museum and Institute, Chiba, Japan (catalogue code CBM-ZW) and at the Colección Poliquetológica, Universidad Autónoma de Nuevo León (catalogue code UANL). A key and a comparative table of diagnostic characters for species of *Claviramus* are also included; the information is as complete as available based on original descriptions and redescriptions provided by Cochrane (2000) and Fitzhugh (2002).

Taxonomic account

Order Sabellida Latreille, 1825
Family Sabellidae Latreille, 1825

Genus *Claviramus* Fitzhugh, 2002

Claviramus Fitzhugh, 2002: 412, 414–415.

Type species. *Sabella candela* Grube, 1863.

Claviramus kyushuensis sp. nov.

http://zoobank.org/AF7C503A-E9B9-4424-840B-191F1718015A

Figs 1–3

Material examined. Ariake Sound, Kyushu, Japan, Stn 20D, 32°31.070'N, 130°14.037'E, 20 m depth, sandy mud bottoms, collected by dredge by K. Mori, 17 September 2005. **Holotype** CBM-ZW 1123, **Paratypes** CBM-ZW 1124-1126 (three paratypes: two complete, one lacking crown), UANL 8130 (three paratypes: two complete, one lacking crown).

   Diagnosis. Subdistal ends of some radioles with lateral margins extended, thin, as foliaceous flanges (Figs 1E–G, 2F), some with a short, distal filament or cirrus (Fig. 1G). Glandular ridge on chaetiger 2 present. Abdominal shields well developed (Figs 1B, 2C). Dorsal pockets of collar present exposing large vascular loops (Fig. 1D). Anterior peristomial ring not extending beyond ventral collar margins. Ventral margin of collar with a shallow mid-ventral incision forming two discrete rounded lappets (Figs 1B, C). Thoracic tori not contacting shields (Fig. 1B). Thoracic uncini with tips of main fangs bifid (Fig. 3C–D).

   Description. Sabellid worm with eight thoracic (eight in all types) and ten abdominal chaetigers (9–16 in paratypes CBM ZW 1124-1126, UANL 8130). Trunk length 2.5 mm (1.6 mm in paratype CBM-ZW 1125, 3.2–4.7 mm in paratypes UANL 8130), body width 0.7 mm (0.3 mm in paratype CBM-ZW 1126, 0.5–1.3 mm in paratypes UANL 8130). Radiolar crown 1.1 mm length (1.3–2.1 mm in paratypes UANL 8130), with seven radioles in each branchial lobe (7–9 in paratypes UANL 8130).

   Palmate membrane absent. Subdistal ends of some radioles with lateral margins extended, thin, as foliaceous flanges; overall shape oblong (Figs 1E–G, 2F) with a mid-ventral incision occupying a quarter of flange length; some tips with a short, distal filament (Fig. 1G). Other radioles with unflanged tips, filiform (Fig. 2D) or with broken tips (Fig. 2E). Largest pinnules located at 3/4 of radiole length (Fig. 2D). Radiolar eyes absent. Two pairs of ventral radiolar appendages, as long as half of radiolar crown length. Dorsal lips narrow, triangular, longer than wide. Ventral lips rounded, low. Dorso-lateral margins of collar fused to faecal groove; dorsal pockets present (Figs 1A, D, 2A); large vascular loops visible on dorsal pockets of collar (Fig. 1D); ventral sacs absent. Ventral margin of anterior peristomial ring as broadly triangular lobe, not extending beyond collar margins. Ventral collar margin with a shallow mid-ventral incision forming two discrete rounded lappets (Figs 1B, C, 2B). Lateral collar margins slightly oblique, with ventral margin slightly higher than dorsal. Thoracic and abdominal shields well developed (Figs 1B, C, 2C). Collar shield divided transversally into three nearly rectangular sections with lateral margins indented (Fig. 2B). A pair of white triangular glandular pads in the ventral side of collar, as lung-shaped. Shields from chaetigers 2 to 8 rectangular, broad, entire (Figs 1B, 2B). Abdominal shields forming two squares divided by faecal groove (Figs 1B, 2C). Narrow glandular ridge on chaetiger 2 present, most notorious laterally (Fig. 1A, D). Thoracic tori not contacting shields (Fig. 1B, C). Thoracic notopodial fascicles in chaetiger 1 as short as rows of
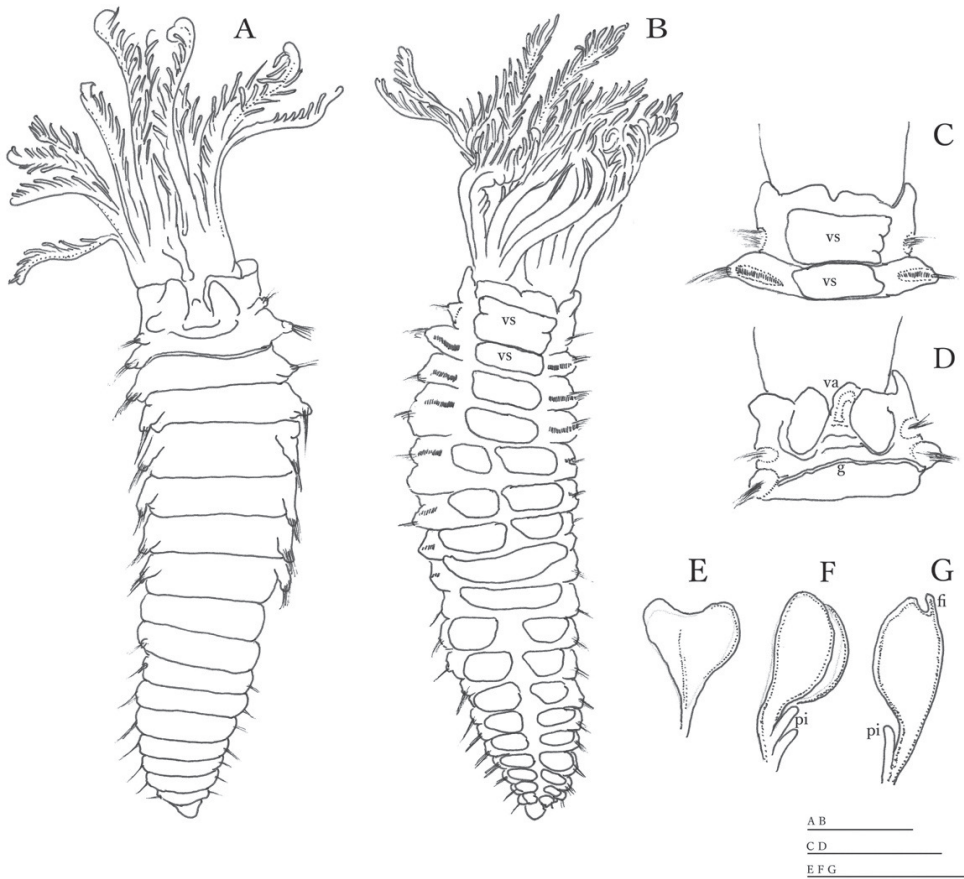
Figure 1. *Claviramus kyushuensis* sp. nov., holotype. **A** Body, dorsal view **B** same, ventral view **C, D** collar and second chaetiger, ventral and dorsal views, respectively **E–G** distal foleaceous flanges. Abbreviations: fi: filament, g: glandular ridge, pi: pinnule, va: vascular loop, vs: ventral shield. Scale bars: 0.5 mm (**A–D**), 0.2 mm (**E–G**).

narrowly hooded chaetae (collar chaetae) (Fig. 3A). Notopodial fascicles in chaetigers 2–8 with superior group of narrowly hooded chaetae and two inferior rows of broadly hooded chaetae (Figs 2I, 3B). Thoracic neuropodial uncini acicular (Fig. 2G); main fang bifid, surmounted by 5–6 rows of small equal-sized teeth (Fig. 3C, D), breast as a narrow swelling; handles very elongate (Fig. 2G). Abdominal neuropodial fascicles with one or two transverse rows of narrowly hooded chaetae (Fig. 3E). Abdominal notopodia with avicular uncini (Figs 2H, 3F); main fang surmounted by 7–9 rows of small teeth equal in size, occupying a half of the main fang length (Fig. 3F); breast well developed; handles short (Fig. 2H). Pygidium triangular without eyes neither cirrus (Figs 1B, 2C). Anus ventral. Tubes not preserved. Paratypes mature hermaphrodites with full-developed oocytes and sperm in thoracic and abdominal segments.

Etymology. The specific epithet is named after type locality, Kyushu, Japan.
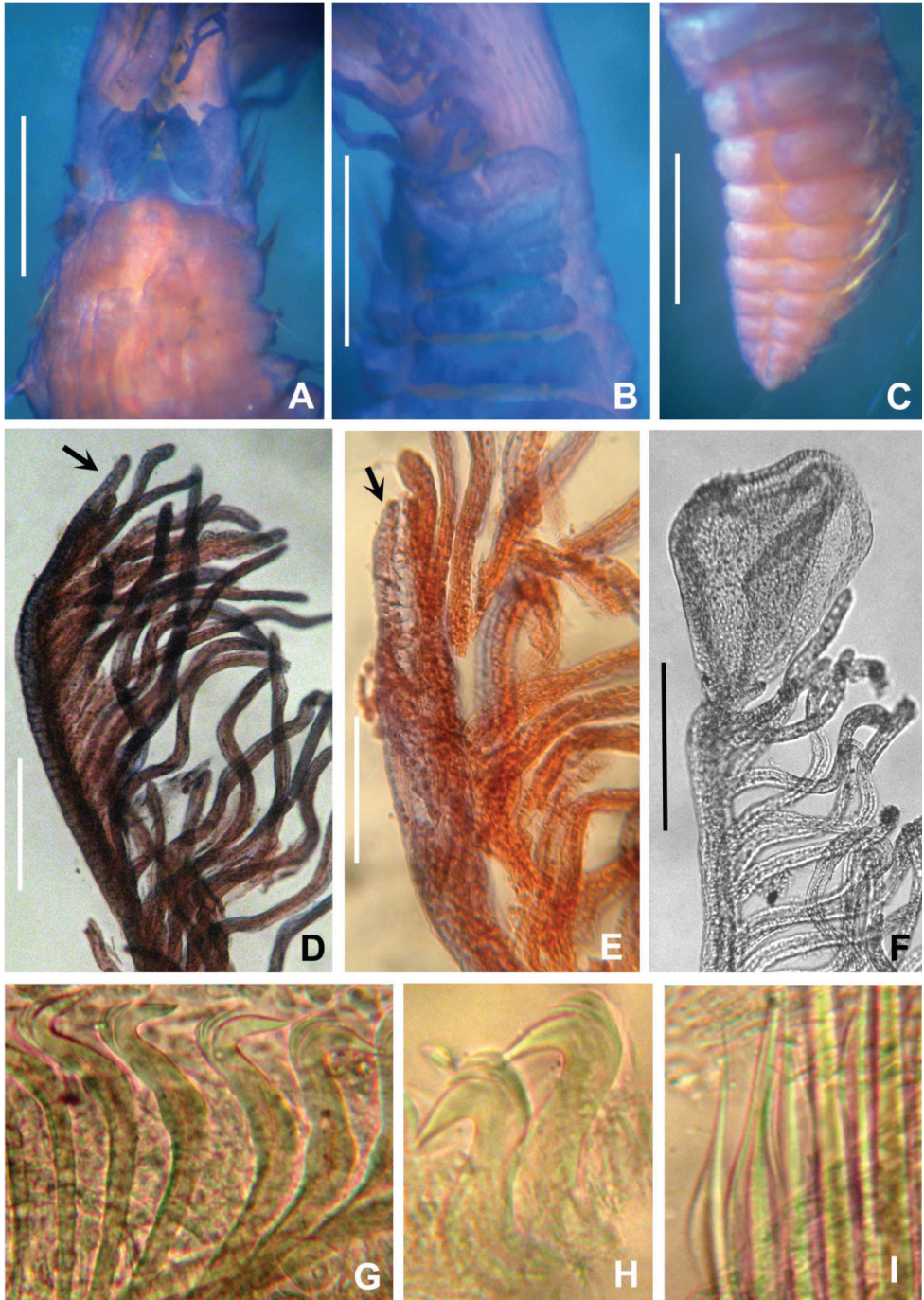
Figure 2. Paratype of *Claviramus kyushuensis* sp. nov. **A** Anterior thoracic segments, dorsal view **B** same, ventral view **C** posterior abdomen **D–F** radiolar tips **G** thoracic uncini **H** abdominal uncini **I** thoracic chaetae. Arrows in **D** and **E** point to radiolar tips, entire in **D**, broken in **E**. Scale bars: 0.5 mm (**A–C**), 150 um (**D–F**).
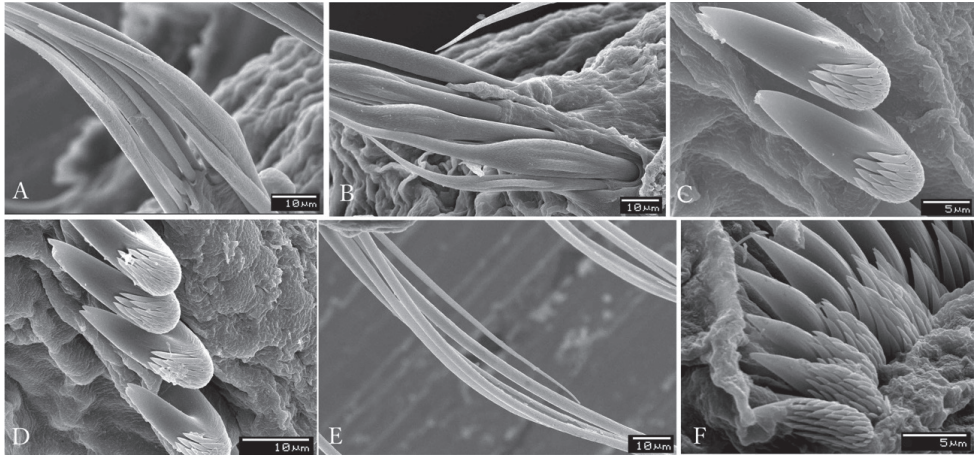
Figure 3. *Claviramus kyushuensis* sp. nov., scanning electron microscope images of chaetae and uncini. **A** Collar chaetiger with narrowly hooded chaetae **B** second thoracic chaetiger with superior group of narrowly hooded chaetae and inferior broadly hooded chaetae **C** uncini from seventh thoracic torus **D** uncini from fourth thoracic torus **E** elongate, narrowly hooded chaetae from eighth abdominal chaetiger **F** uncini from the seventh abdominal torus.

Table 1. Species of *Claviramus* from the world after Cochrane (2000) and Fitzhugh (2002).

Species name	Glandular ridge on chaetiger 2	Abdominal glandular shields	Mid-ventral incision of distal radiolar flanges	Ventral margin of collar	Ventral shield of collar	Main fang of thoracic uncini	Pygidial eyes	Type locality
Claviramus candelus (Grube, 1863)	Absent	Present	? (Short, less than 1/4 of the flange length, fide figure of Langerhans)	Even in height	Rectangular, entire	?	Present	Adriatic Sea
Claviramus grubei Fitzhugh, 2002	Present	Absent	Short, less than 1/4 of the flange length	With shallow mid-ventral incision	?	?	Absent	Thailand, Phuket Island
Claviramus oculatus (Langerhans, 1884)	Absent	Absent	Short, less than 1/4 of the flange length	With shallow mid-ventral incision	Rectangular, divided transversally into 2 areas (superior wider than inferior one)	?	Present	Madeira
Claviramus kyushuensis sp. nov.	Present	Present	Medium, 1/2 of the flange length	With shallow mid-ventral incision	Rectangular, divided transversally into 3 nearly equal sized sections with lateral margins indented	Bifid in frontal view	Absent	Ariake sound, Kyushu, Japan

Remarks. Among the species currently recognized in *Claviramus*, *C. kyushuensis* sp. nov., is unique by having a collar shield rectangular, divided transversally into three nearly equal-sized sections; a glandular ridge on chaetiger 2; abdominal shields well developed; main fang of thoracic uncini with bifid tips and the presence of a short, distal filament in some radioles.

Claviramus grubei has also a glandular ridge on chaetiger 2, a short mid-ventral incision of distal radiolar flanges and radiolar tip filaments, but it differs of *C. kyushuensis* sp. nov., by lacking abdominal shields (present in *C. kyushuensis* sp. nov.) (Table 1).

Claviramus kyushuensis sp. nov., differs from *C. oculatus* and *C. candelus* mainly by lacking pygidial eyes (present in *C. oculatus* and *C. candelus*) and having a collar shield rectangular, divided transversally into three nearly equal-sized sections (entire in *C. candelus*, divided into two areas in *C. oculatus*) (Table 1).

In addition, SEM images used in this study reveals that tips of main fangs of thoracic uncini are bifid (Fig. 3C, D). This peculiarity has been only reported in *Amphicorina triangulata* López & Tena, 1999 by Cepeda and Lattig (2017). However, in *A. triangulata*, the presence of a large tooth above the main fang in the midline, followed by a third tooth offset from midline, and then followed by series of smaller teeth, is remarkable. In *Claviramus kyushuensis* sp. nov., all rows of teeth above the main fang are nearly equal-sized (Fig. 3C, D).

Key to species of *Claviramus*

1	With ventral shields on abdominal segments	**2**
–	Without ventral shields on abdominal segments	**3**
2	Ventral margin of collar entire; glandular ridge on chaetiger 2 absent; with pygidial eyes	***C. candelus***
–	Ventral margin of collar incised; glandular ridge on chaetiger 2 present; without pygidial eyes	***C. kyushuensis* sp. nov.**
3	With pygidial eyes; glandular ridge on chaetiger 2 absent	***C. oculatus***
–	Without pygidial eyes; glandular ridge on chaetiger 2 present	***C. grubei***

Discussion

Claviramus was erected based on the presence of prominent foliaceous flanges, at the distal ends of radioles (Fitzhugh 2002). However, in specimens reviewed here, these leaf-like structures are easily broken off and are present only in some radioles (other radioles have entire filiform tips revealed by presence of skeleton cells). Cochrane (2000) also showed broken radioles in some specimens belonging to *C. candelus*. Under this scenario, it is evident that many specimens were wrongly identified under *Jasmineira*.

However, *Jasmineira* and *Claviramus* may also distinguishable based on the presence of inferior thoracic bayonet notochaetae (absent in *Claviramus*), uncinial morphology (Fitzhugh 1989; Cochrane 2000) and presence of a breaking plane sensu Cochrane (2003) or abscission zone sensu Tovar-Hernández (2008). The abscission zone refers to crowns where there is a distinct point immediately above the radiolar bases, where the radioles become detached from the branchial basis.

Acknowledgements

References

Cepeda D, Lattig P (2017) New reports and description of a new species of Sabellidae (Annelida) for the Iberian Peninsula and Balearic Archipelago. Marine Biology Research 13(8): 832–853. https://doi.org/10.1080/17451000.2017.1303576

Claparède E (1870) Les Annélides Chétopodes du Golfe de Naples. Supplément. Mémoires de la Société de physique et d'histoire naturelle de Genève 20: 365–542. https://doi.org/10.5962/bhl.title.2142

Cochrane SJ (2000) Taxonomy and systematics of selected marine soft-bottom fan-worms (Polychaeta: Sabellidae: Sabellinae). Ph.D. Thesis, University of St. Andrews, Scotland, UK, 296 pp. http://research-repository.st-andrews.ac.uk/ http://hdl.handle.net/10023/7112

Fitzhugh K (2002) Fan worm polychaetes (Sabellidae: Sabellinae) collected during the Thai-Danish Bioshelf Project. Phuket Marine Biological Center Special Publication 24: 353–424.

Grube AE (1863) Beschreibung neuer oder wenig bekannter Anneliden. Zahlreiche Gattungen. Archiv für Naturgeschichte, Berlin 29: 37–69. https://doi.org/10.5962/bhl.part.9306

Krøyer H (1856) Bidrag til Kundskab af Sabellerne. Kongelige Danske Videnskabernes Selskabs Forhandlinger, 1–36.

Langerhans P (1880) Die Wurmfauna von Madeira III. Zeitschrift für Wissenschaftliche Zoologie 34: 87–143.

Langerhans P (1884) Die Wurmfauna von Madeira IV. Zeitschrift für Wissenschaftliche Zoologie 40: 247–285.

Latreille PA (1825) Familles naturelles du règne animal, exposées succinctement et dans un ordre analytique avec l'indication de leurs genres. J.-B. Baillière, Paris, 570 pp. https://doi.org/10.5962/bhl.title.16094

López E, Tena J (1999) A new species of *Amphicorina* (Polychaeta: Sabellidae: Sabellinae) from the Chafarinas Islands (Western Mediterranean). Cahiers de Biologie Marine 40: 329–35.

Nishi E, Tanaka K, Taru M, Kupriyanova EK, Rzhavsky A (2017) Chapter 5 Sabellidae and Serpulidae. In: Japanese Association of Sessile Organisms (Eds) Methods of identification of fouling organisms. Kouseishya Kouseikaku Co., Ltd., Tokyo, 88–102. [in Japanese]

Nishi E, Tanaka K, Tovar-Hernández MA, Giangrande A (2009) *Dialychone*, *Jasmineira* and *Paradialychone* (Annelida: Polychaeta: Sabellidae) from Japan and adjacent waters, including four new species description. Zootaxa 2167: 1–24. https://doi.org/10.11646/zootaxa.2167.1.1

Tovar-Hernández MA (2008) Phylogeny of *Chone* Krøyer, 1856 (Polychaeta: Sabellidae) and related genera. Journal of Natural History 42: 2193–2226. https://doi.org/10.1080/00222930802254714

RESEARCH ARTICLE

Multiple paternity assessed in the cuttlefish *Sepiella japonica* (Mollusca, Cephalopoda) using microsatellite markers

Liqin Liu[1,2], Yao Zhang[1], Xiaoyu Hu[1], Zhenming Lü[1,2], Bingjian Liu[1], Li Hua Jiang[2], Li Gong[1]

1 *National Engineering Laboratory of Marine Germplasm Resources Exploration and Utilization, College of Marine Sciences and Technology, Zhejiang Ocean University, Zhoushan 316022, China* **2** *National Engineering Research Center for Facilitated Marine Aquaculture, Zhejiang Ocean University, Zhoushan 316022, China*

Corresponding author: *Li Gong* (gongli1027@163.com)

Citation: Liu L, Zhang Y, Hu X, Lü Z, Liu B, Jiang LH, Gong L (2019) Multiple paternity assessed in the cuttlefish *Sepiella japonica* (Mollusca, Cephalopoda) using microsatellite markers. ZooKeys 880: 33–42. https://doi.org/10.3897/zookeys.880.33569

Abstract

Multiple paternity was demonstrated for seven clutches of eggs and 40 offspring sampled from these clutches in the cuttlefish *Sepiella japonica* from Fujian Shacheng Harbor Cultivation Base (Fujian Province, China), using four microsatellite DNA markers. It was observed that female cuttlefish copulated with different males. In this study, genotyping data suggest that at least three paternal allele genotypes were present in all seven clutches indicating that at least two males were responsible for each brood. Combined with behavioral observations, this study provides evidence for sperm competition and multiple paternity in *S. japonica*.

Keywords

genetic diversity, mating; polyandry, reproductive strategy, sperm competition

Introduction

The cuttlefish *Sepiella japonica* Sasaki, 1929 (Mollusca, Cephalopoda) is a commercially important marine species in China. Production from wild stocks reached 60,000 tons in Zhejiang Province and accounted for more than 9.3% of provincial fishing

catches in 1957 (Liu 2002; Wu et al. 2010). The resource of *S. japonica* has declined since the 1980s due to over-fishing and pollution (Jiang et al. 2014). To enhance production, artificial breeding methods are being developed in China and successful aquaculture techniques have been established in recent years (Yin et al. 2013). However, studies have revealed that the populations and individual genetic diversity in this species has declined under artificial conditions (Song and Wang 2009; Xu et al. 2011). The factors affecting the maintenance of genetic diversity have been a primary concern of conservation biologists.

An important factor that affects the genetic diversity of a population is the effective population size (Ne) which in turn is greatly influenced by the mating system of a species (Hoekert et al. 2002). The mating system influences Ne through changing the number of individuals contributing to subsequent generations (Brown et al. 2005). In a polyandrous mating system, females mate with several males within a single reproductive cycle in which the clustered offspring are descended from multiple males (Pearse and Anderson 2009). In such a mating system, Ne increases, and, as a result, maximizes the genetic diversity of the offspring within a single reproductive season (Sugg and Chesser 1994; Balloux and Lehmann 2003). Some studies have confirmed that a polyandrous mating system is frequent in marine cephalopods including *Octopus vulgaris* Sasaki, 1929 (Quinteiro et al. 2011), *Graneledone boreopacifica* Nesis, 1982 (Voight and Feldheim 2009), *Sepioteuthis australis* Quoy & Gaimard, 1832 (van Camp et al. 2004), *Sepia apama* Gray, 1849 (Naud et al. 2005), *Loligo pealeii* LeSueur, 1821 (Buresch et al. 2001), and *Loligo bleekeri* Keferstein, 1866 (Iwata et al. 2005). It is worth noting that the female of these species carries stored sperm from more than one male, and Ne will therefore be significantly higher (Pearse and Anderson 2009). Previous studies have shown that female *S. japonica* store sperm in the seminal receptacle found in the buccal membrane (Hanlon et al. 1999; Naud et al. 2005). All else being equal, long-term sperm storage enhances the opportunity for multiple matings of this species (Olsson et al. 1994; Ross 2001). Moreover, multiple matings of female *S. japonica* has actually been observed (Wada et al. 2006). Polyandry, coupled with sperm storage, is an important reproductive strategy for maximizing the genetic diversity of offspring in *S. japonica*.

In recent years, multiple paternity in several marine species has been documented using different genetic markers including allozymes, DNA fingerprinting, RAPDs, and microsatellites. Microsatellites are the preferred marker because they are widely distributed in the genomes of most organisms and are highly polymorphic (Jarne and Lagoda 1996). Paternity studies based on microsatellites have become increasingly common, and the number of studies using microsatellites has increased (Hoekert et al. 2002; Laloi et al. 2004; Takagi et al. 2008). Several microsatellite markers have been isolated and characterized for *S. japonica* and used to evaluate the genetic structure of its populations (Wu et al. 2010; Lü et al. 2017). In this study, we used the previously described microsatellite markers to investigate whether multiple paternity occurs in *S. japonica*. We observed multiple mating and paternity in this species and discussed the possible factors contributing to this reproductive strategy.

Materials and methods

Sample collection

Sexually mature adult *S. japonica* were obtained from the Fujian Shacheng Harbor Cultivation Base (Fujian Province, China). A sample of 200 wild adults was captured using traps and kept mixed into a cage (9 m^3). Seawater parameters were continuously maintained at 25–27 °C and 23‰ salinity. From this sample, seven mating pairs were randomly chosen as breeders to produce the next generation. All behavioral interactions were recorded using closed-circuit television with infrared to observe individual animals. Each mating pair was gently captured and placed in a spawning tank until oviposition. Egg strings derived from each clutch were transferred to a hatchery tank. After hatching, 280 offspring were randomly collected for population genotyping, maintained in a tank until they reached a pre-determined age. The muscles from the mantle cavity of parents and offspring were taken and placed in 95% ethanol and stored at –20 °C until DNA extraction. Seven clutches (called A–G) were analyzed.

DNA extraction and amplification

Total genomic DNA was isolated from each offspring and from the muscular tissue of the respective parents using the standard method of phenol-chloroform (Towner 1991). The concentration of DNA was estimated by a spectrophotometer (Nanodrop ND-2000, Thermo Electron Corporation, USA) and then the quality was assessed in 0.8% agarose gel. Three microsatellite loci, chosen from four loci (CL168, CL327, CL3354, CL904) developed specifically for *S. japonica* by Lü et al. (2017) were used to study genotypes for parents and their offspring.

The amplifications were carried out in a 2720 thermal cycler (ABI, USA) and in a 10 uL reaction volume: 2–10 ng DNA (0.5 μL), 0.5 μL of each forward and reverse primers, 5 μL 2×Es Taq MasterMix and 3.5 μL of double distilled water. The Polymerase Chain Reaction (PCR) conditions were initial denaturation for 5 min at 94 °C, followed by 30 cycles of denaturation for 40 s at 94 °C, annealing for 40 s at a primer-specific annealing temperature, extension for 40 s at 72 °C. PCR products were detected using capillary electrophoresis (BIOptic's Qsep100 dna-CE, Taiwan) and allele size was estimated using Q-Analyzer software.

Data analyses

Parents and their offspring were genotyped by determining alleles at three of the four microsatellite loci. We considered evidence from at least two loci to be necessary for estimation of multiple paternity, because evidence from one locus may have been caused by mutations or genotyping error (Davy et al. 2011). We determined paternal

alleles through subtracting the maternal alleles from offspring in a brood following the technique of FitzSimmons (1998). The minimum number of sires for a clutch was assigned by counting the number of paternal alleles at each locus. Any instance of more than two possible paternal alleles at any loci indicated multiple paternity in a clutch (Buresch et al. 2001). In addition to manual reconstruction, we attempted to estimate paternal number, as genotypes, to corroborate our results using GERUD 2.0 (Jones 2005). Progeny genotypes were tested for conformity with Mendelian inheritance patterns using the X^2 test (P < 0.05). Exclusion probabilities were assessed using the program CERVUS v. 2.0 (Marshall et al. 1998).

Results

Behavioral observations

Mating behavior in *S. japonica* involves courtship of a female by a male, and females may copulate with multiple males. Mating pairs mated in the head-to-head position during which males transfer spermatophores to the buccal membrane of the females or to an internal seminal receptacle (Fig. 1). The spermatophores that are deposited around the buccal area extrude the sperm mass to form spermatangium. Then the spermatangia attach to the buccal membrane where slowly released sperm are used for fertilization. We found that the male flushed water strongly when he was close to the female buccal area prior to mating with the female. This behavior is thought to dislodge sperm from previous males. We also found obvious courtship rituals and agonistic behaviors after sexual maturity. Males are generally capable of mating early in life (3–6 months maturity) and will continue to mate until senescence. However, the females do not generally lay eggs after copulating until fully mature. The duration of spawning in *S. japonica* varied from 21 to 30 days. Females lay multiple eggs (from tens to hundreds of thousands) by extruding them from the ovary and then they die shortly after spawning.

Paternity analysis

Three of the four microsatellite markers were chosen to test paternity in seven offspring clutches. These loci exhibited three or more alleles and were polymorphic in each individual. We chose the locus which followed Mendelian inheritance to analyze paternity. Two hundred and eighty-seven individuals were genotyped at three loci, seven adult females and 280 offspring. The analysis was highly reproducible. We analyzed paternity including sampled males and non-sampled males that had copulated with females prior to capture. The exclusionary power of paternity assignments varied between 0.951 and 0.981. Maternal and offspring genotypes for each clutch are given in Table 2.

Almost all females were heterozygous at these loci (CL168, CL327, CL3354, CL904), except for CL327 (160/160) in the clutch B female. For clutches A and E,

Figure 1. *S. japonica* mating in the head-to-head position.

Table 1. Microsatellite loci used for paternity assessment in *Sepiella japonica.*

Locus	Repeat motif	Primer Sequences(5'-3')	Ta(°C)	GenBank Accession
CL168	$(AAC)_6$	F:ACAATCAACGGCTGTAAAGTCA	55	KU306816
		R:GACTATGGTTTGGATTTGGCAT		
CL3354	$(CTG)_5...(TGC)_5$	F:CCTCGGCTTCTGATGAAAAT	55	KU306828
		R:AGCCTTACTTCTGCAACATG		
CL904	$(AT)_8$	F:TCTAGGCCTGTGGTTAATGT	55	KU306823
		R:TGATCGTTACTTGATGGCAG		
CL327	$(TA)_6$	F: ACAGCATCTTCTGGTAAGCCAT	58	KX839255
		R: TAGTCCTGTCACCACAGTTATGC		

three different alleles which the father contributed were observed at the three chosen loci, suggesting that these two clutches had been sired by at least two males. The offspring of four females (B, C, D, and F) had three or four paternal alleles in each locus, and three paternal genotypes were observed in all loci. The number of paternal genotypes at these three loci indicated that females B, C, D, and F had mated with three different males. Within clutch G, five different alleles were detected at loci CL168 and CL3354, two of which were from maternal alleles. Clutch G showed four alleles for the locus CL904 in addition to the two alleles detected in the female. Four different paternal genotypes were estimated in clutch G, suggesting the female G was fertilized by at least four different males.

Discussion

We observed female *S. japonica* mating with different males during the reproductive period, a behavior also recorded in other species of cephalopods (Hall and Hanlon 2002; Naud et al. 2005). The benefits of multiple mating not only may raise the potential

Table 2. Genotypes of maternal cuttlefish, offspring and estimated paternal cuttlefish of *Sepiella japonica*.

Maternal Genotype			Offspring Genotype					Estimated Paternal Genotype			
Clutch Code	Locus	Genotype	I	II	III	IV	V	1	2	3	4
A	CL168	155/170	155/160(21)	155/165(10)	175/170(9)			160/165	175/160		
	CL3354	240/260	240/250(3)	260/270(18)	240/230(19)			250/270	230/270		
	CL327	140/170	130/170(2)	140/160(15)	140/170(17)	160/170(6)		130/170	160/140		
B	CL168	175/185	175/180(12)	180/185(13)	185/200(5)	160/185(10)		180/180	180/200	160/200	
	CL3354	230/250	230/240(21)	235/250(9)	230/235(9)	230/250(1)	230/230(1)	240/230	235/235	240/235	
	CL327	160/160	145/160(16)	155/160(13)	150/160(11)			145/155	145/150	155/150	
C	CL168	150/160	140/150(14)	150/155(10)	140/160(12)	136/150(4)		140/140	140/136	150/136	
	CL3354	200/230	195/230(16)	195/200(6)	200/225(11)	210/230(3)	225/230(4)	200/195	230/195	195/225	
	CL327	140/154	136/140(13)	140/150(6)	136/154(13)	140/140(3)	150/154(5)	136/136	150/140	136/150	
D	CL168	160/180	175/180(13)	160/175(15)	165/180(5)	160/165(6)	160/160(1)	175/165	175/160	175/165	
	CL3354	220/240	220/235(14)	230/240(7)	255/240(2)	220/225(8)	220/245(9)	235/255	235/245	230/225	
	CL327	150/180	145/150(14)	160/180(6)	145/180(15)	150/160(1)	180/180(4)	145/160	145/160	160/180	
E	CL3354	260/270	250/260(29)	260/263(10)	260/265(1)			250/263	250/265		
	CL904	210/230	205/230(2)	200/210(4)	200/230(26)	205/210(4)	210/220(4)	200/220	205/200		
	CL327	140/160	135/140(24)	140/145(8)	135/160(4)	140/150(4)		135/135	145/150		
F	CL168	150/160	140/150(15)	140/160(8)	145/150(9)	150/180(7)	160/180(1)	140/180	145/145	140/145	
	CL3354	240/250	240/250(26)	240/240(1)	240/250(1)	250/260(10)	240/260(2)	250/260	240/250	240/260	
	CL904	220/230	220/230(9)	215/230(15)	210/230(9)	230/230(7)		215/210	230/215	230/210	
G	CL168	160/150	160/170(5)	140/160(20)	160/160(2)	150/160(4)	130/160(9)	170/160	170/150	150/130	130/140
	CL3354	220/250	240/250(16)	225/250(1)	220/240(12)	220/225(10)	220/250(1)	240/220	240/225	225/220	250/240
	CL904	260/280	250/280(7)	250/260(14)	260/270(15)	240/260(1)	260/280(2)	250/270	240/250	240/270	280/270

Notes: The numbers in the brackets represent number of offspring.

for genetic diversity but also increases the possibility of offspring survival (Mann et al. 1966; Jennions and Petrie 2000). Female *Euprymna tasmanica* Pfeffer, 1884 that mated with different males had larger eggs than those that mated with one male, indicating that females may obtain nourishment from the seminal fluid of several males (Squires et al. 2012). Male cephalopods exhibit "flushing behavior" in which they remove fresh spermatangia from previous males (Hanlon et al. 1999). In *Sepia esculenta* Hoyle, 1885, the males remove sperm by using the hectocotylus instead of flushing water (Wada et al. 2005). The males in this study also exhibited such behavior, flushing the buccal area of the female with water, when mating with a previously mated female.

Microsatellite markers are particularly useful in paternity studies because of their polymorphism, codominance, and repeatability. Cephalopod biologists have determined multiple paternity in many species, including squid (van Camp et al. 2004; Shaw and Sauer 2004; Iwata et al. 2005), and *Graneledone boreopacifica* Nesis, 1982 (Voight and Feldheim 2009). In this study, at least three paternal allele genotypes were found in all seven clutches indicating that at least two males were responsible for each brood. This result was in accordance with that of Naud et al. (2004), where multiple paternity was also found in *Sepia apama*. Multiple paternity in *S. japonica* offspring indicates that sperm from different males must be mixed within the female's reproductive tract. These sperm deposited around the buccal mass were used differentially to fertilize eggs (Shaw and Sauer 2004; Walker et al. 2006), after a process of sperm competition (Hanlon et al. 1999; Hall and Hanlon 2002) or mediation by female choice (Eberhard 1996).

Despite the prevalence of multiple paternity in cephalopod species, these studies show widely differing incidences of multiple paternity. In our study, multiple paternity was demonstrated in all sampled clutches (100%). In *Sepia apama*, one-third of the females mated with multiple males and 67% of females' eggs had multiple sires (Naud et al. 2004). Several factors have been confirmed to be related to the variance in incidence of multiple paternity observed in cephalopod species, e.g., sperm allocation, mating systems, sperm competition, and female choice (Wada et al. 2005; Wada et al. 2010). Moreover, as suggested for the squid *Loligo bleekeri* by Iwata et al (2005), males who were the last to mate fertilized 85–100% eggs in four broods tested. However, in the multiple paternity study of *Loligo pealeii*, the mate order is not the most important factor in determining paternity (Naud et al. 2004; Buresch et al. 2009); however, no clear hypothesis has yet emerged to explain which factor is essential in the multiple paternity of *S. japonica*. Further work should be carried out to understand paternity patterns and to investigate different factors affecting multiple paternity in this species.

Acknowledgements

References

Balloux F, Lehmann L (2003) Random mating with a finite number of matings. Genetics 165: 2313–2315.

Brown RC, Woolliams JA, McAndrew BJ (2005) Factors influencing effective population size in commercial populations of gilthead seabream, *Sparus aurata*. Aquaculture 247: 219–225. https://doi.org/10.1016/j.aquaculture.2005.02.002

Buresch KM, Hanlon RT, Maxwell MR, Ring S (2001) Microsatellite DNA markers indicate a high frequency of multiple paternity within individual field-collected egg capsules of the squid *Loligo pealeii*. Marine Ecology Progress Series 210: 161–165. https://doi.org/10.3354/meps210161

Buresch KC, Maxwell MR, Cox MR, Hanlon RT (2009) Temporal Dynamics of Mating and Paternity in the Squid *Loligo Pealeii*. Marine Ecology Progress Series 387: 197–203. https://doi.org/10.3354/meps08052

Davy CM, Edwards T, Lathrop A, Bratton M, Hagan M, Henen B, Nagy KA, Stone J, Scott Hillard L, Murphy RW (2011) Polyandry and multiple paternities in the threatened Agassiz's desert tortoise, *Gopherus agassizii*. Conservation Genetics 12: 1313–1322. https://doi.org/10.1007/s10592-011-0232-y

Eberhard WG (1996) Female Control: Sexual Selection by Cryptic Female Choice. Princeton University Press, New York, 501 pp.

Fitzsimmons NN (1998) Single paternity of clutches and sperm storage in the promiscuous green turtle (*Chelonia mydas*). Molecular Ecology 7: 575–584. https://doi.org/10.1046/j.1365-294x.1998.00355.x

Hall K, Hanlon R (2002) Principal Features of the Mating System of a Large Spawning Aggregation of the Giant Australian Cuttlefish *Sepia Apama* (Mollusca: Cephalopoda). Marine Biology 140: 533–545. https://doi.org/10.1007/s00227-001-0718-0

Hanlon RT, Ament SA, Gabr H (1999) Behavioral aspects of sperm competition in cuttlefish, *Sepia officinalis* (Sepioidea: Cephalopoda). Marine Biology 134: 719–728. https://doi.org/10.1007/s002270050588

Hoekert WEJ, Neufe´glise H, Schouten AD, Menken SBJ (2002) Multiple paternity and female-biased mutation at a microsatellite locus in the Olive Ridley sea turtle (*Lepidochelys olivacea*). Heredity 89: 107–113. https://doi.org/10.1038/sj.hdy.6800103

Iwata Y, Munehara H, Sakurail Y (2005) Dependence of Paternity rates on alternative reproductive behaviors in the squid *Loligo bleekeri*. Marine Ecology Progress Series 298: 219–228. https://doi.org/10.3354/meps298219

Jarne P, Lagoda PJL (1996) Microsatellites, from molecules to populations and back. Trends. Ecology Evolution 11: 424–429. https://doi.org/10.1016/0169-5347(96)10049-5

Jennions, MD, Petrie M (2000) Why Do Females Mate Multiply? a Review of the Genetic Benefits. Biological Reviews 75: 21–64. https://doi.org/10.1017/S0006323199005423

Jiang LH, Zhu AY, Wu CW, Su YQ, Zhang JS, Dong ZY (2014) Tetracycline Immersion tagging of cuttlefish, *Sepiella japonica*, larvae. Journal of the Word Aquaculture Society 45: 342–349. https://doi.org/10.1111/jwas.12116

Jones AG (2005) GERUD 2.0: a computer program for the reconstruction of parental genotypes from half-sib progeny arrays with known or unknown parents. Molecular Ecology Notes 5: 708–711. https://doi.org/10.1111/j.1471-8286.2005.01029.x

Laloi D, Richard M, Lecomte J, Massotm M, Clobert J (2004) Multiple paternity in clutches of common lizard *Lacerta vivipara*: data from microsatellite markers. Molecular Ecology 13: 719–723. https://doi.org/10.1046/j.1365-294X.2004.02102.x

Liu Y D (2002) General Situation of Fisheries Development in Cape Verde. Chinese Fisheries Economics 2: 1–50.

Lü Z M, Hou L, Gong L, Liu LQ, Chen YJ, Guo BY, Dong YH, Wu CW (2017) Isolation and analysis on Est microsatellites of *Sepiella japonica* by novo high-throughput transcriptome sequencing. Oceanologia et Limnologia Sinica 48: 877–883.

Mann T, Martin AW, Thiersch JB (1966) Spermatophores and Spermatophoric Reaction in the Giant Octopus of the North Pacific, *Octopus Dofleini Martini*. Nature 211: 1279–1282. https://doi.org/10.1038/2111279a0

Marshall TC, Slate J, Kruuk LEB, Pemberton JM (1998) Statistical confidence for likelihood-based paternity inference in natural populations. Molecular Ecology 7: 639–655. https://doi.org/10.1046/j.1365-294x.1998.00374.x

Naud MJ, Shaw PW, Hanlon RT, Havenhand JN (2005) Evidence for biased use of sperm sources in wild female giant cuttlefish (*Sepia apama*). Proceedings of the Royal Society B 72: 1047–1051. https://doi.org/10.1098/rspb.2004.3031

Naud MJ, Hanlon RT, Hall KC, Shaw PW, Havenhand JN (2004) Behavioural and Genetic Assessment of Reproductive Success in a Spawning aggregation of the Australian Giant Cuttlefish, *Sepia apama*. Animal Behaviour 67: 1043–1050. https://doi.org/10.1016/j.anbehav.2003.10.005

Olsson M, Gullberg A, Tegelströ H (1994) Sperm competition in the sand lizard, *Lacerta agilis*. Animal Behaviour 48: 193–200. https://doi.org/10.1006/anbe.1994.1226

Pearse DE, Anderson EC (2009) Multiple paternity increases effective population size. Molecular Ecology 18: 3124–3127. https://doi.org/10.1111/j.1365-294X.2009.04268.x

Quinteiro J, Baibai T, Oukhattar L, Soukri A, Seixas P, Rey-Mendez M (2011) Multiple paternity in the common octopus *Octopus vulgaris* (Cuvier, 1797), as revealed by microsatellite DNA analysis. Molluscan Research 31: 15–20. https://doi.org/10.1007/s10750-017-3399-5

Ross KG (2001) Molecular ecology of social behavior: analyses of breeding systems and genetic structure. Molecular Ecology 10: 265–284. https://doi.org/10.1046/j.1365-294x.2001.01191.x

Shaw PW, Sauer WHH (2004) Multiple Paternity and Complex Fertilisation Dynamics in the Squid *Loligo Vulgaris* Reynaudii. Marine Ecology Progress Series 270: 173–179. https://doi.org/10.3354/meps08052

Song WW, Wang CL (2009) Genetic diversity of *Sepiella maindroni* in cultured and natural population. Oceanologia et Limnologia Sinica 40: 590–595.

Squires ZE, Wong BBM, Norman MD, Stuart-Fox D (2012) Multiple Fitness Benefits of Polyandry in a Cephalopod. PLoS ONE 7: e37074. https://doi.org/10.1371/journal.pone.0037074

Sugg DW, Chesser RK (1994) Effective Population Sizes with Multiple Paternity. Genetics 137: 1147–1155.

Takagi M, Sakai K, Taniguchi N (2008) Direct evidence of multiple paternities in natural population of viviparous Japanese surfperch by allelic markers of microsatellite DNA loci. Fisheries Science 74: 976–982. https://doi.org/10.1111/j.1444-2906.2008.01615.x

Towner P (1991) Purification of DNA. Essential molecular biology: a practical approach. In: Brown TA (Ed.) The Practical Approach Series, vol. 1. Oxford University Press, Oxford, 47–68.

Voight JR, Feldheim KA (2009) Microsatellite inheritance and multiple paternity in the deep-sea octopus *Graneledone boreopacifica* (Mollusca: Cephalopoda). Invertebrate Biology 128: 26–30. https://doi.org/10.1111/j.1744-7410.2008.00152.x

Van Camp LM, Donnellan SC, Dyer AR, Fairweather PG (2004) Multiple Paternity in Field- and Captive-Laid Egg Strands of *Sepioteuthis Australis* (Cephalopoda: Loliginidae). Marine and Freshwater Research 55: 819–823. https://doi.org/10.1071/MF03179

Wada T, Takegaki T, Mori T, Natsukari Y (2006) Reproductive behavior of the Japanese spineless cuttlefish *Sepiella japonica*. Venus 65: 221–228.

Wada T, Takegaki T, Mori T, Natsukari Y (2010) Sperm Removal, Ejaculation and Their Behavioural Interaction in Male Cuttlefish in Response to Female Mating History. Animal Behaviour 79: 613–619. https://doi.org/10.1016/j.anbehav.2009.12.004

Wada T, Takegaki T, Mori T (2005) Sperm Displacement Behavior of the Cuttlefish *Sepia Esculenta* (Cephalopoda: Sepiidae). Journal of Ethology 23: 85–92. https://doi.org/10.1007/s10164-005-0146-6

Walker D, Power AJ, Sweeney-Reeves MJ, Avise JC (2006) Multiple paternity and female sperm usage along egg-case strings of the knobbed whelk, *Busycon carica* (Mollusca; Melongenidae). Marine Biology 151: 53–61. https://doi.org/10.1007/s00227-006-0463-5

Wu CW, Chi CF, He GY, Lü ZM, Xu MY (2010) Isolation via enrichment and characterization of ten polymorphic microsatellite loci in the cuttlefish, *Sepiella maindroni* de Rochebruns. Acta Oceanologica Sinica 29: 121–124. https://doi.org/10.1007/s13131-010-0083-2

Xu MY, Ye YY, Guo BY, Qi PZ, Wu CW (2011) Optimization of the ISSR system for *Sepiella maindroni* and genetic diversity of the cultured population. Oceanologia et Limnologia Sinica 42: 538–542.

Yin F, Sun P, Peng SM, Tang BJ, Zhang D, Wang CL, Mu CK, Shi ZH (2013) The respiration, excretion and biochemical response of the juvenile common Chinese cuttlefish, *Sepiella maindroni* at different temperatures. Aquaculture 402: 127–132. https://doi.org/10.1016/j.aquaculture.2013.03.018

RESEARCH ARTICLE

Sperm ultrastructure of *Pochazia shantungensis* (Chou & Lu) and *Ricania speculum* (Walker) (Hemiptera, Ricaniidae) with phylogenetic implications

Zhen Jiang[1], Jianing Liu[1], Daozheng Qin[1]

1 *Key Laboratory of Plant Protection Resources and Pest Management of the Ministry of Education, Entomological Museum, Northwest A&F University, Yangling, Shaanxi 712100, China*

Corresponding author: *Daozheng Qin* (qindaozh@nwsuaf.edu.cn)

Abstract

The sperm ultrastructure of two ricaniid species, *Pochazia shantungensis* (Chou & Lu) and *Ricania speculum* (Walker), was investigated using light and transmission electron microscopy. Both species have monoflagellate sperm, the shape and ultrastructure of the mature spermatozoon of these two species are similar in morphology, and 128 spermatozoa are organized into sperm bundles with their heads embedded in a homogenous matrix forming the spermatodesmata. The individual sperm is filiform and includes the head, neck and flagellum. The head is needle-like, with a bilayer acrosome and an inferior elongated nucleus which is formed of homogeneously compact and electron-dense chromatin. The neck region is indistinct and is comprised of the centriole and centriole adjunct with a homogeneous dense substance. The long flagellum has the typical 9 + 9 + 2 axoneme microtubule pattern and two symmetrical mitochondrial derivatives with an orderly array of cristae flanking both sides, and a pair of well-developed fishhook-shaped accessory bodies. Current evidence shows that ricaniid species have D-shaped mitochondrial derivatives in cross-section and a serrated electron-dense region. The phylogenetic relationship of Fulgoroidea with other superfamilies in Auchenorrhyncha is briefly discussed.

Keywords

Introduction

Spermatozoa are highly specialized male gametes in sexually reproductive animals, and are characterized by patterns of rapid and divergent morphological evolution (Birkhead et al. 2009). Comparative morphological and ultrastructural investigations of insect sperm not only contribute to better understanding of the interspecific morphological differences and provide additional characters for taxonomic analysis, but also may help elucidate phylogenies and the evolutionary history of the group (Jamieson 1987, Alves et al. 2006, Dallai et al. 2008, Araújo et al. 2009, 2010, 2011, Vitale et al. 2011, Dallai 2014).

Planthoppers (Fulgoroidea) are among the most dominant and diverse groups of phytophagous hemipterans with 13,600 species worldwide (Urban and Cryan 2007, Bourgoin 2019). Many species in this group are economically significant pests of major agricultural crops due to their high reproductive potential and capacity to transmit plant pathogens (Urban and Cryan 2007). Up to the present, studies on the sperm ultrastructure of planthoppers have addressed four species, including *Nilaparvata lugens* (Stål) and *Muellerianella fairmairei* Perris (in Delphacidae), *Ricania marginalis* (Walker) (in Ricaniidae) and *Cixius nervosus* Linnaeus (in Cixiidae) (Folliot and Maillet 1970, Dai et al. 1996, Tian et al. 2006). It was found that the acrosome complex of *Nilaparvata lugens* was a monolayer and branched-shaped structure and was wrapped by a membrane (Dai et al. 1996). Tian et al. (2006) revealed the axoneme in the sperm tail of *R. marginalis* (Fulgoroidea) consists of 9 + 9 + 2 microtubules. In addition, Soulier-Perkins and Bourgoin (1998) explored the copulatory mechanisms in Fulgoromorpha and found that sexual selection, three modes of deposition and sperm storage occurs within the Fulgoromorpha. Planthoppers transfer sperm directly or by using a spermatophore; transferred into the spermatheca at the bursa copulatrix ductus level within the bursa (Soulier-Perkins and Bourgoin 1998).

Ricaniidae is one of the larger families of the superfamily Fulgoroidea, currently containing 432 species in 64 genera (Bourgoin 2019). Members of this family are distributed widely in the Afrotropical, Australian, Indo-Malayan and Oceania regions, and primarily around the tropics. A few species are major agricultural pests (Bu and Liang 2011). Here we examined the fine morphology and ultrastructure of the sperm of two more ricaniid species, *Pochazia shantungensis* (Chou and Lu) and *Ricania speculum* (Walker) using light and transmission electron microscopy. This study aims to provide additional characters useful for comparison with other species in the family and provides additional foundations for future taxonomic and phylogenetic analyses of Fulgoroidea.

Materials and methods

Source of specimens

Adult males of *P. shantungensis* (Chou & Lu) and *R. speculum* (Walker) in Ricaniidae of the superfamily Fulgoroidea (Hemiptera, Fulgoromorpha) (Szwedo 2018) were used in this study. All samples were collected from shrub woodland on the campus of

Northwest A&F University, Shaanxi Province, China (34°15.60'N, 108°03.62'E, elev. 562 m) in the peak of the summer in 2016.

Light microscopy

To determine the total sizes of the spermatozoa of *P. shantungensis* and *R. speculum*, live adult males of these two species were selected. After rapid dissection under a binocular microscope (Motic SMZ-168, China) in a 0.9% physiological saline solution on an ice tray, sperm samples were spread freely before being extracted and mounted in glycerol using clean microscope slides with cover slips. Pictures were taken using a stereomicroscope (LEICA M205 A, Nussloch, Germany). The mean length of sperm and their heads were measured based on five individuals of each species and three sperm from each individual using the Leica Application Suite System Software.

Transmission electron microscopy (TEM)

Male adults of the two species were dissected in a 2.5% glutaraldehyde solution containing 3% sucrose in phosphate-buffered saline (PBS, 0.1 M, pH 7.2) to obtain the seminal vesicles. The seminal vesicles were then transferred immediately into cold fixative solution at 4 °C overnight. After rinsing with PBS (0.1 M, pH 7.2) for 5, 10, 15, and 20 min, respectively, and 30 min twice thereafter, the samples were post-fixed in 1% osmium tetroxide (in 0.1 M PBS, pH 7.2) at 4 °C for 1.5 h and were then rinsed again with PBS in the same procedure noted above.

Samples were dehydrated in a series of ethanol solutions (30%, 50%, 70%, 80%, and 90% for 15 min and 100% for 20 min twice) and infiltrated overnight in a mixture of LR-White resin (London Resin Company, Reading, U.K.) and alcohol (1:1) followed by infiltration with pure LR-White resin twice (for 4 h and 8 h, respectively) at room temperature. The samples were then incubated at 60 °C for 48 h.

Ultrathin sections (70 nm) were cut with a diamond knife on the Leica EM UC7 ultramicrotome (Leica, Nussloch, Germany), floated with 3% aqueous solution of uranyl acetate for 10–15 min, and refloated with 4% lead citrate solution for 8–10 min. All samples were examined under JEM-1230 transmission electron microscope (JEOL, Tokyo, Japan) or a Hitachi HT7700 transmission electron microscope (Hitachi, Tokyo, Japan) at 80 kV.

Results

Pochazia shantungensis (Chou & Lu, 1977)

Description. The mature spermatozoa of *P. shantungensis* are held together (totally 128 spermatozoa per spermatodesm) in the form of coiled sperm bundles in the seminal

vesicles. Anterior ends of heads are embedded in a homogenous matrix that forms the spermatodesmata (Fig. 1A, B, D). The spermatozoon is long and filiform when it is separated from the bundles and exposed to a 0.9% saline solution (Fig. 1C). It is approximately 127 μm in mean length and has an elongate single head (about 16 μm) and a conventional single flagellum (about 111 μm).

The head is formed by the nucleus and the acrosome. The acrosome has an irregular saccular acrosomal vesicle and a perforatorium, both located anterior to the nucleus (Figs 1E, 2A, B, 3A, B). Between the base of the perforatorium and the anterior portion of the nucleus is a noticeable transition (Figs 1E, 2B, 3C–E). The acrosome gradually invaginates posteriorly to form a subacrosomal space in which the anterior part of the elongated nucleus is inserted (Figs 2B, 3C, D). The nuclei, different in shape (Figs 2B, 3B–N), are full of homogeneous condensed chromatin and are separated from each other by a cell membrane (Fig. 1D). The ovoid nucleus measures approximately 0.94 μm in diameter in cross-section; in longitudinal-section, it turns into a cylinder-shape (Fig. 2A, B).

The nucleus-flagellum transition region has a centriole and centriolar adjunct (Fig. 2B, C). The centriole starts near the terminal incurvation of the nucleus and terminates anterior of the axoneme (Fig. 2B, C); it is parallel to the moderately electron-dense centriole adjunct (Fig. 2B). The centriole adjunct contains dense granules between the accessory bodies and mitochondrial derivatives in longitudinal profile (Fig. 2B, C); in cross-section the centriole adjunct arises near the end of the nucleus and terminates anterior to the mitochondrial derivatives (Fig. 3I–K). The nucleus is wrapped by the centriolar adjunct (Figs 2B, C, 3I–M). In several transverse profiles of spermatozoa, the posterior nucleus region overlaps the different regions of accessory bodies and mitochondrial derivatives (Fig. 3G–L).

The flagellum region contains an axoneme, two mitochondrial derivatives and two accessory bodies (Fig. 4A–D); they are parallel to each other throughout most of the length of the flagellum (Fig. 2B–D). The axoneme arises from the centriole (Fig. 2C). It is composed of two innermost microtubules, nine outermost accessory microtubules, and nine doublets, showing the typical 9 + 9 + 2 microtubules arrangement in insects (Fig. 4D, G). The mitochondrial derivatives and accessory bodies are symmetrical in size and diameter in cross-section (Fig. 4A–D). Each mitochondrial derivative is made up of one serrated electron-dense area, one small oval electron-lucid portion and one mitochondrial cristae region (Fig. 4C). In longitudinal-section, the mitochondrial derivatives are positioned lateral to the axoneme and are initiated near the extreme base of the centriole adjunct (Fig. 2B–D). The cristae are perpendicular to the longitudinal axis, bearing regular intervals (42 nm) between adjacent derivatives (Fig. 2E). The accessory bodies are fishhook-shaped; they originate from the centriolar adjunct between the axoneme and mitochondrial derivatives (Fig. 4B–D).

Close to the posterior sperm tip, the axoneme becomes disorganized step by step, and the accessory bodies gradually taper to a cone-shape, while the mitochondrial derivatives disappear (Fig. 4E, F). At the terminal region of the flagellum, the doublet microtubules are the last to disappear (Fig. 4H).
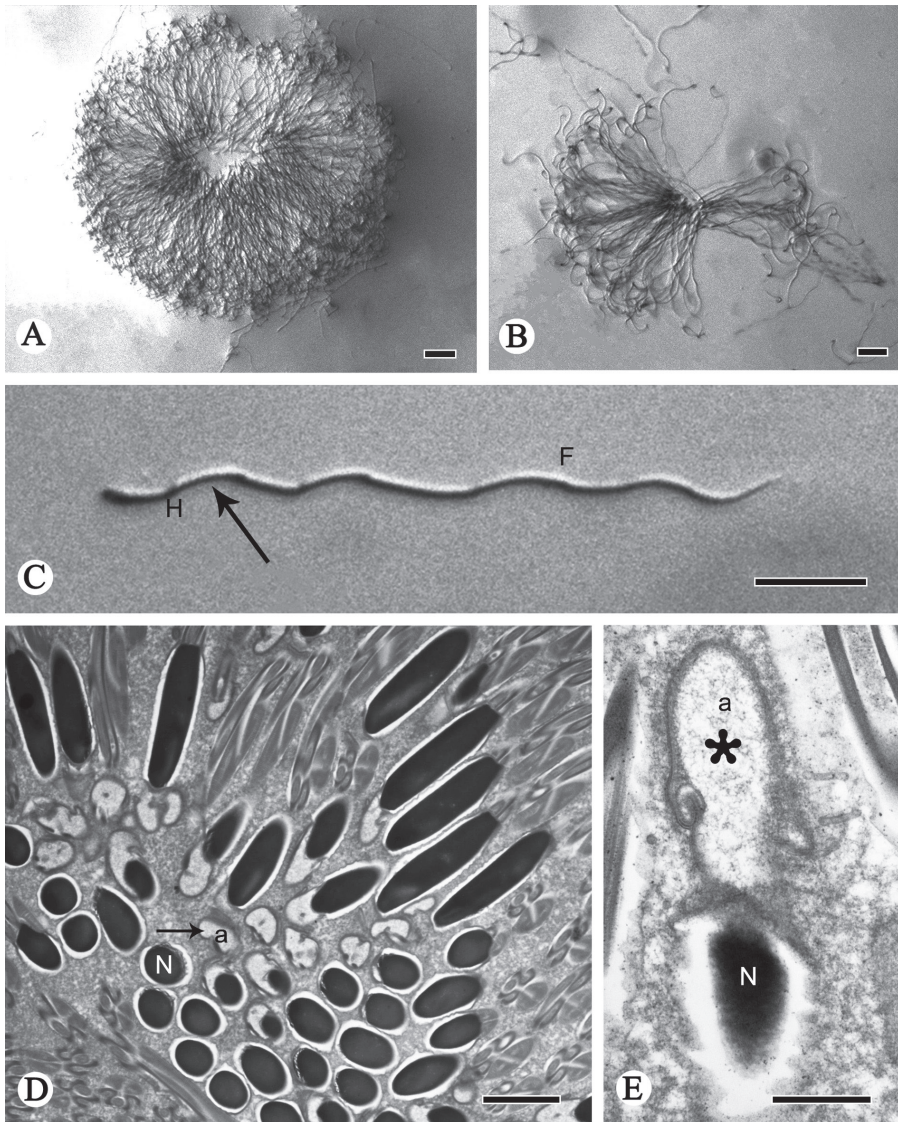
Figure 1. TEM and light micrographs of spermatozoa and spermatodesms of *P. shantungensis*. **A, B** Light micrographs of spermatodesm and spermatozoa **C** light micrograph of a single spermatozoon with the head (**H**, arrow) and wavy flagellum (**F**) **D, E** TEM micrographs of cross-sections of spermatozoa, showing the acrosome (**a**) and nucleus (**N**). Arrow shows head cluster, asterisk indicates the acrosome. Scale bars: 20 μm (**A–C**); 2 μm (**D**); 0.5μm (**E**).

Ricania speculum (Walker, 1851)

Description. Mature spermatozoa of *R. speculum* are similar to those of *P. shantungensis* in morphology insofar as they also have a number of spermatozoa (totally 128 spermatozoa per spermatodesm) organized into sperm bundles with their heads embedded
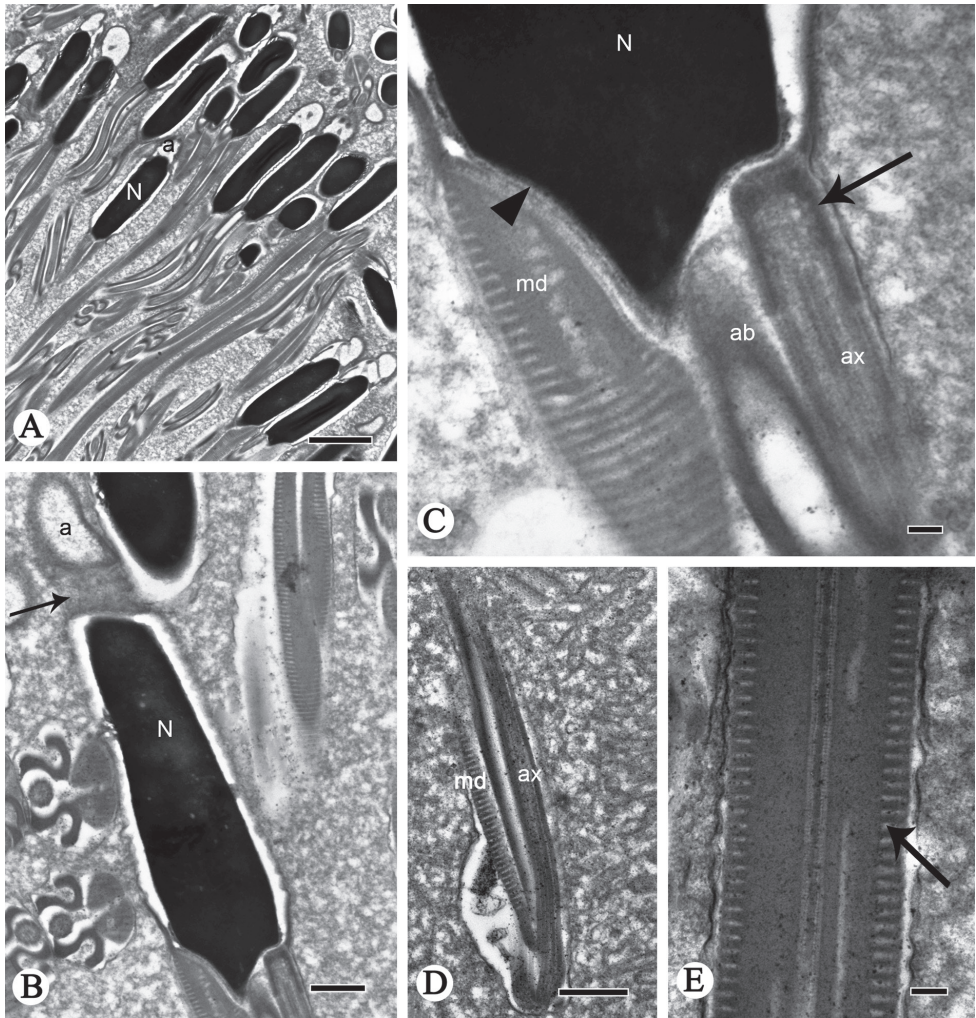
Figure 2. Longitudinal sections of spermatozoa of *P. shantungensis*. **A, B** Spermatozoa, showing acrosome (**a**), nucleus (**N**), arrow indicates connection area between acrosome and nucleus **C** nucleus-flagellum transition, showing nucleus (**N**), mitochondrial derivatives (**md**), accessory body (**ab**), axoneme (**ax**), arrow indicates centriole, triangular arrowhead indicates centriolar adjunct **D, E** flagella of sperm, showing axoneme (**ax**), mitochondrial derivatives (**md**) and cristae (arrow). Scale bars: 2 μm (**A**); 0.5 μm (**B, D**); 0.1 μm (**C, E**).

in a homogenous matrix (Fig. 5A, C–D). The individual sperm is filiform, measuring 196 μm in average length (Fig. 5B), with a linear head and distinct flagellum, approximately 24 μm and 172 μm in length, respectively.

The sperm head of *R. speculum* is elongated and filiform, formed by a short acrosome and an elongated nucleus (Figs 5B, 6B). The conical acrosome contains a dothideoid acrosomal vesicle and perforatorium with the latter made of electron-dense fiber
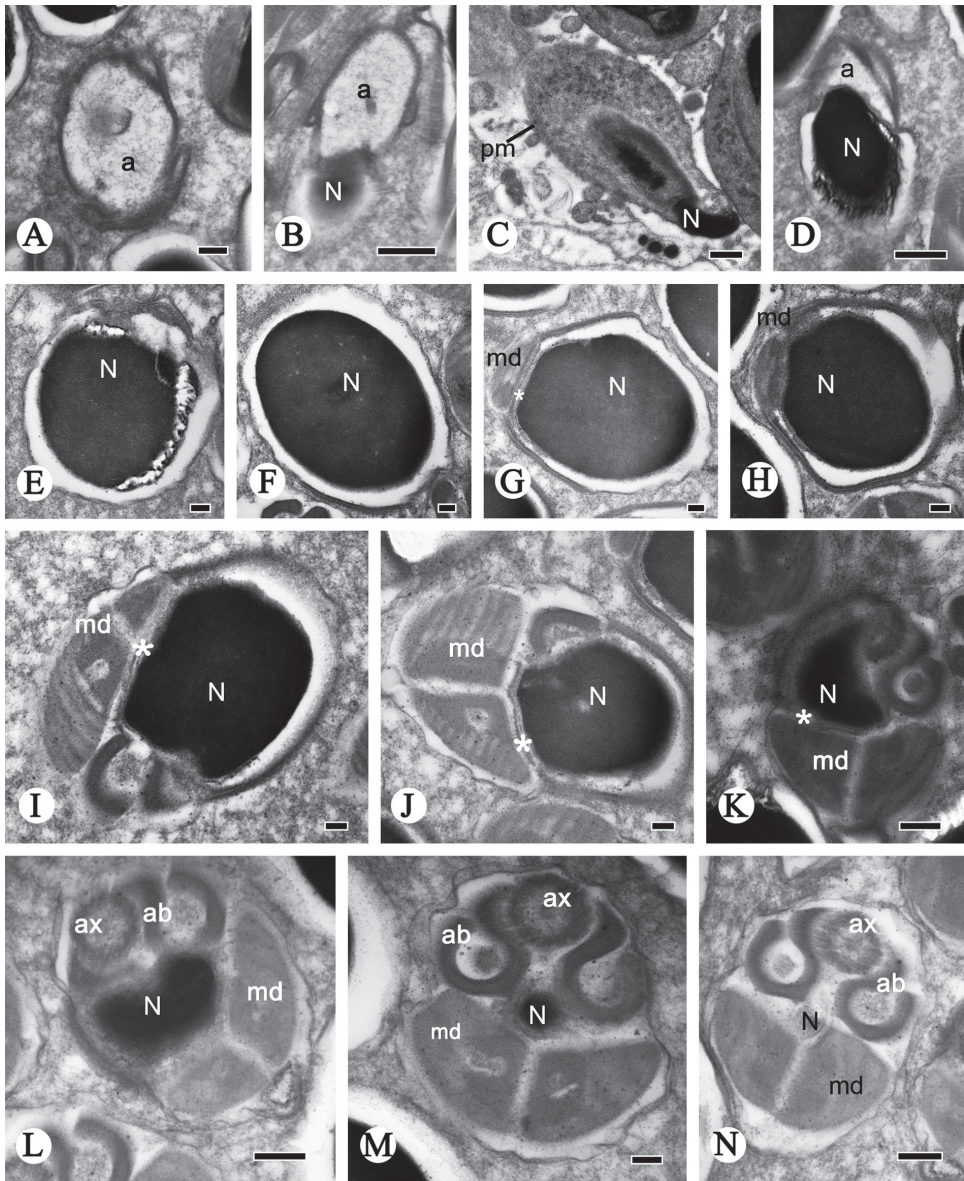
Figure 3. Cross-sections of spermatozoa of *P. shantungensis*. **A** Acrosome, showing the dothideoid acrosome **B–E** serial cross-sections of head showing the dothideoid acrosome (**a**), the nucleus (**N**), and the plasma membrane (**pm**) **F** oval nucleus (**N**) **G–N** nucleus-flagellum transition region, showing the nucleus (**N**), mitochondrial derivatives (**md**), accessory bodies (**ab**), axoneme (**ax**). The asterisk indicates the centriolar adjunct (**ca**). Scale bars: 0.5 µm (**B–D**); 0.2 µm (**A, K, L, N**); 0.1 µm (**E–J, M**).

substructures (Fig. 6B). A transition region is visible between the acrosome and the anterior portion of the nucleus (Fig. 6B). Anteriorly the nucleus is surrounded by the acrosome which is filled with numerous fibrous substructures; posteriorly it increases
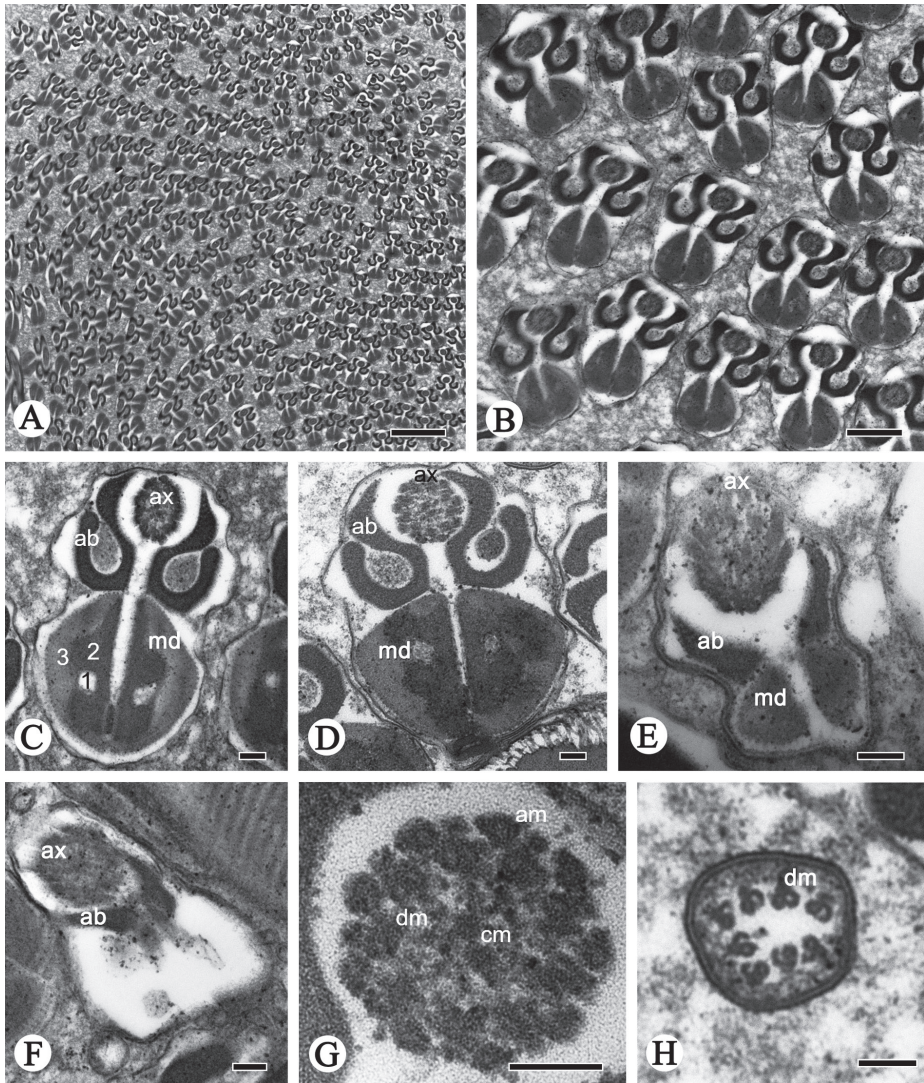
Figure 4. Cross-sections of the sperm flagellum of *P. shantungensis*. **A–D** Flagella, showing axoneme (**ax**), fishhook-shaped accessory bodies (**ab**), D-shaped mitochondrial derivatives (**md**), containing oval lucent region (**1**), serrated electron-dense region (**2**) and mitochondrial cristae region (**3**) **E–F** flagellum, mitochondrial derivatives slowly disappear, axonemes (**ax**) become disordered, accessory bodies (**ab**) become smaller **G** axoneme, showing the typical 9 + 9 + 2 pattern, nine outermost accessory microtubules (**am**), nine doublet microtubules (**dm**) and two innermost central microtubules (**cm**) **H** Showing doublet microtubules finally disappearing. Scale bars: 2 μm (**A**); 0.5 μm (**B**); 0.1 μm (**C–H**).

in diameter and changes from a mushroom-shape to a meniscus shape and finally to an oval-shape (Fig. 7B–D). The nucleus, approximately 0.99 μm in diameter, is filled with compact chromatin and takes on different shapes (Figs 6C, 7B–I).

In the nucleus-flagellum transition region, the centriole and centriolar adjunct that lie next to the nucleus are abrupt (Fig. 6A, C). The centriole is formed by dense
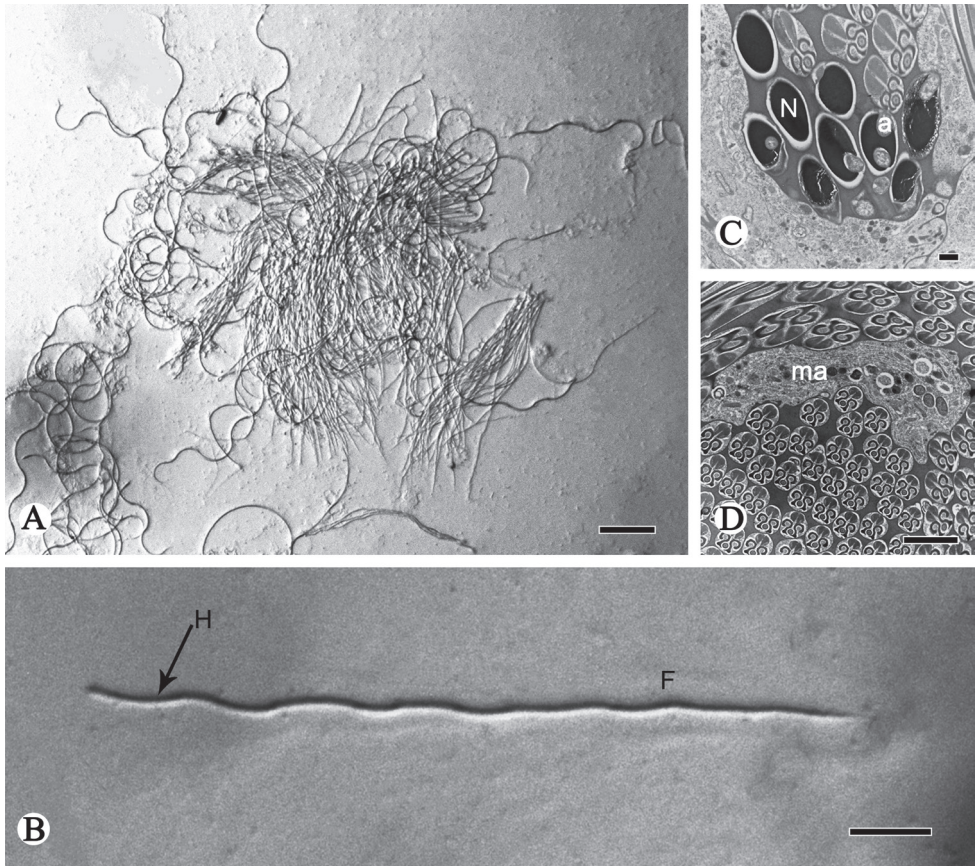
Figure 5. TEM and light micrographs of spermatozoon and spermatodesms of *R. speculum*. **A** Light micrograph of spermatodesm **B** light micrograph of spermatozoon with the head (**H**, arrow) and flagellum (**F**) **C, D** cross-sections of the oval nucleus (**N**), showing the acrosome (**a**) and homogenous matrix (**ma**). Scale bars: 50 μm (**A**); 20 μm (**B**); 0.5 μm (**C**); 2 μm (**D**).

microtubules that originate from the end of the pyknotic nucleus and end above the front of the axoneme (Figs 6B, 7G–H). The centriolar adjunct is composed of moderate electron-dense substances, connecting mitochondrial derivatives with the nucleus (Figs 6B, 7E–I).

The cross-section of the flagellum region consists of an axoneme, two symmetrical accessory bodies and two mitochondrial derivatives (Fig. 8A, B). The axoneme of the flagellum of *R. speculum* has a typical 9 + 9 + 2 microtubule pattern, comprised of two central microtubules, nine inner doublet microtubules and nine outermost single accessory microtubules (Fig. 8C). The mitochondrial derivatives have evident parallel cristae arranged in the periphery and are formed by three different portions: a serrated electron-dense region, a central clear area and a mitochondrial cristae region (Fig. 8B). The cristae are perpendicular to the axis of the derivatives and are at regular intervals (about 46 nm) between adjacent derivatives (Fig. 6D). Between the axoneme and the mitochondrial derivatives are large, fishhook-shaped accessory bodies (Fig. 8A, B);
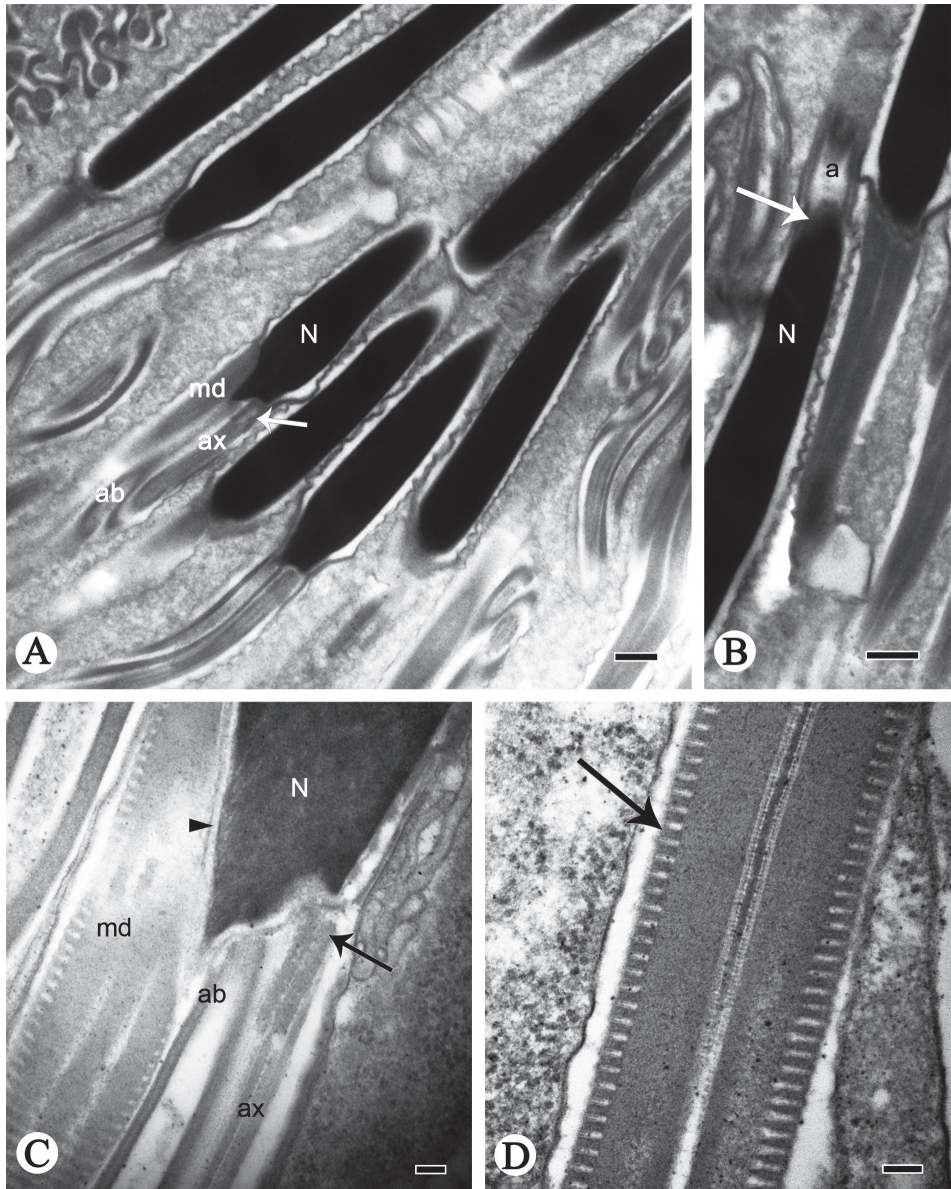
Figure 6. Longitudinal sections of spermatozoa of *R. speculum*. **A, B** Acrosome (**a**), nucleus (**N**), axoneme (**ax**), accessory bodies (**ab**) and mitochondrial derivatives (**md**), arrow indicates acrosome and nucleus connection area **C** nucleus-flagellum transition, showing nucleus (**N**), mitochondrial derivatives (**md**), accessory bodies (**ab**), axoneme (**ax**), arrow indicates centriole, triangular arrowhead indicates centriolar adjunct **D** sperm flagellum, showing cristae (arrow) arranged in mitochondrial derivatives (**md**). Scale bars: 0.5 µm (**A, B**); 0.1 µm (**C, D**).

they are composed of electron-dense material (Fig. 8B). Close to the posterior sperm tip, the mitochondrial derivative is first to end (Fig. 8E), followed by the accessory bodies, while the axoneme gradually becomes disorganized (Fig. 8B, D–F).
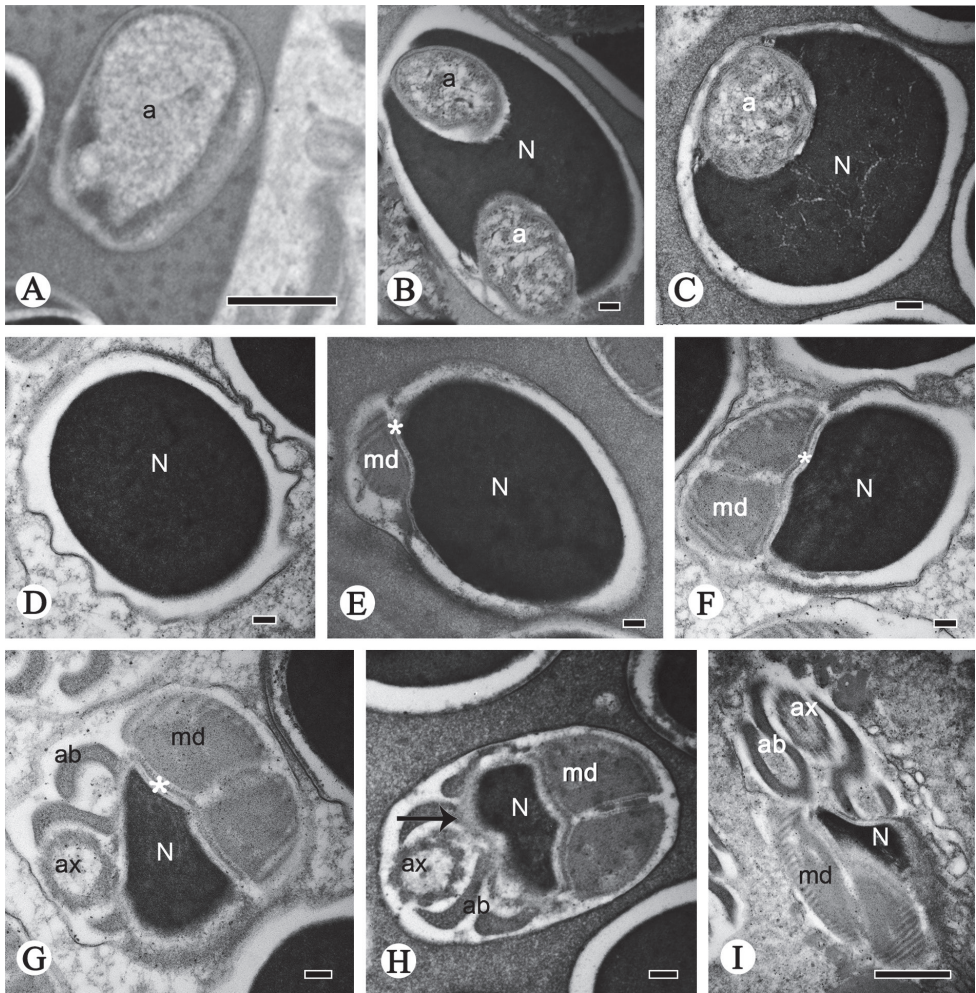
Figure 7. Cross-sections of spermatozoa of *R. speculum*. **A** Showing acrosome (**a**) **B, C** transition region between the acrosome (**a**) and nucleus (**N**), showing acrosome (**a**) on both sides of the nucleus (**N**), until it locates on just the one side of nucleus (**N**) **D** oval nucleus (**N**) **E–I** nucleus-flagellum transition region, showing the nucleus (**N**), mitochondrial derivatives (**md**), accessory bodies (**ab**), axoneme (**ax**), the asterisk indicates the centriolar adjunct (**ca**) and the arrow indicates the centriole (**c**). Scale bars: 0.5 μm (**A, I**); 0.1 μm (**B–H**).

Discussion

This study shows that the mature spermatozoa of these two ricaniid species are similar in quantity and morphology. Both are monoflagellate sperm and both have a straight and needle-like head, an inconspicuous neck, and the conventional long and sinuate flagellum. This study also reveals that *P. shantungensis* and *R. speculum* both have D-shaped mitochondrial derivatives with three particular regions (a serrated electro-dense region, an oval lucent area and mitochondrial cristae region) (Figs 4C, 8B), similar to the previous investigations in other ricaniid species, *Ricania marginalis* (Walker, 1851) and *Euricania clara* Kato, 1932 (Tian et al. 2006, Jiang and Qin 2018). However,
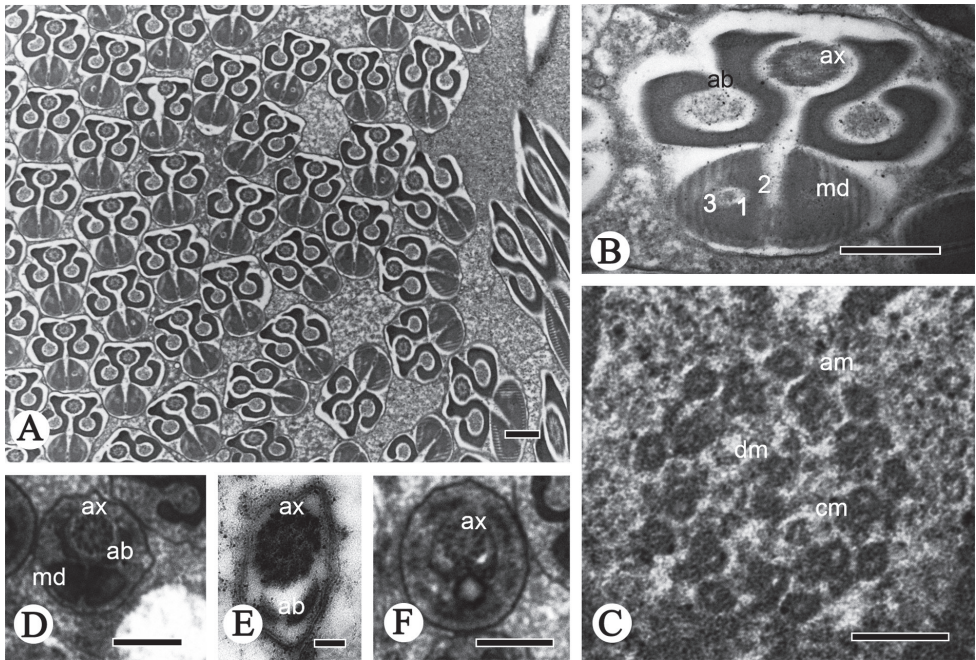
Figure 8. Cross-sections of the sperm flagellum of *R. speculum*. **A, B** Flagella, showing the axoneme (**ax**), accessory bodies (**ab**) and mitochondrial derivatives (**md**) including oval electron-lucid portion (**1**), an electron-dense region (**2**), and one mitochondrial cristae region (**3**) **C** axoneme, showing the typical 9 + 9 + 2 pattern, nine outermost accessory microtubules (**am**), a pair of central microtubules (**cm**), and doublet microtubules (**dm**) in between **D** flagellum, showing the axoneme (**ax**), accessory bodies (**ab**) and mitochondrial derivatives (**md**) **E–F** flagellum without mitochondrial derivatives (**md**). Scale bars: 0.5 μm (**A, B, D, F**); 0.1 μm (**C, E**).

there are several differences between *P. shantungensis* and *R. speculum*. For example, the length of the sperm of *P. shantungensis* (about 127 μm) is shorter than in *R. speculum* (about 196 μm). The acrosome of the sperm is cap-shaped in longitudinal-section in *P. shantungensis* (Fig. 2B) but cylindrical in *R. speculum* (Fig. 6B). These differences may provide additional morphological evidence for species recognition in Ricaniidae.

The number, size and cross-sectional shape of mitochondrial derivatives are different in different insect groups (Phillips 1970, Dallai et al. 1995, Lino-Neto and Dolder 2001, Gracielle et al. 2009, Mancini et al. 2009, Gottardo et al. 2012, Dias et al. 2013, Zhang et al. 2016). For most Sternorrhyncha species, individualised sperm is stored in the seminal vesicle. The spermatozoon flagellum is formed by an axoneme, a 9 + 9 + 2 axoneme microtubule, two accessory bodies and two mitochondrial derivatives (absent in Aleyrodoidea and Coccoidea) (Vitale et al. 2011, Labina et al. 2014, Barcellos et al. 2017). However, in Auchenorrhyncha, spermatozoa are aggregated into bundles in the seminal vesicle, intrude into a homogenous matrix to forming a spermatodesm. Current evidence also suggests that sperm structure in Cicadoidea, Cercopoidea, Cicadelloidea and Fulgoroidea have typical characteristics, viz. a cylindrical

and bilayer acrosome, a 9 + 9 + 2 axoneme microtubule pattern, two mitochondrial derivatives. Except Cicadoidea and Cercopoidea, other auchenorrhynchans have two accessory bodies (Folliot and Maillet 1970, Cruz-Landim and Kitajima 1972, Kubo-Irie et al. 2003, Chawanji et al. 2005, 2006, Araújo et al. 2010, Zhang and Dai 2012, Su et al. 2014, Zhang et al. 2016, Dallai et al. 2016). It seems that these two suborders (Cicadomorpha and Fulgoromorpha) have undergone different evolutionary routes, which lead to great changes in the axoneme of the flagellum.

Spermatodesmata were described as rope-like in Cicadoidea, Cicadelloidea and Fulgoroidea (Chawanji et al. 2005, Su et al. 2014, Jiang and Qin 2018), and ball-like in Membracoidea and Cercopoidea (Araújo et al. 2010, Zhang and Dai 2012, Hodgson et al. 2016) (Table 1). In Aphididae, Coccoidea and Psylloidea (Sternorrhyncha), spermatodesmata are elongate with the sperm aligned in one direction (Robison 1972, Vitale et al. 2011, Hodgson et al. 2016, Barcellos et al. 2017). It is possible that the rope-like spermatodesm of Cicadoidea, Cicadelloidea and Fulgoroidea could be plesiomorphic. In Coccoidea, spermatozoa transferred into the female tractus via bundles of spermatozoa (Robinson 1977). In Cicadomorpha, spermatozoa are not transferred free but connected to median rods forming spermatodesmes before being deposited into the female bursa copulatrix (Robertson and Gibbs 1937, Maillet 1959, Chevaillier 1962, Boulard 1965). The family Cercopidae exhibit a special spermatodesmata (type I) different from Cicadidae, Ledridae and Ulopidae (type II) (Soulier-Perkins and Bourgoin 1998). Because the anterior ends of the heads in Ricaniidae are embedded in a homogenous matrix that forms the spermatodesmata, it seems that the spermatozoa of Ricaniidae are very likely not free, but delivered in bundles in the female copulatory tractus using a spermatophore containing spermatozoa fixed in a spermatodesmata (type II).

Previous studies have shown that the mitochondrial derivatives of Psylloidea are asymmetric in diameter and filled by paracrystalline material (Gottardo et al. 2016). But they are symmetrical with two different regions, including a paracrystalline region and a less electron-dense region in Fulgoroidea (Cruz-Landim and Kitajima 1972, Chawanji et al. 2005, 2006, Zhang and Dai 2012, Su et al. 2014, Hodgson et al. 2016, Jiang and Qin 2018). This study found a pair of symmetrical accessory bodies in Ricaniidae, like those found in Aethalionidae (in Membracoidea) and Cicadellidae (Kubo-Irie et al. 2003, Araújo et al. 2010, Zhang and Dai 2012, Su et al. 2014, Zhang et al. 2016). In Aethalionidae, it has also three different regions (a clear, less electron-dense region, a dense area and a mitochondrial crista region) (Araújo et al. 2010). Because recent phylogenetic analyses

Table 1. The main characters of sperm in Auchenorrhyncha.

Taxa	Spermatodesmata	Accessory bodies	Axoneme microtubule	Spermatozoa
Cicadoidea	rope-like	0		
Cercopoidea	ball-like	0		aggregated into bundles, intrude into a homogenous matrix to form a spermatodesm
Membracoidea	ball-like	2	9 + 9 + 2	
Cicadelloidea	rope-like	2		
Fulgoroidea	rope-like	2		

support the major relationships as Fulgoroidea + (Membracoidea sister to Cicadoidea + Cercopoidea) (Cryan 2005, Johnson et al. 2018), if in Membracoidea the mitochondrial derivatives are 3-parted as in Ricaniidae, it is very probable that Cicadoidea, Cercopoidea and Cicadelloidea have the the apomorphic state, and Ricaniidae share a plesiomorphic state with Aethalionidae. Recent studies also show that ricaniid species have the D-shaped mitochondrial derivatives in cross-section and a serrated electron-dense region, the accessory body large and fishhook-shaped in cross-section, which is different from Aethalionidae and Cicadellidae (Kubo-Irie et al. 2003, Araújo et al. 2010, Zhang and Dai 2012, Su et al. 2014, Jiang and Qin 2018). We think it is probably a peculiar character and could be considered as synapomorphic of the species in this family. However, more spermatological evidence (especially the characters of mitochondrial derivatives and accessory bodies) would still be needed for phylogenetic analysis of Ricaniidae.

Acknowledgements

References

Alves L, Mancini K, Lino-Neto J, Dolder H (2006) Morphology of the male reproductive system and sperm ultrastructure of *Leucoptera coffeella* (Lepidoptera, Lyonetiidae). Acta Zoologica 87: 131–139. https://doi.org/10.1111/j.1463-6395.2006.00226.x

Araújo VA, Báo SN, Moreira J, Neves CA, Lino-Neto J (2010) Ultrastructural characterization of the spermatozoa of *Aethalion reticulatum* Linnaeus, 1767 (Hemiptera, Auchenorrhyncha, Aethalionidae). Micron 41: 306–311. https://doi.org/10.1016/j.micron.2009.12.001

Araújo VA, Lino-Neto J, Ramalho FDS, Zanuncio JC, Serrão JE (2011) Ultrastructure and heteromorphism of spermatozoa in five species of bugs (Pentatomidae, Heteroptera). Micron 42: 560–567. https://doi.org/10.1016/j.micron.2011.02.001

Araújo VA, Moreira J, Lino-Neto J (2009) Structure and ultrastructure of the spermatozoa of *Trypoxylon* (*Trypargilum*) *albitarse* Fabricius 1804 (Hymenoptera, Apoidea, Crabronidae). Micron 40: 719–723. https://doi.org/10.1016/j.micron.2009.05.003

Barcellos MS, Cossolin JFS, Dias G, Lino-Neto J (2017) Sperm morphology of the leafhopper *Diaphorina citri* Kuwayama (Hemiptera, Sternorrhyncha, Psylloidea, Liviidae). Micron 99: 49–55. https://doi.org/10.1016/j.micron.2017.03.017

Birkhead TR, Hosken DJ, Pitnick S (2009) Sperm Biology: An Evolutionary Perspective. Elsevier, London, 674 pp.

Boulard M (1965) L' apparel genital ectodermique des cigales femelles. Annales de la Société entomologique de France 1: 797–812.

Bourgoin T (2019) FLOW (Fulgoromorpha Lists on The Web): a world knowledge base dedicated to Fulgoromorpha. Version 8, updated 2019-02-10. http://hemiptera-databases.org/flow/ [accessed 11 February 2019]

Bu CP, Liang AP (2011) First record of the genus *Aprivesa* Melichar (Hemiptera, Fulgoromorpha) from south India, with description of one new species. ZooKeys 81: 1–12. https://doi.org/10.3897/zookeys.81.816

Chawanji AS, Hodgson AN, Villet MH (2005) Sperm morphology in four species of African platypleurine cicadas (Hemiptera, Cicadomorpha, Cicadidae). Tissue and Cell 37: 257–267. https://doi.org/10.1016/j.tice.2005.03.006

Chawanji AS, Hodgson AN, Villet MH (2006) Sperm morphology in five species of cicadettine cicadas (Hemiptera, Cicadomorpha, Cicadidae). Tissue and Cell 38: 373–388. https://doi.org/10.1016/j.tice.2006.08.006

Chevaillier P (1962) Cytologie-sur la génèse et la constitution histochimique du spermatodesme des Cercopidae (Homopt., Auch.). Compte Rendus de I' Académie des Sciences 254: 1148–1149.

Chou I, Lu CS (1977) On the Chinese Ricaniidae with descriptions of eight new species. Acta Entomologica Sinica 20(3): 314–322.

Cruz-Landim C, Kitajima EW (1972) Ultrastructure of mature spermatozoa of corn leafhopper *Dalbulus maidis* Del. and W. (Homoptera, Cicadellidae). Journal of Submicroscopic Cytology 4: 75–82.

Cryan JR (2005) Molecular phylogeny of Cicadomorpha (Insecta: Hemiptera: Cicadoidea, Cercopoidea and Membracoidea): adding evidence to the controversy. Systematic Entomology 30: 563–574. https://doi.org/10.1111/j.1365-3113.2004.00285.x

Dai HG, Song XL, Wu XY (1996) Ultrastructure of spermatozoa from the brown planthopper: *Nilaparvata lugens* Stål. Journal of Nanjing Agricultural University 19(2): 109–111.

Dallai R (2014) Overview on spermatogenesis and sperm structure of Hexapoda. Arthropod Structure and Development 43: 257–290. https://doi.org/10.1016/j.asd.2014.04.002

Dallai R, Gottardo M, Beutel RG (2016) Structure and evolution of insect sperm: New interpretations in the age of phylogenomics. Annual Review of Entomology 61: 1–23. https://doi.org/10.1146/annurev-ento-010715-023555

Dallai R, Lombardo BM, Mercati D, Vanin S, Lupetti P (2008) Sperm structure of Limoniidae and their phylogenetic relationship with Tipulidae (Diptera, Nematocera). Arthropod Structure and Development 37: 81–92. https://doi.org/10.1016/j.asd.2007.05.002

Dallai R, Lupetti P, Afzelius BA, Mamaev B (1995) Characteristics of the sperm flagellum in fungus gnats (Insecta, Diptera, Mycetophiloidea). Zoomorphology 115: 213–219. https://doi.org/10.1007/BF00393801

Dias G, Oliveira CM, Lino-Neto J (2013) Sperm morphology and phylogeny of lagriids (Coleoptera, Tenebrionidae). Arthropod Structure and Development 42: 379–384. https://doi.org/10.1016/j.asd.2013.04.002

Folliot R, Maillet PL (1970) Ultrastructure de la spermiogenèse et du spermatozoïde de divers insects Homoptères. In: Baccetti B (Ed.) Comparative Spermatology. Academic Press, New York, 289–300.

Gracielle IMS, Fiorillo BS, Lino-Neto J, Báo SN (2009) Morphology of the male reproductive system and spermiogenesis in *Hypanthidium foveolatum* (Alfken, 1930) (Hymenoptera, Apidae, Megachilinae). Micron 40: 419–425. https://doi.org/10.1016/j.micron.2009.02.003

Gottardo M, Dallai R, Mercati D, Hörnschemeyer T, Beutel RG (2016) The evolution of insect sperm – an unusual character system in a megadiverse group. Journal of Zoological Systematics and Evolutionary Research 54: 237–256. https://doi.org/10.1111/jzs.12136

Gottardo M, Mercati D, Dallai R (2012) The spermatogenesis and sperm structure of *Timema poppensis* (Insecta, Phasmatodea). Zoomorphology 131: 209–223. https://doi.org/10.1007/s00435-012-0158-z

Hodgson AN, Ridgeway JA, Villet MH (2016) Sperm ultrastructure and spermatodesm morphology of the spittle bug *Locris transversa* (Thunberg, 1822) (Hemiptera, Cercopidae). Invertebrate Reproduction and Development 60: 87–94. https://doi.org/10.1080/07924259.2016.1157104

Jamieson BGM (1987) The Ultrastructure and Phylogeny of Insect Spermatozoa. Cambridge University Press, 320 pp. https://doi.org/10.1086/415868

Jiang Z, Qin DZ (2018) Sperm ultrastructure of *Euricania clara* Kato (Hemiptera: Fulgoroidea: Ricaniidae). Acta Entomologica Sinica 61(2): 246–254.

Johnson KP, Dietrich CH, Friedrich F, Beutel RG, Wipfler B, Peters RS, Allen JM, Petersen M, Donath A, Walden KKO, Kozlov AM, Podsiadlowski L, Mayer C, Meusemann K, Vasilikopoulos A, Waterhouse RM, Cameron SL, Weirauch C, Swanson DR, Percy DM, Hardy NB, Terry I, Liu SL, Zhou X, Misof B, Robertson HM, Yoshizawa K (2018) Phylogenomics and the evolution of hemipteroid insects. Proceedings of the National Academy of Sciences of the United States of America: 1–6. https://doi.org/10.1073/pnas.1815820115

Kato M (1932) Notes on some Homoptera from south Manuchuria, collected by Mr. Yukimichi. Kontyû 5: 216–229.

Kubo-Irie M, Irie M, Nakazawa T, Mohri H (2003) Ultrastructure and function of long and short sperm in Cicadidae (Hemiptera). Journal of Insect Physiology 49: 983–991. https://doi.org/10.1016/S0022-1910(03)00161-6

Labina ES, Maryańska-Nadachowska A, Burckhardt D, Kuznetsova VG (2014) Variation in sperm formation patterns in jumping plant-lice (Hemiptera, Psylloidea): a light microscopic study. Folia Biologica 62: 321–333. https://doi.org/10.3409/fb62_4.321

Lino-Neto J, Dolder H (2001) Ultrastructural characteristics of the spermatozoa of Scelionidae (Hymenoptera, Platygastroidea) with phylogenetic considerations. Zoologica Scripta 30: 89–96. https://doi.org/10.1046/j.1463-6409.2001.00058.x

Maillet P (1959) Sur la reproduction des Homoptères (Auchénorhynques). Compte Rendus de I' Académie des Sciences 249: 1945–1946.

Mancini K, Lino-Neto J, Dolder H, Dallai R (2009) Sperm ultrastructure of the European hornet *Vespa crabro* (Linnaeus, 1758) (Hymenoptera, Vespidae). Arthropod Structure and Development 38: 54–59. https://doi.org/10.1016/j.asd.2008.07.001

Phillips DM (1970) Insect sperm: Their Structure and Morphogenesis. The Journal of Cell Biology 44: 243–277. https://doi.org/10.1083/jcb.44.2.243

Robertson A, Gibbs AJ (1937) Spermatogenesis and fertilization in Philaenus spumarius Fallen. Journal Tropical of Medicine and Hygiene 40: 257–262.

Robison WG (1972) Microtubular patterns in spermatozoa of coccid insects in relation to bending. The Journal of Cell Biology 52: 66–83. https://doi.org/10.1083/jcb.52.1.66

Robinson WG (1977) Ultrastructure of Coccoidea sperm. Research Division Bulletin Virginia Polytechnic Institute and State University 127: 35–50.

Soulier-Perkins A, Bourgoin T (1998) Copulatory mechanisms and sexual selection in the Lophopidae (Hemiptera: Fulgoromorpha). Annales de la Société Entomologique de France 34: 149–162.

Su M, Dietrich CH, Zhang YL, Dai W (2014) Ultrastructure of the spermatozoa of *Psammotettix striatus* (Linnaeus) and *Exitianus nanus* (Distant) (Hemiptera, Auchenorrhyncha, Cicadellidae, Deltocephalinae). Arthropod Structure and Development 43: 559–570. https://doi.org/10.1016/j.asd.2014.06.003

Szwedo J (2018) The unity, diversity and conformity of bugs (Hemiptera) through time. Earth and Environmental Science Transactions of the Royal Society of Edinburgh 107: 109–128. https://doi.org/10.1017/S175569101700038X

Tian RG, Yuan F, Zhang YL (2006) Male reproductive system and spermatogenesis in Homoptera (Insecta, Hemiptera). Entomotaxonomia 28(4): 241–253. https://doi.org/10.1016/S1872-2067(06)60034-X

Urban JM, Cryan JR (2007) Evolution of the planthoppers (Insecta, Hemiptera, Fulgoroidea). Molecular Phylogenetics and Evolution 42: 556–572. https://doi.org/10.1016/j.ympev.2006.08.009

Vitale DGM, Brundo MV, Viscuso R (2011) Morphological and ultrastructural organization of the male genital apparatus of some Aphididae (Insecta, Homoptera). Tissue and Cell 43: 271–282. https://doi.org/10.1016/j.tice.2011.05.002

Walker F (1851) List of the specimens of Homopterous insects in the collection of the British Museum. British Museum, Department of Zoology, London 2: 261–636.

Zhang BB, Dai W (2012) Ultrastructure of the spermatozoa of *Cicadella viridis* (Linnaeus) and its bearing on the phylogeny of Auchenorrhyncha. Micron 43: 978–984. https://doi.org/10.1016/j.micron.2012.03.022

Zhang BB, Lyu QH, Hua BZ (2016) Male reproductive system and sperm ultrastructure of *Furcatopanorpa longihypovalva* (Hua and Cai, 2009) (Mecoptera, Panorpidae) and its phylogenetic implication. Zoologischer Anzeiger – A Journal of Comparative Zoology 264: 41–46. https://doi.org/10.1016/j.jcz.2016.07.004

RESEARCH ARTICLE

ZooKeys

A peer-reviewed open-access journal

Launched to accelerate biodiversity research

The impact of a new genus on the molecular phylogeny of Hemisphaeriini (Hemiptera, Fulgoromorpha, Issidae)

Songping Zhao[1], Thierry Bourgoin[2], Menglin Wang[1]

1 *Key Laboratory of Southwest China Wildlife Resources Conservation of the Ministry of Education, China West Normal University, Nanchong, Sichuan Province, 637009, China* **2** *Institut de Systématique, Évolution, Biodiversité, ISYEB-UMR 7205 MNHN-CNRS-Sorbonne Université-EPHE, Muséum national d'Histoire naturelle, CP 50, 57 rue Cuvier, F-75005 Paris, France*

Corresponding author: *Menglin Wang* (wangmenglin123@126.com)

Abstract

A new genus, *Retaldar* **gen. nov.** of the family Issidae (Hemisphaeriinae, Hemisphaeriini) is described from Guangxi Province of China. A revised molecular analysis for the Hemisphaeriini based on partial sequences of 18S, 28S, COXI and Cytb, provides evidence for a new lineage within the subtribe Mongolianina. With two subgroups of genera now identified, the monophyly of Mongolianina is discussed from both a morphological and a molecular basis.

Keywords

Hemisphaeriinae, molecular, morphology, new species, Oriental, planthoppers

Introduction

Recently Wang et al. (2016) proposed important changes to the classification of the planthopper family Issidae based on the first molecular analysis of the family. Supported also by a new set of morphological characters, several new lineages were identified forming a major group including almost all Oriental genera in the subfamily Hemisphaeriinae Melichar, 1906 sec. Wang et al. (2016). This important monophyletic unit

currently groups around 100 genera and 486 species distributed in the Oriental region (Bourgoin 2019) with a few taxa in the New World such as *Picumna* Stål, 1864 (Wang et al. 2016). The subfamily is divided into four tribes according to the following topology: (Kodaianellini Wang, Zhang & Bourgoin, 2016 + (Sarimini Wang, Zhang & Bourgoin, 2016 + (Parahiraciini Cheng & Yang, 1991 + Hemisphaeriini Melichar, 1906))) (Wang et al. 2016). The last tribe currently contains 28 genera and is divided into two sister subtribes: Mongolianina Wang, Zhang & Bourgoin, 2016 (6 genera) and Hemisphaeriina Melichar, 1906 (11 genera). Two unnamed lineages in each subtribe were also identified in the Wang et al. (2016) analysis. They were not discussed being considered as artificial due to sampling bias: several taxa belonged to the same genus (viz. *Mongoliona* Distant, 1909 and *Hemisphaerius* Schaum, 1850). Beside these 17 Hemisphaeriini genera, 11 other genera still remain in an *incertae sedis* position within the Hemisphaeriini (Bourgoin 2019).

In this paper, we describe and sequence the genes (18S, 28S (D3–D5) and (D6–D7), COXI and Cytb) of a new species of Hemisphaeriini from Guangxi Province of China, and provide several sequences for other known genera. These new data allow the reassessment of the subtribal division of Hemisphaeriini proposed by Wang et al. (2016).

Materials and methods

The specimens were collected by net capture and stored in alcohol. The genitalia were separated from the insect body using micro-scissors, and then boiled in 10% NaOH solution for few minutes until muscles were completely dissolved leaving tegumentary structures. After rinsing in distilled water several times to clean the residual NaOH solution, the abdomen was subsequently transferred to glycerine for final dissection and observation. Genitalia were finally conserved under the specimen in genital vials. Photographs for external morphology and genitalia characters were taken using Leica DFC camera attached to Leica M205FA stereomicroscope and further refined with LAS X software. Morphological interpretations and subsequent terminologies follow Bourgoin (1987, 1993) for male and female genitalia respectively, Emeljanov (1971) for the term "hypocostal plate" on the forewing and Bourgoin et al. (2015) for wing venation. The type specimens are deposited in China West Normal University, Nanchong, Sichuan Province, China.

Total genomic DNA was extracted from the legs of type specimens using a Sangon Ezup column animal genomic DNA purification kit. The genes (18S, 28S, COXI, Cytb) were amplified using the same primers and amplification procedure as in Wang et al. (2016). DNA sequencing was conducted at Sangon Company (Shanghai, China). Taxon sampling includes all Hemisphaeriini taxa available from a previous analysis (Wang et al. 2016) for which several new sequences are added (Table 1). Both the newly described genus and an undescribed *Mongoliana* species from Thailand (*Mongoliana* sp. 1) were included in the new analysis. From Wang et al. (2016), 11 genera representing all major lineages were used as outgroups, plus a new species of the genus *Rhombissus*

Table 1. Taxa sampling used for the phylogeny tree and corresponding sequence numbers registered in GenBank. The symbol * denotes new added sequences in this study.

Taxa name	Collecting location	Gene 18S (1F–5R)	Gene 18S (3F–Bi)	Gene 18S (A2–9R)	Gene 28S (D3–D5)	Gene 28S (D6–D7)	COXI	Cytb
Hemisphaeriini								
Ceratogergithus pseudotessellatus (Che, Zhang & Wang, 2007)	China	KX761574	–	KX761576	KX761444	KX702806	KX702919	KX702906
Ceratogergithus spinosus (Che, Zhang & Wang, 2007)	China	KX761491	KX761491	KX761491	KX761532	KX761521	KX761502	KX761513
Choutagus longicephalus Zhang, Wang & Che, 2006	China	KX650620	KX650620	KX650620	KX761450	KX702810	KX761460	–
Clypeosmilus centrodasus Gnezdilov & Soulier-Perkins, 2017	Vietnam	–	–	KX761575	–	–	KX761470	KX761474
Eusudasina nantouensis Yang, 1994	China	JX196136	–	–	–	–	HM052838	HM452266
Euxaldar lenis Gnezdilov, Bourgoin & Wang, 2017	Vietnam	KX761573	–	KX761565	KX761412	–	–	–
Gergithoides carinatifrons Schumacher, 1915	China	–	KX761538	KX761538	–	KX702805	KX761555	KX702905
Gergithoides rugulosus (Melichar, 1906)	China	JX196163	–	–	–	–	HM052835	HM452279
Gergithus yunnanensis Che, Zhang & Wang, 2007	China	KX702831	KX702831	KX702831	KX761456	MN381848*	KX702924	KX702915
Hemisphaerius palaemon Fennah, 1978	China	KX761486	KX761486	KX761486	KX761526	KX761517	KX761497	KX761508
Hemisphaerius rufovarius Walker, 1858	China	KX702825	KX702825	KX702825	KX761454	KX702812	KX702923	KX702913
Hemisphaerius lysanias Fennah, 1978	Vietnam	KX702833	KX702833	KX702833	KX761404	KX702860	KX702933	KX702883
Hemisphaerius coccinelloides (Burmeister, 1834)	Philippines	KX702834	KX702834	KX702834	KX761405	KX702861	KX702934	KX702884
Hemisphaerius sp.	Laos	KX702835	KX702835	KX702835	KX761406	KX702862	KX761556	KX702885
Hemisphaerius testaceus Distant, 1906	China	JX196135	–	–	–	–	HM052831	HM452258
Macrodaruma pertinax Fennah, 1978	Vietnam	KX702832	KX702832	KX702832	KX761402	KX702859	KX702931	KX702882
Macrodaruma sp.	China	KX702828	KX702828	KX702828	KX761399	KX702857	KX702927	KX702881
Maculergithus multipunctatus (Che, Zhang & Wang, 2007)	China	KX702816	KX702816	KX702816	KX761443	KX702804	KX702918	KX702904
Maculergithus nonomaculatus (Meng & Wang, 2012)	China	KX761492	KX761492	KX761492	KX761533	KX761522	KX761503	KX761514
Mongoliana triangularis Che, Wang & Chou, 2003	China	–	–	KX761561	KX761528	–	–	KX761510
Mongoliana sinuata Che, Wang & Chou, 2003	China	KX702820	KX702820	KX702820	KX761448	–	KX761459	KX702908
Mongoliana sp.1	Thailand	–	–	MN422135*	MN381854*	–	–	MN332233*
Mongoliana sp. 2	China	KX761572	MN422136*	KX761566	KX761534	MN381849*	–	–
Mongoliana serrata Che, Wang & Chou, 2003	China	JX196160	–	–	–	–	HM052830	HM452272
Neogergithoides tubercularis Sun, Meng & Wang, 2012	China	KX702822	KX702822	KX702822	KX761451	MN381845*	KX761558	KX702910
Ophthalmosphaerius trilobulus (Che, Zhang & Wang, 2006)	China	KX702826	KX702826	KX702826	KX761455	KX702813	KX761462	KX702914
Retaldar yanitubus sp. nov.	China	MN381856*	MN381856*	MN381856*	MN381853*	MN381851*	MN381857*	MN332232*
Thioniini								
Thionia sp.	Panama		KX761539	KX761539	KX761407		KX702935	KX702886

Taxa name	Collecting location	Gene 18S (1F–5R)	Gene 18S (3F–Bi)	Gene 18S (A2–9R)	Gene 28S (D3–D5)	Gene 28S (D6–D7)	COXI	Cytb
Hysteropterini								
Celyphoma quadrupla Meng & Wang, 2012	China	KX702815	KX702815	KX702815	KX761442	KX702803	KX702917	KX702903
Mulsantereum maculifrons (Mulsant & Rey, 1855)	France	KX761569	KX761569	KX761569	KX761400	MN381847*	KX702928	KX761551
Issini								
Issus coleoptratus (Fabricius, 1781)	France	KX761568	KX761568	KX761568	KX761403	KX761560	KX702932	KX761550
Kodaianellini								
Kodaianellissus intorqueus Wang, Bourgoin & Zhang, 2017	China	KX761476	KX761476	KX761476	KX761480	KX761482		KX761472
Kodaianella bicinctifrons Fennah, 1956	China	KX702814	KX702814	KX702814	KX761441	KX702802	KX761458	KX702902
Sarimini								
Sarima bifurca Meng & Wang, 2016	China	KX702819	KX702819	KX702819	KX761447	KX702808	KX702921	KX761552
Tetrica sp.	China	KX702821	KX702821	KX702821	KX761449	KX702809	KX702922	KX702909
Parahiraciini								
Flavina hainana (Wang & Wang, 1999)	China	KX702824	KX702824	KX702824	KX761453	MN381846*		KX702912
Fortunia sp.	China	KX761487	KX761487	KX761487	KX761527	KX761518	KX761498	KX761509
Neodurium hamatum Wang & Wang, 2011	China	KX702818	KX702818	KX702818	KX761446	MN381844*	KX702920	
Rhombissus sp.	China	MN381855*	MN381855*	MN381855*	MN381852*	MN381850*		MN332231*

Gnezdilov & Hayashi, 2016 (*Rhombissus* sp.) from the issid tribe Parahiraciini. All sequences are registered in GenBank with their accession numbers provided in Table 1. Contigs assembly was made using the software SEQMAN from package DNASTAR v5.01 (www.dnastar.com). MEGA v7.0 (Kumar et al. 2016) was used for performing alignments. IQTREE v1.4.1 (Nguyen et al. 2015) was used for maximum likelihood phylogenetic analysis using 10,000 ultrafast bootstraps (Minh et al. 2013) with substitution model automatically selected for partitions unlinked; other parameters were used as per default. FIGTREE v1.1.2 (Rambaut 2016) was used to visualize the tree.

Taxonomy

Hemisphaeriini Melichar, 1906
Mongolianina Wang, Zhang & Bourgoin, 2016

Retaldar gen. nov.
http://zoobank.org/9A9AD297-9A97-44C2-B710-B1B34A0D1817

Type species. *Retaldar yanitubus* sp. nov., here designated.
  Etymology. Genus name masculine from the free combination of the latin word '*rete*' meaning network as for the reticulated forewings and the suffix '-*aldar*' from the genus *Euxaldar* Fennah, 1978.
  Diagnosis. This new genus is similar to the genus *Clypeosmilus* Gnezdilov & Soulier-Perkins, 2017 in general appearance, but differs by: 1) a more complex and

obscure reticular venation of the forewing (Fig. 1) while a simpler pattern is found in *Clypeosmilus* (Gnezdilov and Soulier-Perkins 2017, fig. 1A); 2) an asymmetrical male genitalia with the periandrium more developed on right side and the aedeagus processes emerging at different levels, more posteriorly on right side (Figs 9, 10) while it is symmetrical in *Clypeosmilus* (Gnezdilov and Soulier-Perkins 2017, fig. 3A); 3) gonostyli with ventral margin deeply convex (Fig. 8), while it is much more elongated in *Clypeosmilus* (Gnezdilov and Soulier 2017, fig. 3C). The new genus is also similar to the genus *Eusudasina* Yang, 1994, from which it differs also by its more complex reticulate venation and by its longer frons, around 1.2 times longer (in middle) than broad at widest part (Figs 3, 21), only around 0.9 times longer in *Eusudasina* (Chan and Yang 1994, fig. 34C). With *Euxaldar* Fennah, 1978, *Retaldar* gen. nov. shares the general form of the gonostyli, which is strongly developed ventrally (Fennah 1978, fig. 251; Gnezdilov et al. 2017, fig. 8) but definitively differs by its distal postero-ventral protuberance (Fig. 8) and by its near-symmetric subapical processes on the periandrium (Figs 9, 10) while they are asymmetrical in the former (Gnezdilov et al. 2017, figs 1, 2).

Description. Head with compound eyes slightly wider than pronotum, almost same width as mesonotum (Fig. 1). Vertex rectangular, obviously broader than long at midline, anterior margin almost straight, lateral margins nearly parallel, posterior margin slightly roundly concave at middle; median carina absent on disc (Fig. 1). Frons obviously longer than wide, gradually broadening from dorsal margin to below the level of antennae, then curved to frontoclypeal suture (Figs 3, 21); dorsal margin slightly concave, lateral margins slightly broaden below level of compound eyes, median carina nearly invisible. Frons with numerous tiny tubercles on the whole disc. The tubercles larger on the lateral areas, arranged into a vertical line on each side of frons (Figs 3, 21). Frontoclypeal suture straight (Figs 3, 21). Gena in lateral view flattened and oblique (Fig. 2). Clypeus in lateral view with a protuberance below frontoclypeal suture slightly surpassing the gena (Fig. 2); in ventral view, clypeus without median carina (Figs 3, 21). Rostrum reaching midcoxae; apical segment slightly shorter than subapical one. Antennae with scape extremely short, pedicel rounded (Figs 3, 21). Pronotum triangular, apical margin roundly convex, posterior margin nearly straight, with some faint small nodules on each side or nodules invisible, median carina absent (Figs 1, 19, 20). Mesonotum triangular, a little longer than pronotum in midline, without carina on the disc; with (Fig. 1) or without (Figs 19, 20) some faint small nodules in lateral part apically. Forewings obviously longer than broad, without hypocostal plate, with elevated irregular reticular venations and venation poorly recognizable, costal margin and posterior margin subparallel, costal margin roundly convex, apical margin straight and oblique inward to posterior margin (Fig. 4), CuP obvious, Pcu and A1 fused exceeding middle of clavus (Figs 1, 4). Hindwing one-lobed. Metatibia with two lateral spines on apical half and seven spines apically.

Male genitalia. Anal tube in lateral view long and curved (Fig. 6). Pygofer long triangular in lateral view, posterior margin roundly convex (Fig. 6). Gonostyli irregularly quadrangular in profile, almost as high as long, dorsal margin nearly straight, ventral margin strongly convex with a strong posteroapical protuberance, caudo-ventral angle rounded (Figs 6, 8). Capitulum of gonostyli finger-shaped, with a small peaked
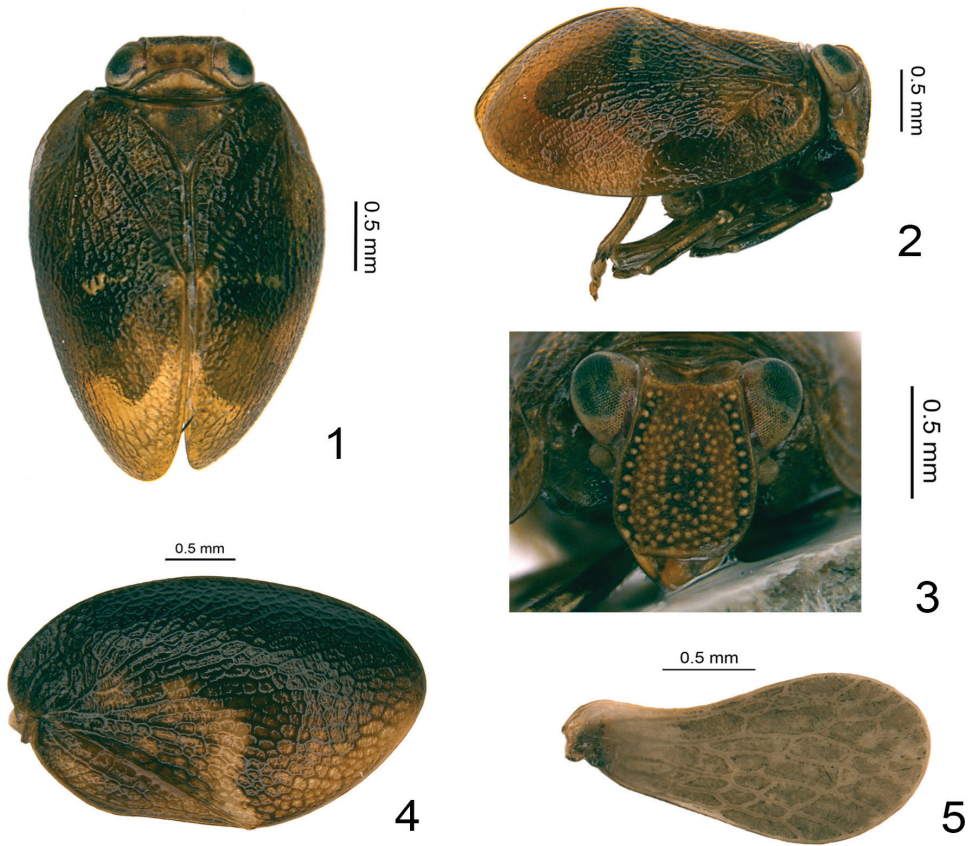
Figures 1–5. *Retaldar yanitubus* sp. nov. **1** adult (holotype, male), dorsal view **2** adult (holotype, male), lateral view **3** adult (holotype, male), frontal view **4** forewing (paratype, female) **5** hindwing (paratype, female).

spine (Fig. 8). Periandrium tubular, subapical nearly symmetric, medially constricted and slightly asymmetric in ventral view. Aedeagus processes asymmetric, right one emerging more posteriorly than left one (Figs 9, 10). Aedeagus a little longer than dorsolateral lobe and ventral lobe of periandrium (Figs 9, 10).

Female genitalia. Anal tube in dorsal view a little longer than wide (Fig. 12). Gonoplacs nearly rectangular in lateral view, apical margin rounded (Fig. 13), in dorsal view fused at middle near base, broadest near base, outer lateral margins straight and roundly convex at base (Fig. 14). Gonapophysis IX in lateral view long and narrow, boat-shaped (Fig. 16); in dorsal view nearly triangular, basal half broader than apical half, with a spine on each side (Fig. 15); gonospiculum bridge developed (Fig. 16). Gonocoxa VIII long rectangular (Fig. 18). Three teeth at apex and three keeled teeth on outer lateral margin of anterior connective lamina of gonapophysis VIII (Fig. 18). Endogonocoxal process membranous (Fig. 18).

Distribution. China (Guangxi).
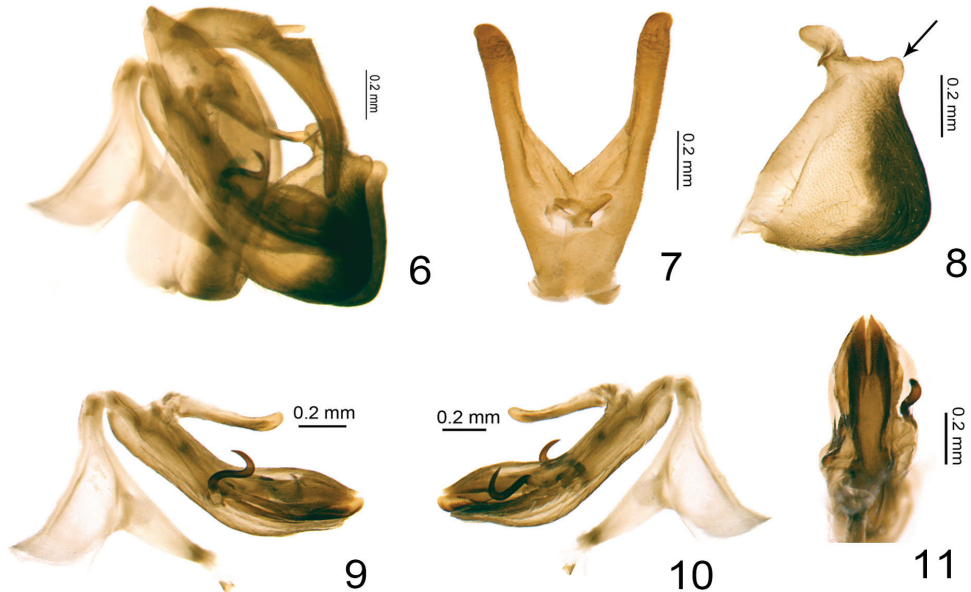
Figures 6–11. *Retaldar yanitubus* sp. nov., holotype. **6** male genitalia, lateral view **7** male anal tube, dorsal view **8** gonostylus, lateral view **9** phallic complex, left lateral view **10** phallic complex, right lateral view **11** apical half of phallic complex, ventral view. The arrows on Fig. 8 indicates the distal postero-ventral protuberance of gonostyli.

Retaldar yanitubus sp. nov.

http://zoobank.org/7098817F-FAE5-4A30-AE8A-3D4E7DAE2EA1

Etymology. Specific epithet built by the arbitrary combination of the alphabet letter "Y" and "anal tube" latinised into "*anitubus*", referring to the Y-shaped male anal tube in dorsal view.

Diagnosis. The species is close to *Clypeosmilus centrodasus* Gnezdilov & Soulier-Perkins, 2017, from which it differs by its generic characters (complex reticular venation (Fig. 1), more or less quadrangular gonostyli bearing a postero-apical protuberance) and the form of the male anal tube, which is deeply concave on the apical margin, Y-shaped in dorsal view (Fig. 7), while very shallowly concave and cylindrical in the latter species (Gnezdilov and Soulier-Perkins 2017, fig. 3E). From *Euxaldar guangxiensis* Zhang, Chang & Chen, 2018, another Guangxi species, it differs by: 1) its tegmina pattern black (Fig. 19) to dark tawny with a yellow slender or broader transverse marking (Figs 1, 4, 20), while it is dark brown with more than four yellow irregular markings in *E. guangxiensis* (Zhang et al. 2018, figs 1, 3); 2) the form of the male anal tube which is obviously protruded in the later (Zhang et al. 2018, fig. 10), and 3) the base of periandrium with a finger-shaped dorsal process (Figs 9, 10), while it is with three dorsal processes in *E. guangxiensis* (Zhang et al. 2018, figs 15a, b, 16a, b).
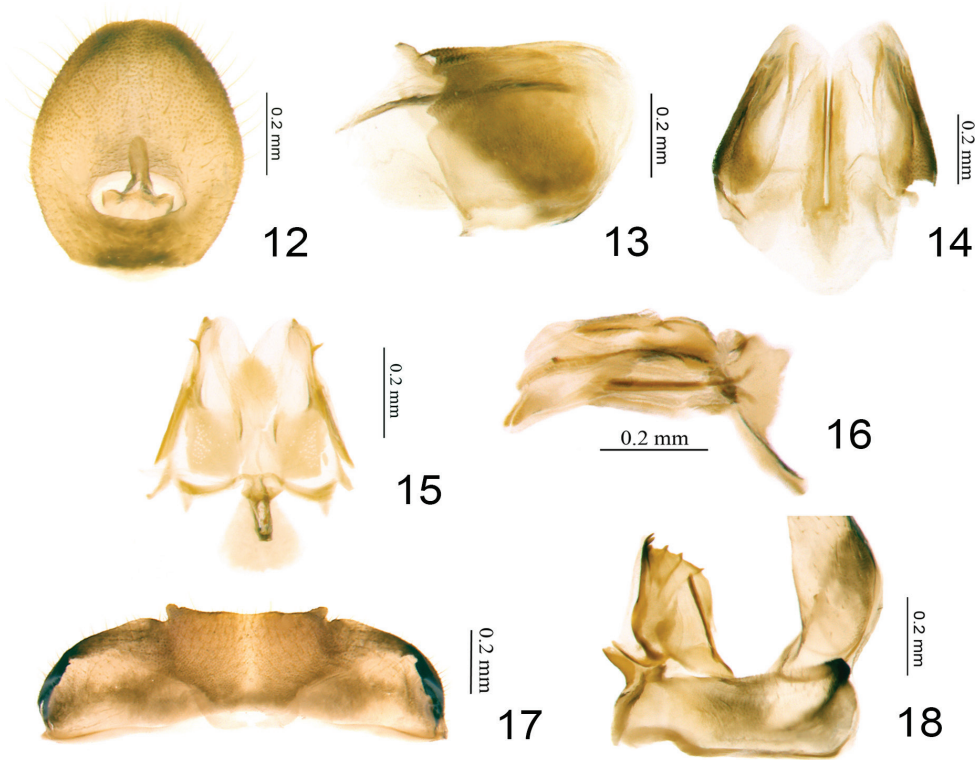
Figures 12–18. *Retaldar yanitubus* sp. nov., paratype. **12** female anal tube, dorsal view **13** gonoplacs, lateral view **14** gonoplacs, dorsal view **15** gonapophysis IX and gonaspiculum bridge, dorsal view **16** gonapophysis IX and gonaspiculum bridge, lateral view **17** sternite VII **18** gonocoxa VIII and gonapophysis VIII, ventral view.

Type materials. Holotype: ♂, CHINA: Guangxi Province, Jinxiu, Dayaoshan natural reserve, Hekou, 24°14'11"N, 110°14'11"E, 689.9 m, 23 vii 2018, Feilong Yang & Kun Zhao leg.

Paratypes: 2♀♀, same data as for holotype.

Description. Length: male (including forewings) (N =1): 3.1 mm; female (including forewings) (N =2): 3.3–3.4 mm.

Coloration. Vertex tawny, disc with two dark brown circular markings; anterior, lateral and posterior margins tawny (Figs 1, 19, 20). Center of the compound eyes mostly black, surrounded by brown (Figs 1, 3, 20) or compound eyes grayish (Figs 19, 21). Frons mostly tawny, scattered with many yellow nodules on the whole disc (Figs 3, 21); the central area slightly black (Figs 3, 21); lateral areas black, with the yellow nodules arranged into a distinct line on each side (Figs 3, 21); lateral margins tawny (Figs 3, 21). Clypeus in frontal view tawny, with two vertical dark brown markings at middle (Fig. 3) or tawny but the vertical dark brown markings invisible; the basal part black (Fig. 21). Rostrum tawny (Fig. 21). In lateral view gena tawny (Fig. 2), clypeus

Figures 19–21. *Retaldar yanitubus* sp. nov., paratype. **19** adult (female), dorsal view **20** adult (female), dorsal view **21** adult (female), frontal view.

with a broad black oblique patch covering the base of the gena and most part of the clypeus (Fig. 2). Antennae dark brown (Figs 3, 21). Pronotum tawny, with three small yellow nodules present on each side (Fig. 1) or without them (Figs 19, 20), anterior and posterior margins brown (Figs 1, 19, 20). Mesonotum mainly tawny mixed with some black, disc with two small yellow nodules on each side (Fig. 1) or disc black with nodules almost invisible (Figs 19, 20); anterior margin tawny. Forewings dark tawny, with a discontinuous yellow transverse band from the end of clavus to the middle of forewing (Figs 1, 2) or the transverse marking lighter and broader (Figs 4, 20), or the whole forewing black without any markings (Fig. 19); venations tawny or black, reticular and inconspicuous (Figs 1, 2, 4, 19, 20). Hindwing grayish-brown, with grayish reticulate venations (Fig. 5).

Head and thorax. Vertex 2.5 times wider than long in midline, without median carina; anterior margin straight; posterior margin roundly concaved (Fig. 1). Frons 1.2 times longer in middle than broad at widest part, 1.4 times wider at the widest part than apical margin (Fig. 3). Pronotum with posterior margin 3.6 times wider than long in midline, anterior margin roundly protruded (Fig. 1). Mesonotum with anterior margin 2.0 times wider than long in midline, anterior margin straight (Fig. 1). Forewings 1.6 times longer in longest part than widest part (Fig. 4), clavus obvious, the tip reaching to the middle of forewing in dorsal view (Fig. 1). Metatibiotarsal formula: 2–7/7/2.

Male genitalia. Anal tube in lateral view arc-shaped, gradually narrowing from the base to the end, apical part conical (Fig. 6); in dorsal view anal tube Y-shaped with two long straight posterolateral arms, middle part in between deeply concave; in dorsal view arms as long as median part of anal tube (Fig. 7); anal opening located at the basal 1/4 of anal tube, epiproct protruded (Fig. 7). The highest length of pygofer around 3.4 times of the widest length, no basal notch (Fig. 6). Periandrium with a finger-shaped process originated from dorsal margin of base extending to the middle, directed to caudal (Figs 9, 10); dorsolateral lobe of periandrium a little longer than ventral lobe

(Figs 9, 10), the ventral lobe in ventral view rounded in apex (Fig. 11). Aedeagus asymmetric, left hooked process emerging at its mid length, S-shaped, curved and directed dorso-cephalad in lateral view, the tip not exceeding the base of right process (Figs 9, 10); right hooked process almost same length as the left but emerging from its apical 1/4, curved and directed dorsad (Figs 9, 10); apex of aedeagus rounded in lateral view, slightly exceeding dorsolateral and ventral lobe of periandrium (Figs 9, 10). The connective with strongly developed tectiductus (Figs 9, 10).

Female genitalia. Anal tube in dorsal view ovate, widest near middle, 1.2 times longer in midline than widest part, apical margin and lateral margins rounded (Fig. 12); anal opening situated at basal 1/4 (Fig. 12). Gonoplacs in dorsal view fused at middle near base, broadest near base, outer lateral margins straight and roundly convex at base (Fig. 14). Posterior connective lamina of gonapophysis IX in dorsal view nearly triangular, the basal half relatively sclerotized, slightly broader than apical half, apical half membranous, the inner bifurcation at apical 1/3 (Fig. 15); the posterior fibula sclerotized, with a spine on each side on apical 1/4 (Fig. 15). In lateral view, gonapophysis IX long and narrow, dorsal and ventral margins nearly parallel each to another, tip pointed (Fig. 16); gonospiculum bridge in lateral view triangular, needle-like ventrally (Fig. 16). Anterior connective lamina of gonapophysis VIII subrectangular, with three closely situated teeth at apex and three keeled teeth on the outer lateral margin, inner lateral margin without teeth (Fig. 18). Endogonocoxal process membranous, reaching the level of the apical teeth (Fig. 18). Gonocoxa VIII long rectangular, vertical with the gonapophysis VIII (Fig. 18). Hind margin of sternite VII with middle part slightly prominent and truncates in ventral view (Fig. 17).

Molecular data. Genes sequences were registered in GenBank with accession numbers as following: MN381856 (whole 18S), MN381853 (28S D3–D5), MN381851 (28S D6–D7), MN381857 (COXI), MN332232 (Cytb). The COXI sequence of this species differs respectively by 87 bp (over 601 bp: 14.5%) and 103 bp (over 681 bp: 15.1%) from *Eusudasina nantouensis* Yang, 1994 (Genbank accession number: HM052838) and *Clypeosmilus centrodasus* (Genbank accession number: KX761470).

Note. As in the genus *Euxaldar* (Gnezdilov et al. 2017), color and color-pattern variation on forewing is reported in *R. yanitubus* sp. nov. Forewings might be nearly black (Fig. 19) or dark tawny (Figs 1, 2, 20), while color-patterns on the forewing varies from a light yellowish broad traverse band apically curved upward (Fig. 4) to a much thinner band only visible on the middle of forewing (Figs 1, 2) or even absent (Fig. 19).

Phylogenetical analysis

In-group sampling comprised 14 Hemisphaeriini genera and 27 species while 12 other issid genera were used as outgroups (Fig. 22). In all configurations tested, Hemisphaeriini reached a full 100% boostrap (BS). Monophyly of Hemisphaeriina appears less supported (BS=69) than in Wang et al. (2016: BS=98) although the group was recovered in all analyses. Monophyly of Mongolianina is not recovered but appeared
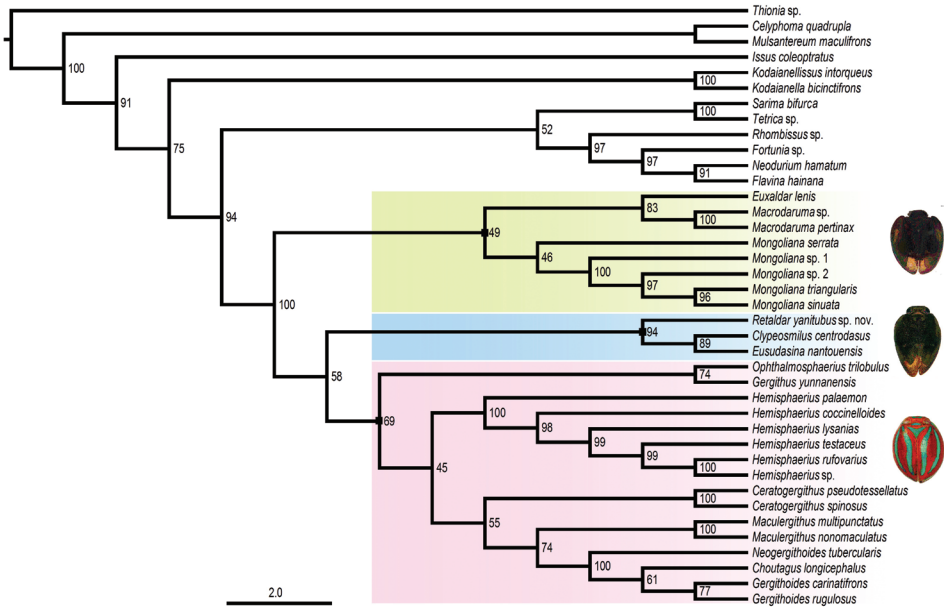
Figure 22. Maximum likelihood tree of Hemisphaeriini based on combined sequences (18S, 28S, COXI, Cytb) with genera of Thioniini, Hysteropterini, Issini, Kodaianellini, Sarimini and Parahiraciini as outgroups. At each node, values denote ML ultrafast bootstrap support

paraphyletic, disclosing a new well-supported lineage (BS=94). It includes *Retaldar* gen. nov. at its base in the following relationship (*Retaldar* + (*Clypeosmilus* + *Eusudasina*)). The other Mongolianina taxa form another weakly supported lineage (BS=49) comprising three taxa in the following relationship: (*Mongoliana* + (*Euxaldar*+ *Macrodaruma*)). In several analyses, these two lineages appear in a sister group relationship.

Discussion

According to their results, Wang et al. (2016) subdivided Issidae into three subfamilies. At their base, Thioniinae Melichar, 1906 with at least two genera, *Thionia* Stål, 1859 and *Cheiloceps* Uhler, 1895 form a monophyletic group sister to the rest of the Issidae. For practical reasons of classification, all New World genera were placed in Thioniinae by Wang et al. (2016), but it is important to note that the subfamily does not necessarily include all of these taxa: *Picumna* Stål, 1864 for instance, never grouped within Thioniinae in their analysis, but in Hemisphaeriinae sec. Wang et al. (2016), although its place is not stabilized. This indicates a mixed origin of New World Issidae, which includes at least an older lineage (*Thionia*, *Cheiloceps*) of Lower Cretaceous origin and another slightly younger one (*Picumna*) originating from the Oriental lineages (Bourgoin et al. 2018). Several other genera are also waiting for a better placement in the issid phylogeny and it might be that other, still younger, taxa have also expanded more

recently from Asia into the Nearctic as proposed by Gnezdilov (2019). Only future phylogenetic analyses including New World genera will help to better understand the heterogeneous composition of the Issidae fauna in the Nearctic.

In the phylogeny of Wang et al. (2016), the second subfamily Issinae Spinola, 1839 was less supported (BS = 72). In all subsequent analyses including more taxa (Bourgoin et al. 2018), this node was no more supported, suggesting a paraphyletic Issinae with Issini sec. Wang et al. (2016), no longer sister to Hysteropterini but moving to sister of Hemisphaeriinae as in this study (Fig. 22). Because in some cases Thioniinae also grouped with Hysteropterini, we suggest that these tribes recover separate subfamily ranks in a basal polytomic node with the following topology [Thioniinae, Hysteropterinae, (Issinae + Hemisphaeriinae)].

Within Hemisphaeriinae, Hemisphaeriini sec. Wang et al. (2016) form a natural group of at least 28 genera (Bourgoin 2019) for which monophyly has always been strongly supported in all our analyses since 2016 with a BS=100. Two lineages were recognized as subtribes: Mongolianina and Hemisphaeriina, both well supported (BS = 95 and 98 respectively) in Wang et al. (2016). Addition of new taxa with an almost full set of sequences for the genes under this study has however slightly modified previous results allowing recognition of three main lineages within Hemisphaeriini while eleven other genera still remain in an *incertae sedis* position.

Hemisphaeriina remains the most diverse subtribe with, at least, 11 described genera, eight having being sequenced and providing the following topology: ((*Ophthalmosphaerius* + *Gergithus*) + (*Hemisphaerius* + (*Ceratogergithus* + (*Maculergithus* + (*Neogergithoides* + (*Choutagus* + *Gergithoides*)))))). Three genera remain unsequenced: *Epyhemisphaerius* Chan & Yang, 1994, *Neohemisphaerius* Chen, Zhang & Chang, 2014 and *Rotundiforma* Meng, Wang & Qin, 2013. Moreover, *Gergithus yunnanensis* Che, Zhang & Wang, 2007 probably belongs to another new genus and *Gergithus* s.s. should remain in an *incertae sedis* position within Hemisphaeriini. According to Gnezdilov (2017), the *Maculergithus* clade might include two different genera.

According to our analysis, Mongolianina should be now restricted to the following genera: (*Mongoliana* + (*Euxaldar* + *Macrodaruma*)), separated from a third new lineage (*Retaldar* + (*Clypeosmilus* + *Eusudasina*)). The support of this last lineage is high (BS= 94) and higher than the Mongolianina lineage itself. Because the monophyly of the Mongolianina lineage itself remains weak and unstable, we prefer to keep provisionally a paraphyletic Mongolianina, including in it this new lineage. When more genera will be sequenced, a better and stronger topology will probably appear. Genera such as *Bruneastrum* Gnezdilov, 2015, *Tapirissus* Gnezdilov, 2014 and *Neotapirissus* Meng & Wang, 2016 should also join this group, but, as for Hemisphaeriina, new morphological analyses are still needed to better identify these lineages without molecular sequencing.

The new species *Retaldar yanitubus* gen. & sp. nov. has a protruded clypeus in lateral view. In the tribe Hemisphaeriini, several other genera also display such a protruded clypeus: *Euxaldar*, *Clypeosmilus* and *Eusudasina*. They also share a plesiomorphic clearly visible CuP on the forewing while this vein is not visible in Hemisphaeriina

(Gnezdilov et al. 2017; Gnezdilov and Soulier-Perkins 2017). Although appearing in two separate lineages, *Retaldar* gen. nov. and *Euxaldar* share also an obscure reticulate forewing venation with the main veins poorly recognizable, while these are clearer in *Clypeosmilus* and *Eusudasina*.

Including more sequenced taxa in the molecular analysis, revisiting morphological characteristics of Hemisphaeriini and investigating the etho-ecology of these fascinating ladybug-like planthoppers is now urgently needed.

Acknowledgements

References

Bourgoin T (1987) A new interpretation of the homologies of the Hemiptera male genitalia, illustrated by the Tettigometridae (Hemiptera, Fulgoromorpha). Proceedings of the 6th Auchenorrhyncha Meeting, Turin (Italy), September 1987, 113–120.

Bourgoin T (1993) Female genitalia in Hemiptera Fulgoromorpha, morphological and phylogenetic data. Annales de la Société Entomologique de France 29(3): 225–244.

Bourgoin T (2019) FLOW (Fulgoromorpha Lists On the Web): a world knowledge base dedicated to Fulgoromorpha. Version 8, updated 3 June 2019. http://hemiptera-databases.org/flow/ [accessed 3 June 2019]

Bourgoin T, Guilbert E, Wang ML (2018) Issidae Molecular K-libration. In: 8th European Hemiptera Congress Abstract book, 24–29 June 2018. Katowice-Zawiercie, Poland, 36.

Bourgoin T, Wang RR, Asche M, Hoch H, Soulier-Perkins A, Stroiński A, Yap S, Szwedo J (2015) From micropterism to hyperpterism: recognition strategy and standardized homology-driven terminology of the forewing venation patterns in planthoppers (Hemiptera: Fulgoromorpha). Zoomorphology 134(1): 63–77. https://doi.org/10.1007/s00435-014-0243-6

Chan ML, Yang CT (1994) Issidae of Taiwan (Homoptera: Fulgoroidea). Chen Chung Book, Taichung, 168 pp.

Emeljanov AF (1971) New genera of planthoppers of the families Cixiidae and Issidae (Homoptera, Auchenorrhyncha) from the fauna of the USSR (Entomologicheskoe Obozrenie 50(3): 619–627). Entomological Review 50(3): 350–354.

Fennah RG (1978) Fulgoroidea (Homoptera) from Vietnam. Annales Zoologici 34(9): 207–279.

Gnezdilov VM (2017) Addenda to the revisions of the genera *Gergithus* Stål and *Hemisphaerius* Schaum (Hemiptera, Auchenorrhyncha, Fulgoroidea: Issidae). Entomological Review 97(9): 1338–1352. https://doi.org/10.1134/S0013873817090123

Gnezdilov VM (2019) A new genus and a new species, representing a new tribe of the family Issidae (Hemiptera: Auchenorrhyncha: Fulgoroidea), from Costa Rica. Zoosystematica Rossica 28(1): 108–115. https://doi.org/10.31610/zsr/2019.28.1.108

Gnezdilov VM, Bourgoin T, Wang ML (2017) Revision of the genus *Euxaldar* Fennah, 1978 (Hemiptera: Fulgoroidea: Issidae). Annales Zoologici (Warszawa) 67(1): 13–20. https://doi.org/10.3161/00034541ANZ2017.67.1.002

Gnezdilov VM, Soulier-Perkins A (2017) *Clypeosmilus centrodasus* gen. et sp. nov., a new genus and species of the family Issidae (Hemiptera: Fulgoroidea) from Northern Vietnam, Proceeding of the Zoological Institute RAS 321(1): 25–31.

Kumar S, Stecher G, Tamura K (2016) MEGA7: Molecular evolutionary genetics analysis version 7.0 for bigger datasets. Molecular Biology and Evolution 33(7): 1870–1874. https://doi.org/10.1093/molbev/msw054

Minh BQ, Nguyen MAT, von Haeseler A (2013) Ultrafast approximation for phylogenetic bootstrap. Molecular Biology and Evolution 30: 1188–1195. https://doi.org/10.1093/molbev/mst024

Nguyen LT, Schmidt HA, von Haeseler A, Minh BQ (2015) IQ-TREE: a fast and effective stochastic algorithm for estimating maximum likelihood phylogenies. Molecular Biology and Evolution 32: 268–274. https://doi.org/10.1093/molbev/msu300

Rambaut A (2016) FigTree v1.4.3: Tree figure drawing tool. http://tree.bio.ed.ac.uk/software/figtree/ [Accessed 4 October 2016]

Wang ML, Zhang YL, Bourgoin T (2016) Planthopper family Issidae (Insecta: Hemiptera: Fulgoromorpha): linking molecular phylogeny with classification. Molecular Phylogenetics and Evolution 105: 224–234. https://doi.org/10.1016/j.ympev.2016.08.012

Zhang ZG, Chang ZM, Chen XS (2018) A new species of the genus *Euxaldar* Fennah, 1978 from China (Hemiptera, Fulgoroidea, Issidae). Zookeys 781: 51–58. https://doi.org/10.3897/zookeys.781.27059

RESEARCH ARTICLE

ZooKeys
Launched to accelerate biodiversity research

A peer-reviewed open-access journal

One new species and three newly recorded species of *Neopallodes* Reitter from China (Coleoptera, Nitidulidae, Nitidulinae)

XiaoXiao Chen[1], Min Huang[1]

1 *Key Laboratory of Plant Protection Resources and Pest Management of the Ministry of Education, Entomological Museum, Northwest A&F University, Yangling, Shaanxi 712100, China*

Corresponding author: *Min Huang* (huangmin@nwsuaf.edu.cn)

Citation: Chen XX, Huang M (2019) One new species and three newly recorded species of *Neopallodes* Reitter from China (Coleoptera, Nitidulidae, Nitidulinae). ZooKeys 880: 75–84. https://doi.org/10.3897/zookeys.880.38033

Abstract

One new species of the sap beetle genus *Neopallodes*, *N. nigrescens* **sp. nov.**, is described and illustrated. New information on the distribution and illustrations of three species, *N. dentatus* Kirejtshuk, 1994, *N. falsus* Grouvelle, 1913 and *N. vietnamicus* Kirejtshuk, 1987, which are newly recorded from China, are also supplemented. A key to species of the genus *Neopallodes* from China is provided.

Keywords

Chinese fauna, Cucujoidea, *Cyllodes*-complex, Cyllodini, distribution

Introduction

The genus *Neopallodes* Reitter, 1884 was proposed for three species from Japan (Reitter 1884). Grouvelle (1892, 1902, 1903) later described another three species in this group although this taxon was treated as a synonym by Grouvelle (1913a). However, C.T. Parsons (1943) regarded *Neopallodes* as a valid genus. Five species from Japan and one species from Chejudo Island, Korea, were recorded by Y. Kurosawa et al. (1985) and M. Chûjô and C.E. Lee (Chûjô and Lee 1992), respectively. Kirejtshuk (1987, 1994, 2011) described 16 species and revised the Palaearctic and Indo-Malayan species. Later, Kirejtshuk (1992) distinguished *Neopallodes* from *Pallodes* Erich-

son, 1843, based on the exposed male anal sclerite from under the transverse pygidial apex, and proposed some additional diagnostic characters for these taxa. Twenty-one species previously placed in *Pallodes* Erichson, 1843 by Grouvelle (1896, 1906) and Reitter (1877) were also transferred to *Neopallodes* by Kirejtshuk (1994). Kirejtshuk (2008) gave a complete species checklist of *Neopallodes*, including 40 East Asian species (mostly in the Palaearchearctic or East-Chinese Province of the Palearctic Region, Indo-Malayan, and Malgassy regions.

Prior to our studies, only three species, *Neopallodes hilleri* Reitter, 1877, *N. inermis* Reitter, 1884, and *N. vicinus* Grouvelle, 1892, have been recorded from China (Kirejtshuk 1992, 1994). Here, we describe one new species and newly record three species from China. A key to the Chinese species of *Neopallodes* is presented.

Materials and methods

All materials for this study are deposited in the Entomological Museum of Northwest A&F University (**NWAFU**), Yangling, China. Most samples were preserved in 99% ethanol, although some were preserved as dried specimens. All photographs were taken using a Leica M205A microscope with a Leica DFC camera, and image stacking was done using LAS (Leica Application Suite) V3.7. Images were retouched with Adobe Photoshop CS6. Illustrations were drawn using Adobe Illustrator CS4.

Morphological terminology follows Kirejtshuk (1994, 2011). Body length measures from the anterior edge of clypeus to the posterior apex of pygidium; body width refers to the maximum width of elytra.

Taxonomy

Neopallodes Reitter, 1884

Neopallodes Reitter 1884: 269; Grouvelle 1892: 849, 1902: 17; Kirejtshuk 1987: 152; 1994: 225; 2008: 119; 2011: 287. Type species: *Pallodes hilleri* Reitter, 1877 (subsequent designation by Kirejtshuk 1994)

Diagnosis. The genus *Neopallodes* can be distinguished from other genera of the *Cyllodes* complex by the following features: distance between metacoxae wider than that between procoxae and mesocoxae; tarsomeres simiple on all legs; male anal sclerite exposed from under truncate pygidial apex. This genus is similar to other cyllodin genera in East Asia, such as *Pallodes*, *Coxollodes* Kirejtshuk 1987, and *Cyllodes* Erichson 1843, but it can be easily distinguished from *Pallodes* and *Coxollodes* in having the exposed male anal sclerite from under the transverse pygidial apex, and from *Cyllodes* in having simple tarsomeres and axillary sclerites absent on the mesoventrite.

Remarks. Congeners of *Neopallodes* are mycophagous, and their adults are associated with the sporocarps and thalli of Agaricaceae (Basidiomycetes). So far, larvae are known to be found on the mycelia of these fungi or in their fruiting bodies (Hayashi 1978; Kirejtshuk 1994; Leschen 1999; Yamashita and Hiji 2007). Yunnan Province accounts for 90% of the wild mushroom species in China (Liu 2014), and, the species in this genus so far collected in China are all distributed in Yunnan Province. This suggests that the abundance of fungi may potentially harbor undiscovered species of this genus.

Key to the species of *Neopallodes* from China*

1	Dorsal surface without color spots (Figs 1, 3, 18)......................................**2**
–	Dorsal surface with dark spots (Figs 19, 20)..**4**
2	Outer apical angle of protibia without distinctly raised tooth (Fig. 9); scutellum subtriangular with round apex (Figs 1, 3); prosternum slightly carinate with moderately subflattened process slightly widened at subtruncate apex and not bend to mesoventrite between mesocoxa; abdominal ventrite 1 much longer than hypopygidium (Figs 2, 4)...**3**
–	Outer apical angle of protibia with distinctly raised tooth; scutellum trapezoidal (Fig. 18); prosternum strongly carinate with process extremely widened at round apex and bend to mesoventrite between mesocoxa; abdominal ventrite 1 scarcely longer than hypopygidium..............***N. dentatus* Grouvelle, 1892**
3	Base of pronotum nearly three times as wide as long; antennal club subequal with or wider than prosternal process, antennal club subequal in length with antennomeres 2–8 together, antennomere 11 about as long as wide, antennomere 9 subequal in length with antennomere11; metaventrite without punctures in the middle and with fine and sparse punctures laterally .... ***N. inermis* (Reitter, 1885)**
–	Base of pronotum nearly 2.4 times as wide as long (Figs 1, 3); antennal club narrower than prosternal process; antennal club distinctly shorter than antennomeres 2–8 together, antennomere 11 wider than long, antennomere 9 shorter than antennomere11 (Fig. 8); metaventrite with fine punctures in the middle and large, sparse punctures laterally (Figs 2, 4)...***N. nigrescens* sp. nov.**
4	Outer apical angle of protibia without distinctly raised tooth; antennal club distinctly shorter than antennomeres 2–8 together; dorsal surface usually without color spots .... ***N. vicinus* Grouvelle, 1892**
–	Outer apical angle of protibia with distinctly raised tooth; antennal club longer than or subequal with antennomeres 2–8 together; dorsal surface usually with distinct, large, blackish spots...**5**

---

* after Kirejtshuk 1994.

5　　　　　Prosternal process flat apically; pronotum without dark spots at base; elytra surface with not quite regular longitudinal rows of punctures ....
.... *N. hilleri* (**Reitter, 1877**)
–　　　　　Prosternal process carinate apically; pronotum with distinct, dark spots at base; elytral surface with distinctly regular longitudinal rows of punctures... **6**
6　　　　　Antennal club longer than antennomeres 2–8 together; elytra with longitudinal rows of punctures not quite regular at basal third; elytra with large, blackish spots at humeral angles; pronotum with two subcircular, blackish spots; protibia with strongly raised tooth. (Fig. 20)...
....*N. vietnamicus* (**Kirejtshuk, 1987**)
–　　　　　Antennal club subequal in length with antennomeres 2–8 together; elytra with clearly longitudinal rows of punctures, including their basal third; elytra without spots at humeral angles; pronotum with two subtriangular, blackish spots; protibia with moderately raised tooth. (Fig.19)...*N. falsus* (**Grouvelle, 1913**)

Neopallodes nigrescens Chen & Huang sp. nov.
http://zoobank.org/C50B513E-2F59-4C59-9199-EF629E6C36F3
Figs 1–17

Type material. *Holotype*, ♂: China: Yunnan Province, Chuxiong City, Zixi Mountain, 2450 m a.s.l., 13-VII-2018, Xiaoxiao CHEN (NWAFU). *Paratypes*, 5♂♂: Yunnan Province, Dali City, Cangshan Mountain, 2610 m a.s.l., 25°39'51"N, 100°07'10"W, 05-VI-2018, Xiaoxiao CHEN (NWAFU); 1♂: Yunnan Province, Qujing City, Junzi Mountain, 2310 m a.s.l., 30-VII-2018, Xiaoxiao CHEN (NWAFU); 2♂♂: Yunnan Province, Qujing City, Yehuagou, 1980 m a.s.l., 05-VII-2018, Xiaoxiao CHEN (NWAFU); 3♂♂, 8♀♀: Same as holotype; 2♂♂: Guizhou Province, Bijie City, Shangdi Mountain, 2240 m a.s.l., 26°52'13"N, 104°18'02"W, 06-VII-2018, Xiaoxiao CHEN (NWAFU).

Description. Body size (♂): length 2.7–3.7, width 2.1–3.1 mm.

Body: Body shiny, dorsum glabrous, abdomen with sparse and inconspicuous hairs, moderately convex dorsally and ventrally. Dorsal and ventral surface blackish with antennae and tarsi lighter, or dorsal surface blackish with elytra brightly brownish orange, ventral surface yellowish brown with metaventrite darker (Figs 1–4).

Dorsal habitus: Head somewhat depressed with medium-sized eyes, punctures larger than eye-facets. Lobes of labrum clearly exposed with short excision (Fig. 5). Mandible exposed from under lobes of labrum, with four small teeth on apical edge (Fig. 15). Length of antenna subequal with head width, scape subcylindrical, slightly curved and about 1.5 times as long as wide, pedicel approximately subcylindrical and nearly 1.5 times as long as wide, antennomere 3 narrowed basally, antennomeres 3 and 4 longer than wide, antennomere 4 longer than antennomere 5, each of antennomeres 5–8 wider than long, antennal club compact and asymmetrical, with length nearly 0.6 times of total antennal length, antennomere 11 shorter than antennomeres 9–10 together (Fig. 8). Pronotum widest at base and arcuately narrowed to apex; anterior edge
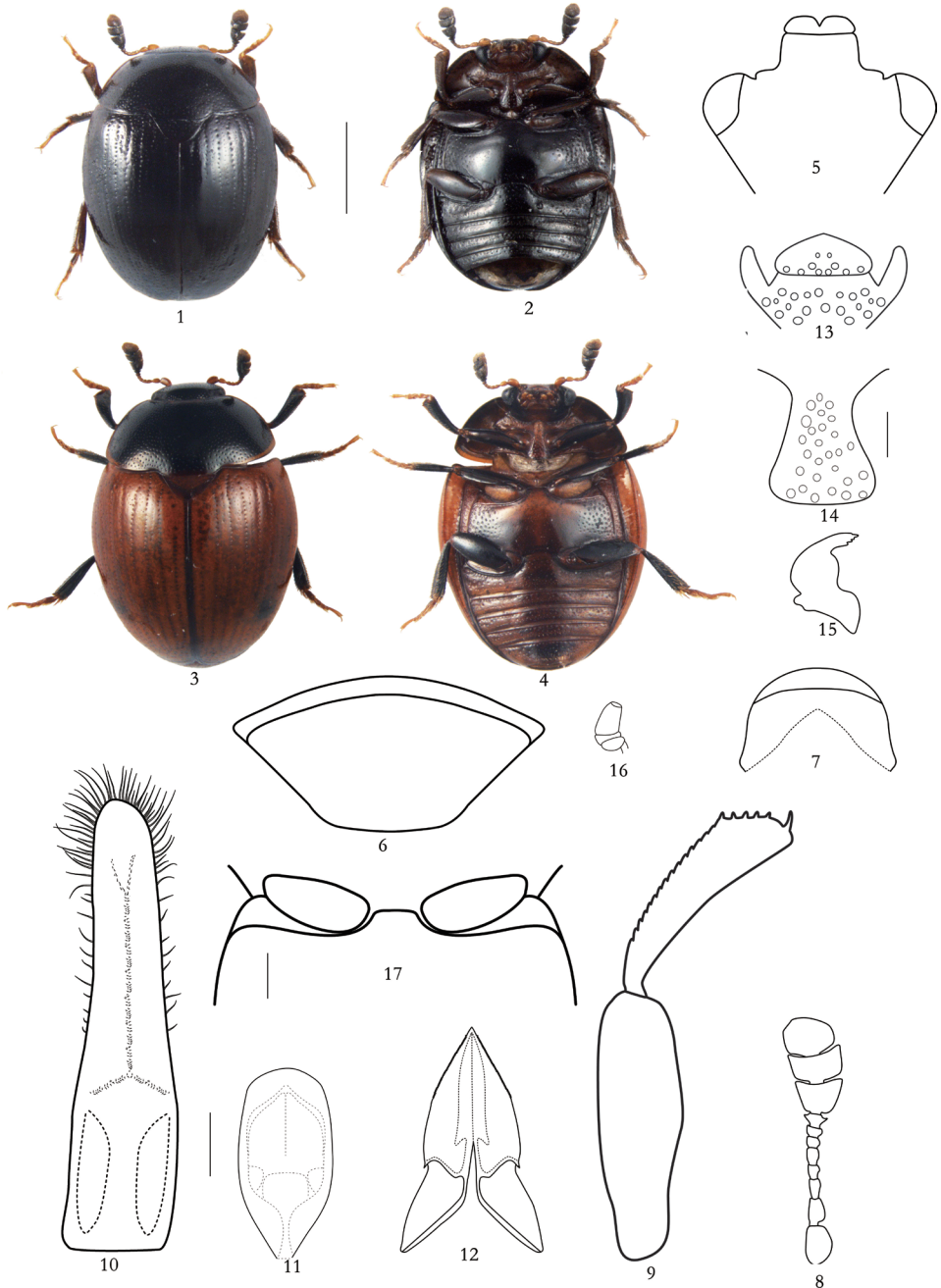
Figures 1–17. *Neopallodes nigrescens* sp. nov. (male) **1, 3** body, dorsal **2, 4** body, ventral **5** head, dorsal **6** pygidium **7** anal sclerite, ventral **8** left antenna, dorsal **9** left profemur and protibia, dorsal **10** tegmen, dorsal **11** penis trunk, dorsal **12** ovipositor, ventral **13** mentum and inner edges of antennal grooves, ventral **14** prosternal process, ventral **15** left mandible, dorsal **16** left maxillary palpus, ventral **17** anterior part of mesoventrite, ventral **1–2, 5–17** specimen from "Yunnan Province, Chuxiong City, Zixi Mountain" **3, 4** specimen from "Yunnan Province, Dali City, Cangshan Mountain" Scale bars: 1 cm (**1–4**); 0.2 cm (**5–12**); 0.2 cm (**13–16**); 0.2 cm (**17**).

deeply emarginate; posterior edge vaulted with clear projection covering base of scutellum, anterior and posterior angles blunt; surface with punctures round, slightly smaller than eye-facets and separated by 2.7–5.7 puncture diameters; interspaces smooth to alutaceous. Scutellum subtriangular with round apex, with punctures scattered and separated by 0.7–1.9 puncture diameters. Elytra about 0.9 times as long as wide together, widest at basal 1/3; surface with regular longitudinal rows of large punctures separated by 0.8–1.3 diameters in rows; rows separated from each other by 5.3–6.9 puncture diameters; interspaces microreticular, between rows of large punctures with irregular row of very fine and sparse punctures. Pygidium markedly wider than long, subtruncate at apex and with dense punctures subequal to those on pronotum (Fig. 6). Anal sclerite slightly wider than long (Fig. 7).

Ventral habitus: Terminal maxillary palpomere elongate and subconical (Fig. 16). Terminal labial palpomere narrowing apically. Mentum pentagonal with sparse, large punctures along posterior edge (Fig. 13). Antennal grooves strongly convergent behind mentum. Prosternum convex medially, with moderately subflattened process, slightly widened at subtruncate apex, and about 1.7 times as wide as scape. Mesoventrite moderately carinate. Metaventrite with finer punctures in middle and coarser punctures laterally. Metepisternum somewhat narrower than antennal club and with distinct, large punctures. Epipleura almost 0.6 times as wide as antennal club long. Abdominal ventrite 1 longest, about 1.6 times as long as hypopygidium and 2.1 times longer than each of ventrites 2–4. Hypopygidium rounded at apex. Submesocoxal line almost rectilinearly deviating from posterior edge of mesocoxal cavity (Figs 2, 4). Distance between metacoxae more than three times as great as that between procoxae, and about twice as great as that between mesocoxae.

Protibia artcuately curved, about as wide as antennal club, with rounded outer apical angle and with apical angle round (Fig. 9); meso- and metatibiae almost subtriangular and slightly narrower than protibia, both with rows of dense setae along outer edge. Femora 1.8 times as wide as corresponding tibiae. Metatarsus shorter than corresponding tibia.

Male genitalia: Tegmen narrow, strongly sclerotized and rounded apically, about 4.3 times as long as wide, with short setae disposed along middle of tegmen and forming an X-like figure; also with long setae along sides and at apex (Fig. 10). Penis trunk about 2.1 times as long as wide and 0.4 times long as tegmen, with apex widely rounded and with two wide apical lobes narrowed apically (Fig. 11).

Female: Body size: length 2.9–3.5, width 2.1–2.8 mm. Ovipositor moderately sclerotized, gonocoxal apex acuminate (Fig. 14).

Variability. Some variation is observable in coloration and punctures. The holotype and paratypes from Chuxiong City, Zixi Mountain, and Qujing City, Yehuagou (all Yunnan Province) are subunicolorous black, while the paratypes from Dali City, Cangshan Mountain, and Qujing City, Junzi Mountain (all Yunnan Province) and from Bijie City, Shangdi Mountain (Guizhou Province) are blackish with brightly brownish elytra.

Diagnosis. *Neopallodes nigrescens* can be distinguished from other species of the genus *Neopallodes* by its unique body color (dorsal surface blackish or with elytra brightly brownish orange), elytra with regular longitudinal rows of large punctures and not quite regular longitudinal rows of small punctures arranged alternately and tegmen

with short setae forming an X-like figure. This taxon is similar to *N. inermis*, but differs from it in: antennal club distinctly shorter than antennomeres 2–8 combined; metaventrite with fine punctures in the middle and with large, sparse punctures laterally; tegmen with short setae forming an X-like figure; penis trunk with round apex.

Name derivation. The specific epithet is derived from the Latin word "*nigrescens*" (= blackening) referring to the color of dorsal surface of most specimens.

Neopallodes dentatus **Grouvelle, 1892**
Figs 18, 21, 22

Neopallodes dentatus Grouvelle 1892: 849
Neopallodes dentatus Kirejtshuk 1994: 230

Material examined. 26♂♂, 22♀♀, China: Yunnan Province, Chuxiong City, Zixi Mountain, 2450 m a.s.l., 25°00'59"N, 101°24'10"W, 13-VIII-2018, Xiaoxiao CHEN (NWAFU); 2♂♂: Shaanxi Province, Ziyang County, Fenghuang Mountain Bell and Drum Tower Scenic Area, 27-VI-2018, Yuru YANG (NWAFU).

Distribution. China (Yunnan, Shaanxi), Myanmar

Neopallodes falsus **Grouvelle, 1913**
Figs 19, 23, 24

Pallodes harmandi Grouvelle 1903:117, non Grouvelle 1902: 17; Grouvelle 1908: 392; Grouvelle 1913:169
Pallodes falsus Grouvelle, 1913b: 398
Neopallodes lindskogi Kirejtshuk 1987: 158
Neopallodes falsus Kirejtshuk 1994: 237

Material examined. 3♂♂, China: Yunnan Province, Yuxi City, Ailao Mountain, 2200 m a.s.l., 20-VII-2017, Xiaoxiao CHEN (NWAFU); 7♂♂, 6♀♀, China: Yunnan Province, Qujing City, Junzi Mountain, 2150 m a.s.l., 14-VII-2017, 30-VII-2018, Xiaoxiao CHEN (NWAFU).

Distribution. China (Yunnan), India, Japan, Myanmar, Nepal

Neopallodes vietnamicus **Kirejtshuk, 1987**
Figs 20, 25, 26

Neopallodes vietnamicus Kirejtshuk 1987: 152.

Material examined. 1♂, China, Yunnan Province, Yuxi City, Mopanshan Forest Park, 2300 m a.s.l., 22-VI-2016, Meike LIU (NWAFU); 2♂♂, China, Yunnan Province,
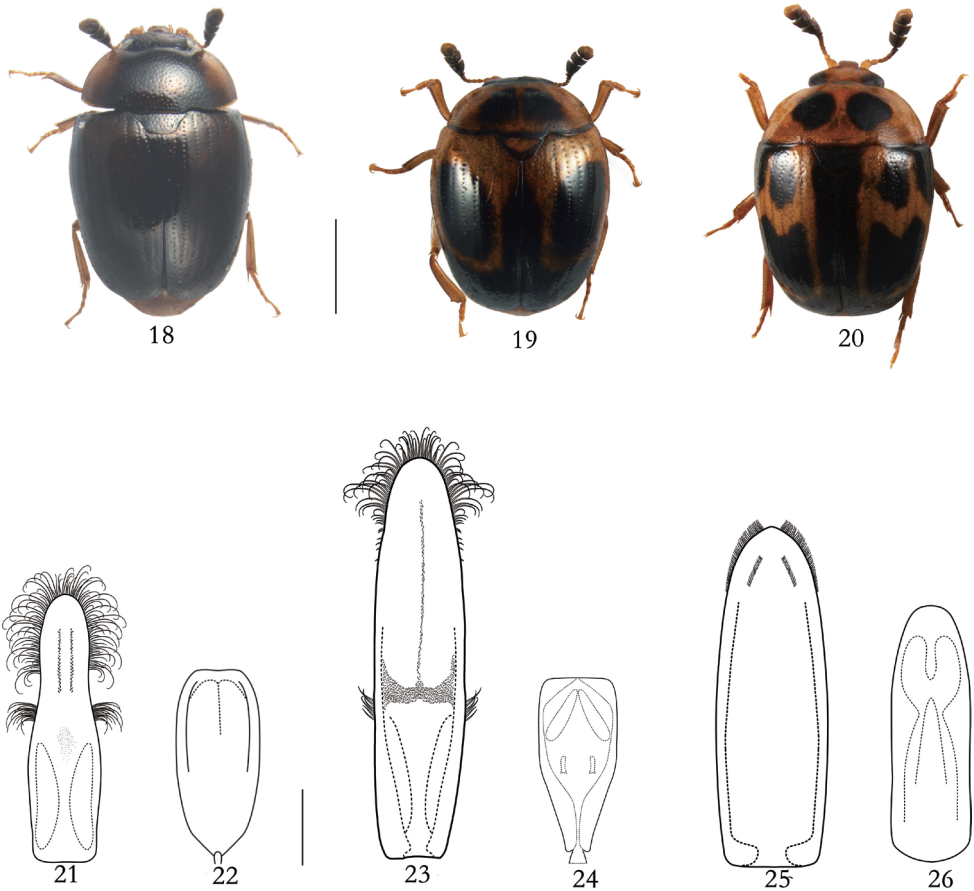
Figures 18–26. *Neopallodes dentatus*, *N. falsus*, and *N. vietnamicus* **18, 21, 22** *N. dentatus* (male): **18** dorsal view **21** tegmen, dorsal **22** penis trunk, dorsal. **19, 23, 24** *N. falsus* (male): **19** dorsal view **23** tegmen, dorsal **24** penis trunk, dorsal. **20, 25–26** *N. vietnamicus* (male): **20** dorsal view **25** tegmen, dorsal **26** penis trunk, dorsal. Scale bars: 1 cm (**18–20**); 0.2 cm (**21–26**).

Yuxi City, Ailao Mountain, 2220 m a.s.l., 20-VII-2017, Xiaoxiao CHEN (NWAFU); 1♂, China: Yunnan, Qujing City, Junzi Mountain, 2300 m a.s.l., 14-VII-2017, Xiaoxiao CHEN (NWAFU).

Distribution. China (Yunnan), India, Myanmar, Vietnam

Acknowledgements

References

Chûjô M, Lee CE (1992) Nitidulidae from Chejudo Island. Esakia 32: 19–24. https://doi.org/10.1295/polymj.24.1301

Grouvelle A (1892) Viaggio de Leonardo Fea in Birmania e regioni vicine. Annali del Museo Civico di Storia Naturale, Genova 12: 833–868.

Grouvelle A (1896) Descriptions de clavicorens d'Afrique et de Madagascar Annales de la Société Entomologique de France 65: 76–78.

Grouvelle A (1902) Coléoptères recueillis dans le Japon central par M. le Dr. Harmand. Bulletin du Muséum National d'Histoire Naturelle, Paris 8: 15–17.

Grouvelle A (1903) Clavicornes de l'Inde septentrionale récoltés par M. Harmand. Annales de la Société Entomologique de France 72: 108–124.

Grouvelle A (1906) Contribution a l'étude des coléoptéres de Madagascar, Nitidulidae, Colydiidaem, Cucujidae, Monotomodae, Cryptophagidae, Dryopidae, Heteroceridae. Annales de la Société Entomologique de France 75: 84–92.

Grouvelle A (1913a) Byturidae, Nitidulidae. In: Schenkling S (Ed.) Coleopterorum catalogus, pars 56. W. Junk, Berlin 15, 223 pp.

Grouvelle A (1913b) Coléoptéres de la région indienne. Annales de la Société Entomologique de France 80: 1–398.

Hayashi N (1978) A contribution to the knowledge of the larvae of Nitidulidae occurring in Japan (Coleoptera: Cucujoidea). Insecta Matsumurana (NS) 14: 1–98.

Kirejtshuk AG (1987) New species of the complex of genera closely related to *Cyllodes* Erichson (Coleoptera, Nitidulidae) from Indochina and adjacent territories. In: Medvedev LN (Ed.) Entomofauna V'etnama. Nauka, Moscow, 157–164. [in Russian with English summary]

Kirejtshuk AG (1992) Sem. Nitidulidae-Blestyanki. In: Ler PA (Ed.) Opredelitel'nasekomykh Dal'nego Vostoka SSSR v shesti tomakh. Tom III. Zhestkokrylye, ili zhuki. Nauka, Sankt-Petersburg, 114–209. [in Russian with English summary]

Kirejtshuk AG (1994) Revision of the genus *Neopallodes* Reitter 1884 (Coleoptera Nitidulidae) from the Palaearctic and Indo-Malayan regions. Tropical Zoology 7: 225–253. https://doi.org/10.1080/03946975.1994.10539256

Kirejtshuk AG (2008) A current generic classification of sap beetles (Coleoptera, Nitidulidae). Zoosystematica Rossica 17: 107–122.

Kirejtshuk AG (2011) "*Paradoxal*" new genus and species of the family Nitidulidae (Polyphaga: Coleoptera) from Afro-Madagascarean and Australian Regions. Zoosystematica Rossica 20: 274–298.

Kurosawa Y, Hisamatsu S, Sasaji H (1985) The Coleoptera of Japan in Color. Vol. 3. Osaka Hoikusha Publishing Co., 500 pp. [in Japanese with English summary]

Leschen RAB (1999) Systematics of Nitidulinae (Coleoptera: Nitidulidae): phylogenetic relationships, convexity and the origin of phallalophagy. Invertebrate Taxonomy 13: 845–882. https://doi.org/10.1071/IT98016

Parsons CT (1943) A revision of Nearctic Nitidulidae (Coleoptera). Bulletin of the Museum of Comparative Zoology 92: 1–278. [213 pls]

Liu T (2014) Development status, problems and countermeasures of wild mushroom industry in Yunnan. Contemporary Economics 19: 86–87. [in Chinese]

Reitter E (1884) Die Nitiduliden Japans. Wiener entomologische Zeitung 3: 257–272, 299–302. https://doi.org/10.5962/bhl.part.13811

Reitter E (1877) Beitrage zur Kaferfauna von Japan. Deutsche entomologische Zeitschrift 21: 369–384. https://doi.org/10.1002/mmnd.4800210221

Yamashita S, Hiji N (2007) Resource use pattern of a mycophagous beetle, *Neopallodes inermis* (Coleoptera, Nitidulidae) on soft fungi, *Collybia* spp. (*Agaricales*). Annals of the Entomological Society of America 100: 222–227. https://doi.org/10.1603/0013-8746(2007)100[222:RUPOAM]2.0.CO;2

REVIEW ARTICLE

A review of the genus *Brachytrycherus* Arrow (Coleoptera, Endomychidae) of mainland China with descriptions of three new species

Ling-Xiao Chang[1], Wen-Xuan Bi[2], Guo-Dong Ren[3]

1 *Science Research Department, Beijing Museum of Natural History, Beijing 100050, China* **2** *Room 401, No. 2, Lane 155, Lianhua South Road, Shanghai, 201100, China* **3** *College of Life Sciences, Hebei University, Baoding 071002, China*

Corresponding author: *Guo-Dong Ren* (gdren@hbu.edu.cn)

Citation: Chang L-X, Bi W-X, Ren G-D (2019) A review of the genus *Brachytrycherus* Arrow (Coleoptera, Endomychidae) of mainland China with descriptions of three new species. ZooKeys 880: 85–112. https://doi.org/10.3897/zookeys.880.34712

Abstract

This paper presents a review of the genus *Brachytrycherus* Arrow from mainland China. Three new species are described and illustrated: *B. bipunctatus* Chang & Bi, **sp. nov.**, *B. denticulatus* Chang & Bi, **sp. nov.**, and *B. humeralis* Chang & Bi, **sp. nov.** The diagnosis, distribution, type locality, biology, and ecology are provided for each species. A key to the species of *Brachytrycherus* known in China is updated.

Keywords

Coleoptera, Endomychidae, new species, taxonomy, China

Introduction

Arrow (1920) established *Brachytrycherus* for two new species from India, *B. perotteti* and *B. madurensis*. This genus belongs to the largest endomychid subfamily Lycoperdininae. In 2005, *Brachytrycherus* was placed in the Amphisternus-group with seven other genera by Tomaszewska (2000, 2005), based on the following characters: mesoventrite with intercoxal process widened laterally towards apex, overlapping parts of coxae, elytra with basal margins thickened and raised, mandible with apical tooth widely chisel-shaped, and male genital segment with an additional internal V- or U-shaped sclerite.

The most recent synopsis of the tribe Amphisternini (Amphisternus-group) was completed by Strohecker (1964), wherein he treated and listed four species of *Brachytrycherus*, and also provided a key to the species of *Brachytrycherus* known at that time. Strohecker (1971) then transferred two species from *Engonius* Gerstaecker to the genus *Brachytrycherus*: *E. opimus* Gorham, 1896 (= *Engonius gemmatus* Arrow, 1928) and *E. femoralis* Arrow, 1928). Shockley et al. (2009a) listed six species in the updated checklist of the entire family. Since then, Chang et al. (2016) described two new species from China, *B. conaensis* and *B. curviantennae*. Furthermore, *B. conaensis* is the first species of the Handsome fungus beetles recorded feeding on Ascomycetes. Prior to the present study, this genus included eight species (Table 1).

During the examination of the Endomychidae collected in China, three new species were recognized and are described here. The recent key of Chang et al. (2016) to species of *Brachytrycherus* known in China is modified and updated.

Table 1. Known species of *Brachytrycherus* and distribution.

Species	Distribution
B. conaensis Chang et al., 2016	China (Xizang)
B. concolor Arrow, 1937	Borneo
B. convexus Strohecker, 1964	India
B. curviantennae Chang et al., 2016	China (Xizang)
B. femoralis (Arrow, 1928)	China (Guangxi), Laos, Vietnam
B. gemmatus (Arrow, 1928)	Laos, Myanmar, Thailand
B. madurensis Arrow, 1920	China (Taiwan), India
B. perotteti Arrow, 1920	India

Materials and methods

Type specimens of the new species described here are deposited in the following institutions or private collections:

BJMNH   Beijing Museum of Natural History, Beijing, China
CBWX   Collection of Wen-Xuan Bi, Shanghai, China
CCLX   Collection of Ling-Xiao Chang, Beijing, China
CSHT   Collection of Hai-Tian Song, Fujian, China
IZCAS   Institute of Zoological, Chinese Academy of Sciences, Beijing, China
MHBU   Museum of Heibei University, Baoding, China
MZPW   Museum and Institute of Zoology, Polish Academy of Sciences, Warszawa, Poland
SHNU   Shanghai Normal University, Shanghai, China

Specimens were examined and described using a Nikon SMZ800 dissecting microscope. The following measurements were made using a Leica M205A dissecting microscope: body length from apical margin of clypeus to apex of elytra; width across both elytra (at widest part); elytral length along suture, including scutellum. The aedea-

gus was boiled in 10% NaOH solution, cleaned, and finally dissected in distilled water. Habitus photos were taken using a Canon Eos 5D III SLR camera and Canon MP-E 65 mm macro lens. All photographs were modified in Adobe Photoshop CC 2015.

Taxonomy

Brachytrycherus **Arrow, 1920**

Brachytrycherus Arrow, 1920: 12.

Type species. *Brachytrycherus perotteti* Arrow, 1920.

Diagnosis. As stated in Chang et al. (2016), species of *Brachytrycherus* resemble those of *Ohtaius* Chûjô and *Gerstaeckerus* Tomaszewska in having the body black or blackish brown, elytral maculae transverse, most often orange or yellow. These genera share the feature of having the mandibles chisel-shaped apically. However, *Brachytrycherus* can be distinguished from these genera by the following combination of characters: 1) body less elongate; 2) head with well-developed gular sutures; 3) mesoventral process with sides parallel; 4) maxillary lacinia with tuft of S-like setae apically (Tomaszewska 2005).

Description (based on Tomaszewska 2005). Body squat-oval to oval, moderately convex to strongly convex, glabrous or minutely pubescent. Colour dark brown to black, usually with orange or yellow markings on elytra.

Head with gular sutures well developed, widely separated, convergent apically. Antennae (Fig. 20A–C) 11-segmented, long and slender or rather stout; antennal club 3-segmented, loose. Mandible with chisel-shaped apical tooth and moderately large subapical tooth. Maxilla with terminal palpomere longer than wide, tapering apically; lacinia with tuft of S-shaped apical spines.

Pronotum transverse, widest near 1/2 of pronotal length or apical 1/3; anterior edge with rater large stridulatory membrane; sides weakly undulate or strongly curved. Prosternal process (Fig. 21A–C) not extending beyond coxae; narrowly separates procoxae, sides weakly curved outwardly or nearly straight, rounded, weakly truncate or emarginate apically. Mesoventral process (Fig. 21A–C) transverse, lateral margins widening apically and overlapping parts of coxae. Elytra anterior edge thickened and raised; sides curved, widest near 1/2 length of elytron; most often with contrasting markings. Tibiae (Fig. 22A–C) most often with sexual characters, in male with different degrees of concavity, curved or tooth.

Abdomen in both sexes with five ventrites. Ventrite V (Fig. 23A–C) almost always with sexual characters, posterior margin in male weakly curved or rounded medially, and/or with longitudinal short wrinkles laterally. Male genital segment with paired apophyses fused along nearly 1/3 of its length basally; dorsal plate undivided; additional, internal, V-shaped sclerite present.

Aedeagus (Fig. 24A–C) rather long, heavily sclerotized, without basal curvature. Median lobe branched apically. Tegmen placed basally, ring-shaped, fused with parameres.

Distribution. Oriental Region (India, Laos, Thailand, South of China).

***Brachytrycherus bipunctatus* Chang & Bi, sp. nov.**
http://zoobank.org/178DF400-CB0E-4775-A034-D1B9C195226C
Figs 1–4

Type material. Holotype (Fig. 1), male, **Hainan**, Fanjia Forest Reserve, 196 m, 19°16.806'N, 109°40.494'E, 17. IV.2016, Xing-Long Bai leg. (MHBU). Paratypes (Fig. 2), 1 female, Hainan, Qiongzhong, Shifangzhen, 22.II.2019, Guo-Dong Ren leg.
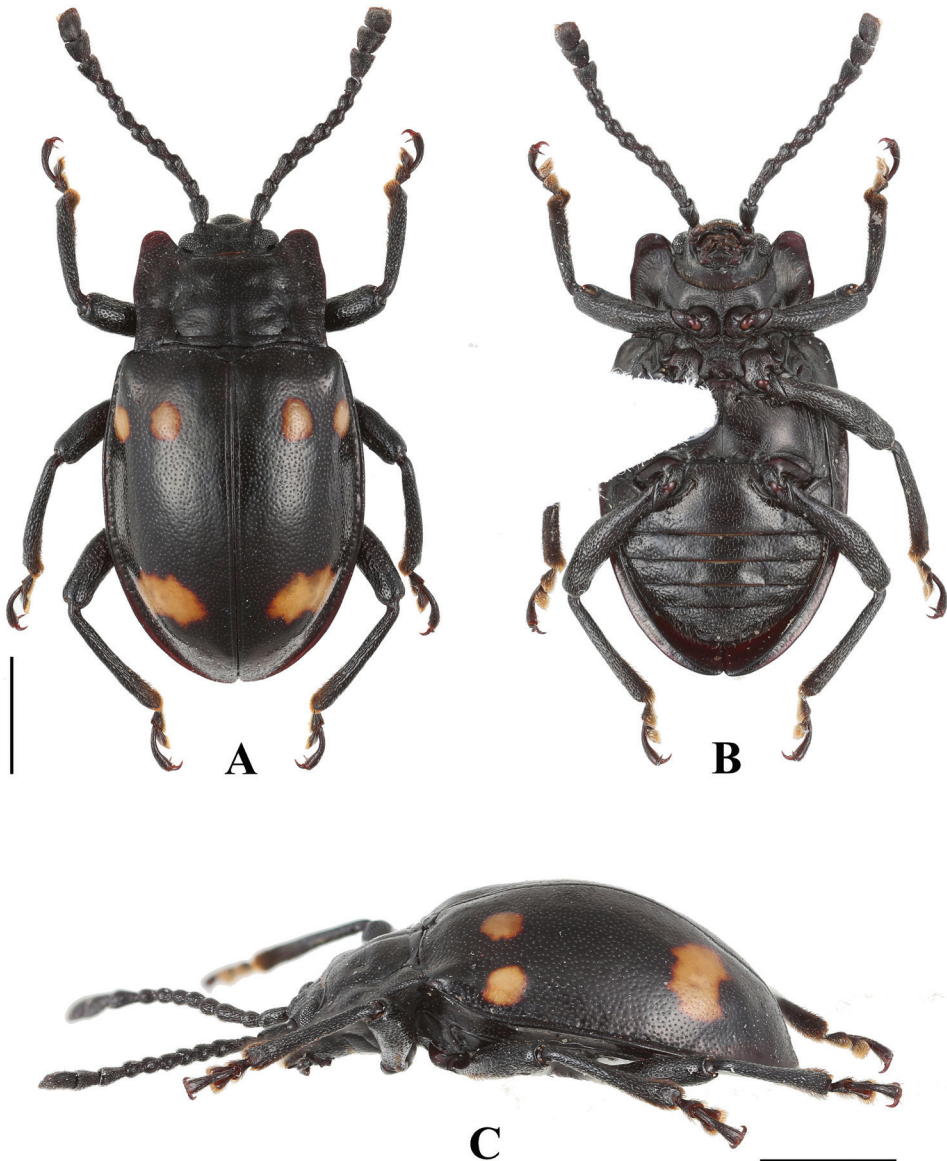
Figure 1. Habitus of *B. bipunctatus* sp. nov. (male). **A** dorsal view **B** ventral view **C** lateral view. Scale bar: 2 mm.
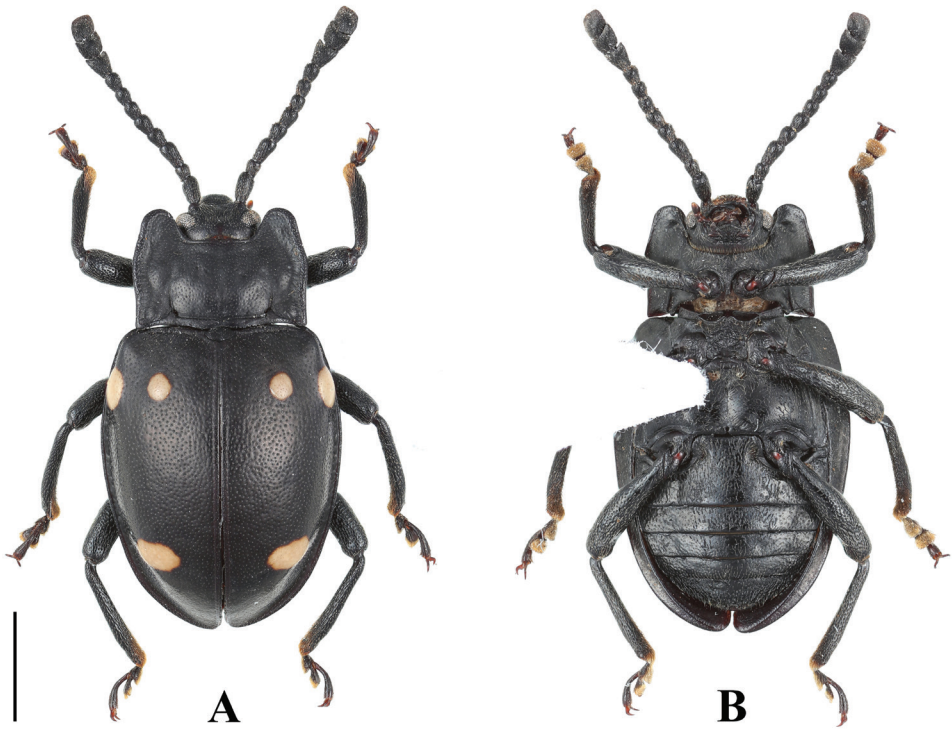
Figure 2. Habitus of *B. bipunctatus* sp. nov. (female). **A** dorsal view **B** ventral view. Scale bar: 2 mm.

(BJMNH); 1 female, Hainan, Dongfang, Mihouling, 11.VI.2008, Yi-Bin Ba & Jun-Tong Lang leg. (MHBU); 2 females, Hainan, Yinggeling. Nankai Township, Fangyuan Village, 21.VII.2013, Bo Cai leg. (CCLX); 1 female, **Yunnan**, Xishuangbanna, Mengla County, Mengla Town, Bubang Village, H: 680 m, 21°36'6"N, 101°35'9"E, Jian-Yue Qiu & Hao Xu leg. (CCLX) (Fig. 2).

Etymology. The specific name is derived from the two apical elytral maculae.

Diagnosis. *Brachytrycherus bipunctatus* can be distinctly separated from all congeners by having two distant spots on the elytral base.

Description. Length 7.6–8.2 mm, width 4.1–4.2 mm. *Body* oval, approximately 2.0 times as long as wide; moderately convex; shiny. Colour black with three yellow maculae on each elytron.

Head. Antenna (Fig. 3A) rather stout, nearly 1/2 body length, with antennomeres 1–8 longer than wide; scape approximately 4.0 times as long as pedicel; antennomere 3 as long as 4 and 5 combined; antennomeres 4–6 nearly length equal; antennomere 6 longer than 7 and antennomere 7 as long as 8; club composed of three antennomeres, moderately broad, weakly flat, loose. Maxilla with terminal palpomere elongated, almost 1.5 times as long as palpomere 3, slightly tapering anteriorly, truncate apically.

Thorax. Pronotum (Fig. 3B) 1.5–1.7 mm long, 2.7–3.1 mm wide; widest near 1/2 of pronotal length; coarsely and densely punctate; anterior and lateral margins moder-
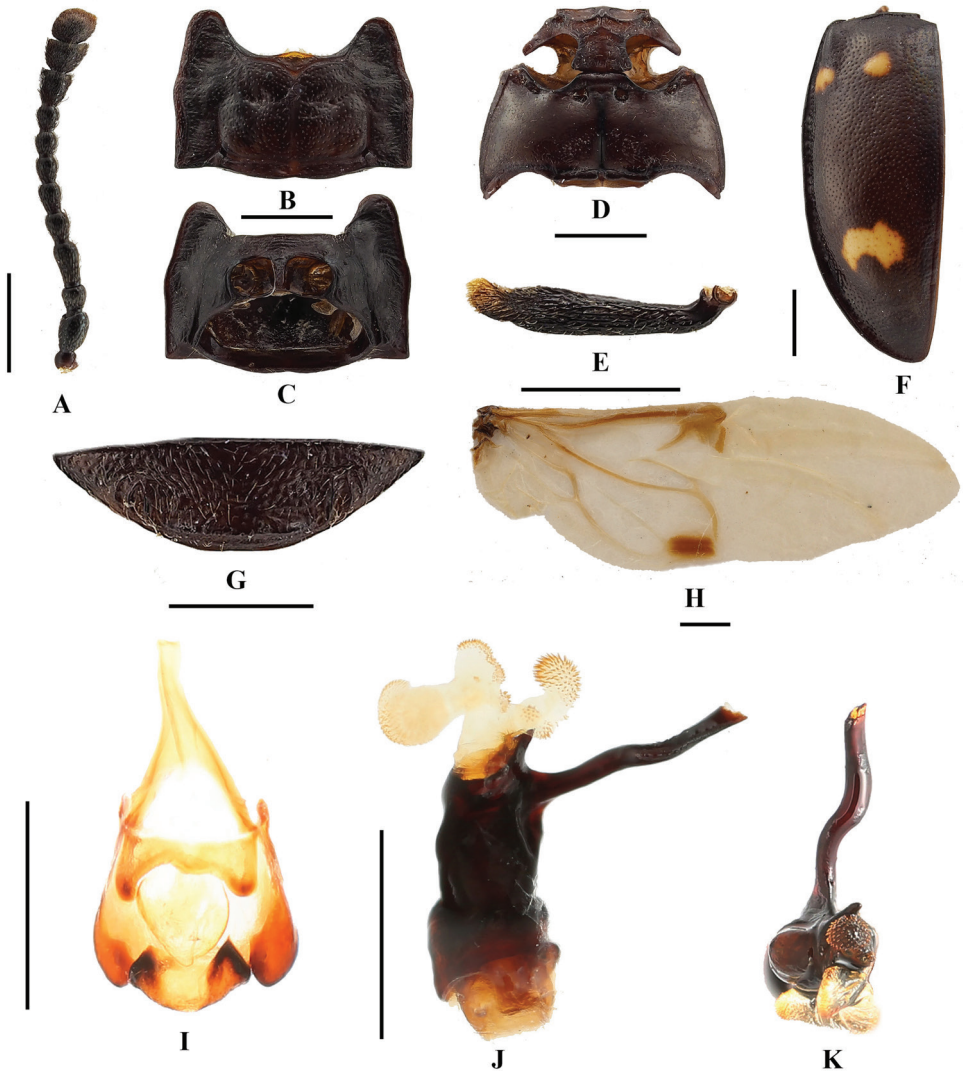
Figure 3. *B. bipunctatus* sp. nov. **A** antenna **B** pronotum **C** proventrite **D** male meso- and metaventrites **E** male protibia **F** elytron **G** male ventrite V of abdomen **H** hind wing **I** male genital segment **J** aedeagus in lateral view **K** aedeagus in apical view. Scale bars: 1 mm.

ately narrowly bordered; anterior edge with rather large stridulatory membrane; sides weakly undulate; front angles produced anteriorly, blunt round; disc weakly convex, two round raised area laterally; transverse wrinkle laterally; median furrow shallow, two small round pits laterally; lateral sulci linear, groove, deep, extending to basal 1/3 length of pronotum; basal sulcus nearly straight, deep. Prosternal process (Fig. 3C) not extending beyond coxae; very narrowly separates procoxae, sides weakly curved outwardly, rounded apically in male; in female rather narrowly, sides nearly straight, weakly truncate apically. Mesoventral process (Fig. 3D) transverse, lateral margins distinctly widening apically in male; in female lateral margins nearly parallel; posterior margin nearly straight.

Figure 4. Habitats of *B. bipunctatus* sp. nov.

Elytra (Fig. 3F) 5.9–6.2 mm long, 3.6–3.9 times as long as and 1.4–1.5 times as wide as pronotum; sides curved, widest near 1/2 length of elytron; densely and coarsely punctate; humeri rather prominent. Each elytron with three orange-yellow maculae. Anterior two elytral maculae nearly oval or round, located behind humeri, size subequal, transverse arrangement, spacing between them subequal diameter of one macula. Posterior macula cloud-form, transverse, outer sides far from elytral lateral margin, inner margin of macula far from elytral suture. Protibia (Fig. 3E) in male with concavity on inner edge of apical 1/4 distinctly, in female without concavity; meso- and metatibiae simple. Hind wing (Fig. 3H) normal.

Ventrite **V** (Fig. 3G) with lateral margins abruptly converging posteriorly, three or four pairs of longitudinal short wrinkles laterally; posterior margin weakly curved medially in male; in female ventrite V lateral margins gently converging posteriorly, without longitudinal wrinkles; posterior margin bluntly round medially. Male genital segment (Fig. 3I) with paired apophyses fused along nearly half of its length apically; dorsal plate undivided; additional, internal, V-shaped sclerite present.

Aedeagus (Fig. 3J–K) rather long, heavily sclerotized, straight. Median lobe branched apically; branch long, in apical view longitudinal Z-shaped; truncate apically. Tegmen placed basally, comparatively large, ring-shaped, parameres rectangle, fused with tegmen.

Biology and ecology. The holotype was hand collected by simple searching, as it is active under the fallen decayed wood in the day (Fig. 4).

Brachytrycherus denticulatus **Chang & Bi, sp. nov.**
http://zoobank.org/E1E38FED-0977-4275-B16A-AF99873C1E60
Figs 5–9

Type material. Holotype (Fig. 5), male, Guangxi, Jinxiu, Guangxi Dayaoshan Nature Reserve Bureau Yinshan Protection Station, 13.VIII.2015, Ling-Xiao Chang leg. (MHBU). Paratypes (Fig. 6), 1 female, same data as holotype (BJMNH); 1 female, Guangxi, Damingshan, Hao-Yu Liu & Ji-Bin Liang leg. (MHBU); 1 male, Guangxi
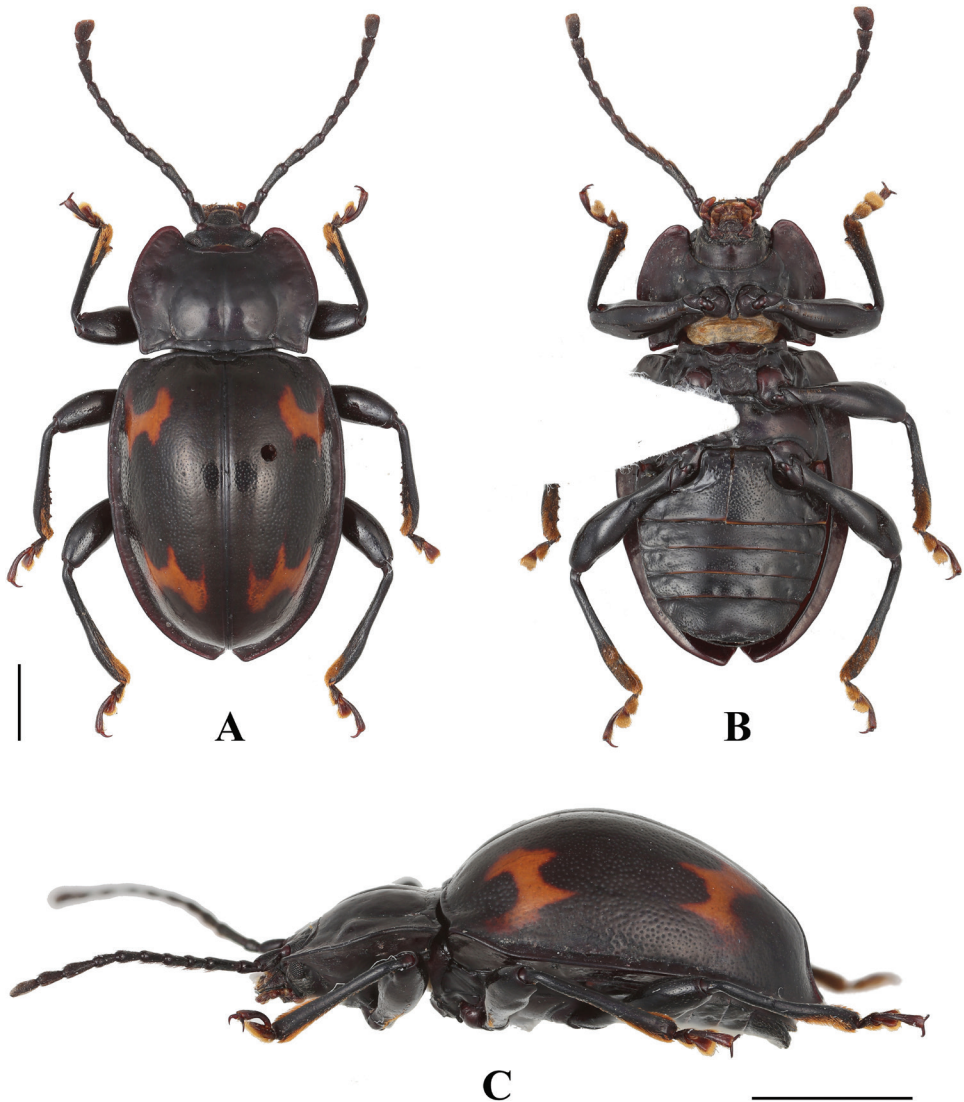
Figure 5. Habitus of *B. denticulatus* sp. nov. (male). **A** dorsal view **B** ventral view **C** lateral view. Scale bars: 2 mm.
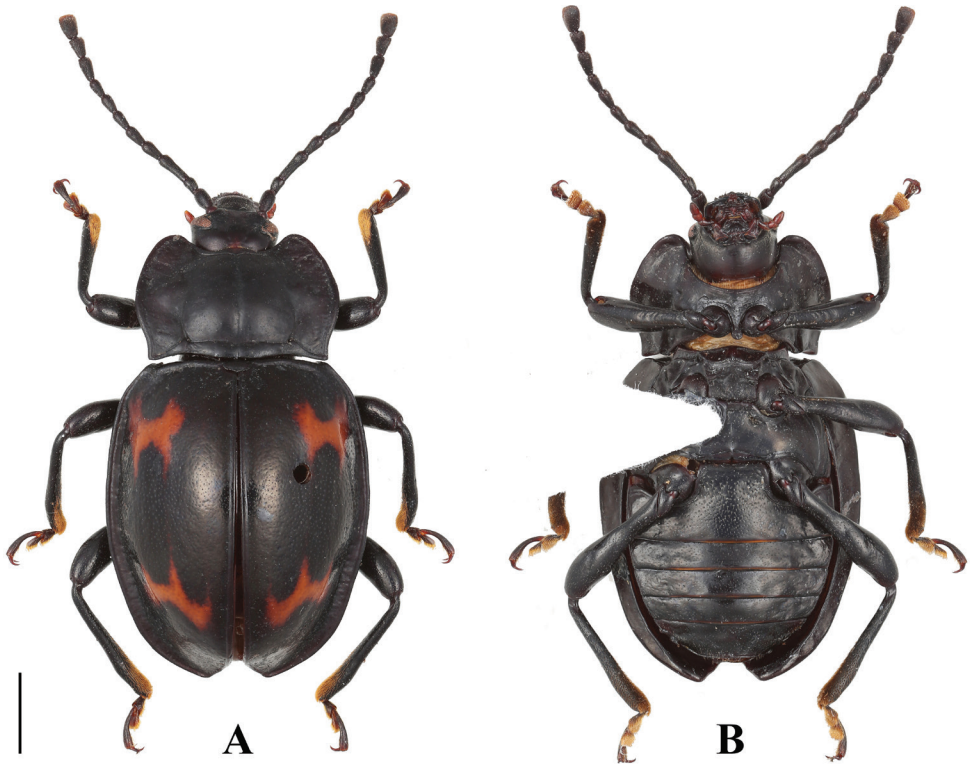
Figure 6. Habitus of *B. denticulatus* sp. nov. (female). **A** dorsal view **B** ventral view. Scale bar: 2 mm.

Prov., Jinxiu County, 16 km, 29.VII.2011, alt. 882–950 m, PENG Zhong leg. (dissected, SHNU); 1 male, Guangxi Prov., Damingshan, Tianping Protect Station, N23.49811, E108.43715, 1230 m, 22.V.2011 N, Xing-Lei Huang Coll. (IZCAS); 1 female, same data except 28.V.2011 (IZCAS); 1 male, Guangxi, Jinxiu, Jiuwanshan, 4.VIII.2015 N, Ling-Xiao Chang leg. (CCLX); 1 male, Guangxi, jinxiu, Yinshan Protection Station, 27.VIII.2016, Yu-Yang Lei leg. (CCLX); 1 male, Guangxi, jinxiu, Dayaoshan, 22-24.IV.2018, Chun-Fu Feng leg. (CCLX); 6 males, 5 females, Guangxi, Damingshan, 1200 m, 28–31.VII.2012, Wen-Xuan Bi leg. (CBWX); 1 male, 1 female, Guangxi, Damingshan, 1200 m, 31.VII.2012, Xiao-Bin Song leg. (CBWX); 1 female, Guangxi, Jinxiu, Yinshanbaohuzhan, 1200 m, 9.VII.2014, Xiao-Bin Song leg. (CBWX); 2 males, 2 females, same data except 10.VII.2014 (CBWX); 1 male, Guangxi, Jinxiu, Laoshanlinchang, 850 m, 18.VII.2014, Xiao-Bin Song leg. (CBWX); 1 male, Guangxi, Nanning, Wuming, Damingshan, N23.49944, E108.44154, 1204 m, 7.VIII.2011, Hai-Tian Song leg. (CSHT).

Etymology. The name refers to the mesotibia serrulated on inner edge in male.

Diagnosis. *Brachytrycherus denticulatus* resembles *B. convexus* in the elytra being strongly convex; posterior elytral maculae transverse, dentate; hind wing reduced to narrow straps. Antenna with club rather narrow (vs. broad in *B. convexus*); *B. denticulatus*
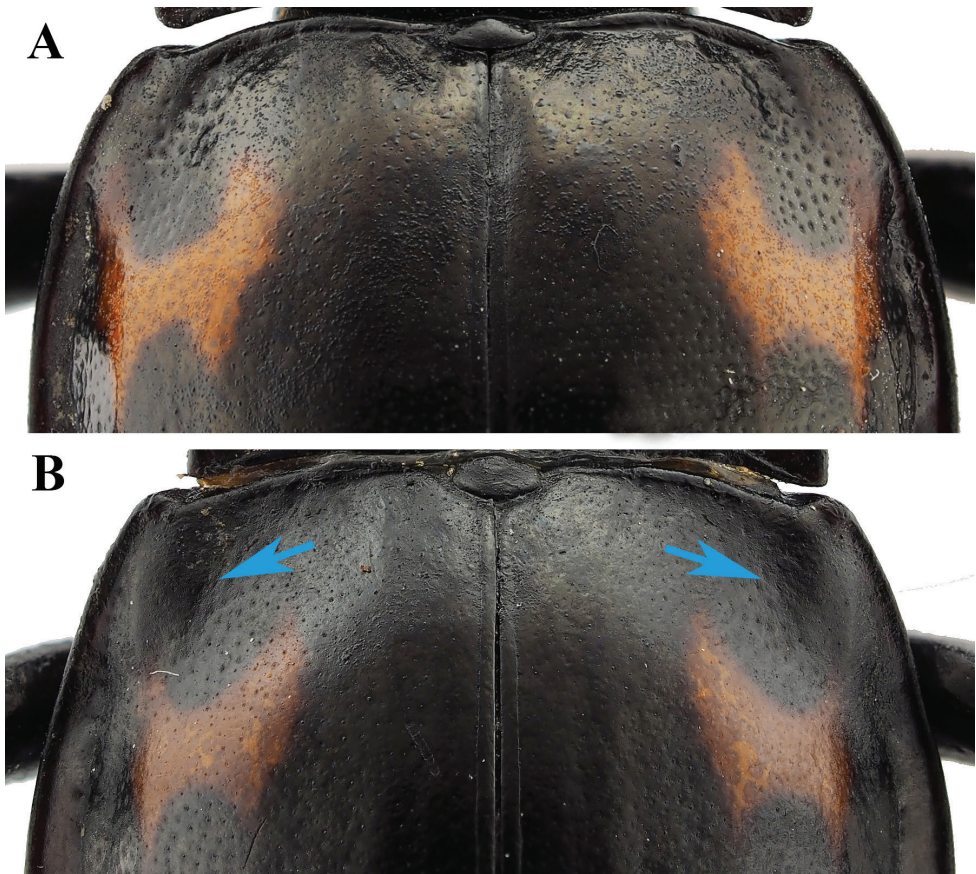
Figure 7. Humeri. **A** *B. denticulatus* sp. nov. **B** *B. humeralis* sp. nov.

pronotum sides strongly curved (vs. weakly rounded and somewhat convergent basally); elytron widest near 1/2 length of elytron (vs. beyond mid-length). *Brachytrycherus denticulatus* is extremely similar to *B. humeralis* sp. nov. in appearance, but the humeri (Fig. 7A) are not distinctly prominent, protibia in male with small sharp tooth near apical 1/4 on inner edge, and mesotibia serrulated on inner edge in male can distinguish *B. denticulatus* from *B. humeralis*.

Description. Length 10.2–13.7 mm, width 5.7–6.9 mm. *Body* broadly oval, approximately 1.8–2.0 times as long as wide; strongly convex; shiny. Colour black with two red-brown maculae on each elytron.

Head. Antenna (Fig. 8A) long and slender, nearly 1/2 body length, with antennomeres 1–8 distinctly longer than wide; scape approximately 4.0 times as long as pedicel; antennomere 3 nearly as long as 4 and 5 combined; antennomere 4 as long as 5, antennomeres 5–8 gradually shorter; club composed of three antennomeres, narrow and moderately flat. Maxilla with terminal palpomere elongate, almost 2.0 times as long as palpomere 3, tapering anteriorly, truncate apically.

Thorax. Pronotum (Fig. 8B) 2.6–3.3 mm long, 4.4–5.4 mm wide; widest behind 1/2 of pronotal length; surface opaque; lateral margins narrowly bordered,
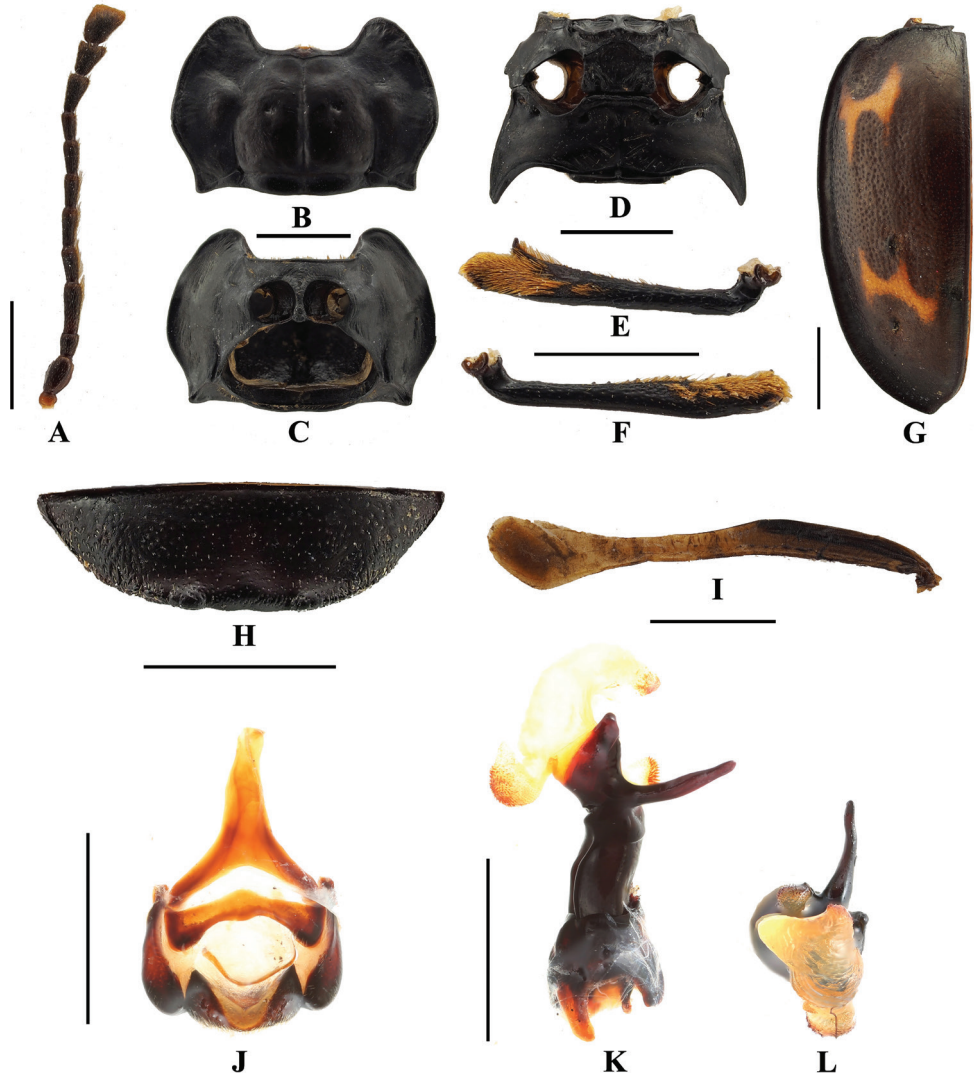
Figure 8. *B. denticulatus* sp. nov. **A** antenna **B** pronotum **C** provenrite **D** meso- and metaventrites **E** male protibia **F** male mesotibia **G** elytron **H** male ventrite V of abdomen **I** hind wing **J** male genital segment **K** aedeagus in lateral view **L** aedeagus in apical view. Scale bars: 1 mm.

sides strongly curved; front angles produced anteriorly, bluntly round; disc weakly convex, with two large round raised areas laterally; transverse wrinkle laterally; median furrow distinct, straight; lateral sulci linear, curved, deep, extending to 1/2 of pronotal length; basal sulcus nearly straight, deep. Prosternal process (Fig. 8C) moderately separates the procoxae, slightly extending beyond coxae; sides curved outwardly, round apically. Mesoventral process (Fig. 8D) transverse, lateral margins barely widening apically, overlapping part of mesocoxae; posterior margin rather straight.

Elytra (Fig. 8G) 7.4–9.3 mm long, 1.3 times as long as wide; 2.8 times as long as and 1.3 times as wide as pronotum, sides curved, widest near 1/2 length of elytron;

Figure 9. Habitats of *B. denticulatus* sp. nov.

densely and moderately coarsely punctate; humeri not prominent. Each elytron with two transverse, irregularly shaped red-brown maculae. Anterior elytral macula bowtie-shaped, located behind humerus, its anterior and posterior margins broadly U-shaped and deeply emarginate. Posterior macula crown-shaped, located at apical 1/3, its anterior margin tridentate, posterior margin widely U-shaped and deeply emarginate. Protibia (Fig. 8E) in male with small sharp tooth near apical 1/4 on inner edge, in female without tooth; mesotibia (Fig. 8F) serrulated on inner edge in male, not serrulated in female. Hind wing (Fig. 8I) reduced to narrow straps, oval shape apically, no longer than the elytra.

Ventrite **V** (Fig. 8H) with lateral margins gently converging posteriorly; posterior margin in male with some small lateral tubercles, one raised area medially; in female ventrite V with posterior margin simple, weakly emarginate medially. Male genital segment (Fig. 8J) with paired apophyses fused along nearly 1/3 of its length basally; dorsal plate undivided; additional, internal, V-shaped sclerite present.

Aedeagus (Fig. 8K, L) rather long, heavily sclerotized, straight. Median lobe branched apically; branch moderately long and rather straight, flat and round apically. Tegmen placed basally, comparatively large, ring-shaped; parameres rather large, rectangle, fused with tegmen.

Biology and ecology. The adults were collected by hand collected from a large pile of dead bamboos in the day (Fig. 9).

Brachytrycherus humeralis Chang & Bi, sp. nov.

http://zoobank.org/99D5DA5E-DB6E-4FB1-A254-FEFBF472B40A

Figs 10–13

Type material. Holotype (Fig. 10), male, Guangxi, Huanjiang, Yangmeiao Protection Station, 4.VIII.2015 N, Ling-Xiao Chang leg. (MHBU). Paratypes (Fig. 11), 1 female, same data as holotype (BJMNH); 1 male, same data as holotype (CCLX); 1 male,
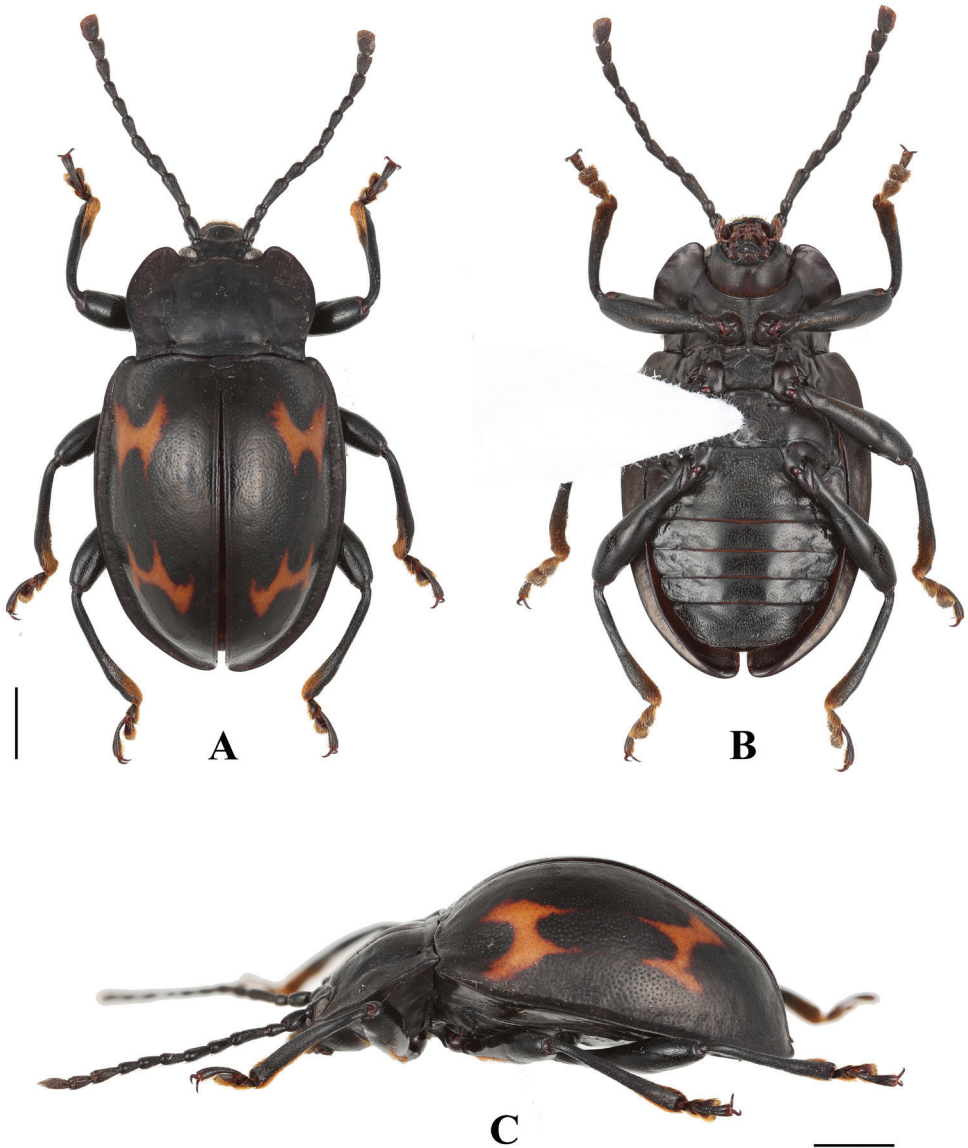
Figure 10. Habitus of *B. humeralis* sp. nov. (male). **A** dorsal view **B** ventral view **C** lateral view. Scale bars: 2 mm.
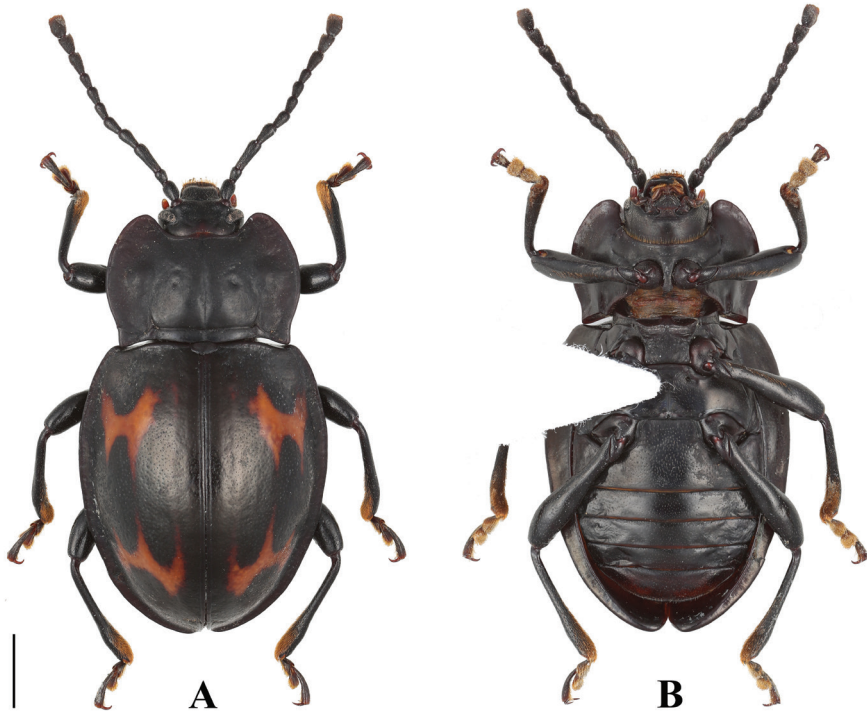
Figure 11. Habitus of *B. humeralis* sp. nov. (female). **A** dorsal view **B** ventral view. Scale bar: 2 mm.

Guangxi, Damingshan, Longteng, Power Station, N23.49811, E108.43715, 1230 m, 20.V.2011 N, Xing-Lei Hhang leg. (IZCAS); 1 male, same data except dissected (IZCAS); 1 female, Guangxi, Jinxiu, Shengtangshan, 700 m, 19.V.1999, Fu-Sheng Huang leg. (I0Z(E)1172359, IZCAS). 1 male, Guangxi, Jinxiu, Yinshan, 27.VIII.2016, Yu-Yang Lei leg. (CCLX).

Etymology. The name refers to the humeri with a distinct raised oval area.

Diagnosis. *Brachytrycherus humeralis* resembles *B. convexus* in the elytra being strongly convex; posterior elytral maculae transverse, dentate; hind wing reduced to narrow straps. However, they can be differentiated by *B. humeralis* with the antennal club that is rather narrow (vs. broad); the pronotum sides are strongly curved (vs. weakly rounded and somewhat convergent basally); and the elytra are widest near 1/2 length of elytron (vs. beyond mid-length). In addition, *B. humeralis* is extremely similar to *B. denticulatus* sp. nov. in appearance. The humeri (Fig. 7B) are distinctly prominent, the protibia in males is without a tooth, raised near apical 1/3 on inner edge, and the simple mesotibia in males can distinguish *B. humeralis* from *B. denticulatus*.

Description. Length 12.5–12.7 mm, width 6.6–7.0 mm. *Body* broadly oval, approximately 1.8–1.9 times as long as wide; strongly convex; shiny. Colour black with two red-brown maculae on each elytron.

Head. Antenna (Fig. 12A) long and slender, nearly 1/2 body length, with antennomeres 1–8 distinctly longer than wide; scape approximately 3.0 times as long as
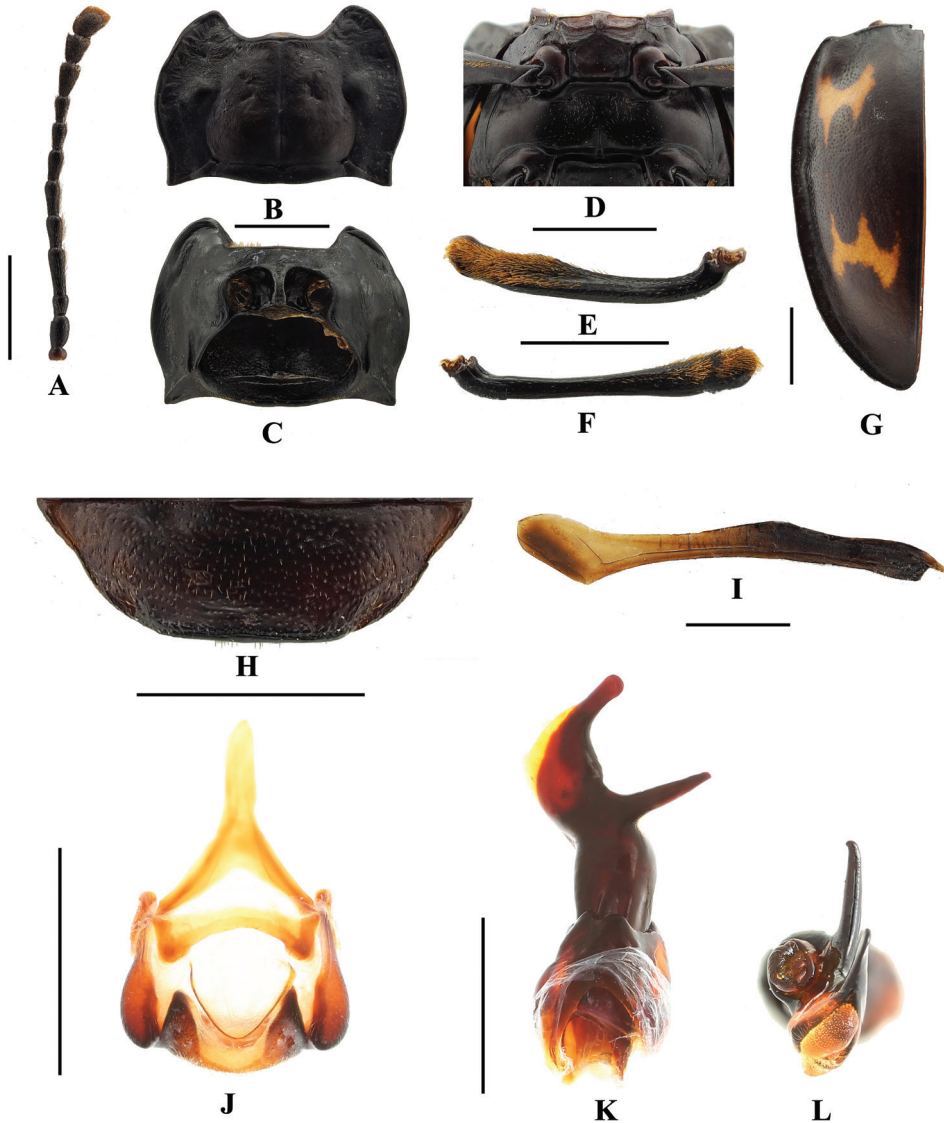
Figure 12. *B. humeralis* sp. nov. **A** antenna **B** pronotum **C** proventrite **D** meso- and metaventrites **E** male protibia **F** male mesotibia **G** elytron **H** male ventrite V of abdomen **I** hind wing **J** male genital segment **K** aedeagus in lateral view **L** aedeagus in apical view. Scale bars: 1 mm.

pedicel; antennomere 3 nearly as long as 4 and 5 combined; antennomere 4 as long as 5, antennomeres 5–8 gradually shorter; club composed of three antennomeres, narrow and moderately flat. Maxilla with terminal palpomere elongate, almost 1.5 times as long as palpomere 3, tapering anteriorly, truncate apically.

Thorax. Pronotum (Fig. 12B) 2.9–3.2 mm long, 5.1–5.3 mm wide; widest 1/2 of pronotal length; surface opaque; lateral margins narrowly bordered, sides strongly curved; front angles produced anteriorly, bluntly round; disc weakly convex, with two large round raised areas laterally; transverse wrinkle laterally; median furrow distinct, straight;

lateral sulci linear, curved, deep, extending to 1/2 of pronotal length; basal sulcus nearly straight, deep. Prosternal process (Fig. 12C) moderately separates the procoxae, slightly extending beyond coxae; sides curved outwardly, round apically. Mesoventral process (Fig. 12D) transverse, lateral margins weakly widening apically and overlapping part of mesocoxae, in some specimens hardly widening apically; posterior margin rather straight.

Elytra (Fig. 12G) 8.9–9.6 mm long, 1.3 times as long as wide; 2.8 times as long as and 1.3 times as wide as pronotum, sides curved, widest near 1/2 length of elytron; densely and moderately coarsely punctate; humeri distinctly prominent. Each elytron with two transverse, irregular red-brown maculae. Anterior elytral macula bowtie-shape, located behind humeri, its anterior and posterior margin widely U-shaped and deeply emarginate. Posterior macula crown-shaped, located at apical 1/3, its anterior margin tridentate, posterior margin widely U-shaped and deeply emarginate. Protibia (Fig. 12E) in male raised near apical 1/3 on inner edge, in female not raised; mesotibia (Fig. 12F) simple. Hind wing (Fig. 12I) reduced to narrow straps, oval shape apically, no longer than the elytra.

Ventrite **V** (Fig. 12H) with lateral margins gently converging posteriorly; posterior margin in male widely raised medially; in female ventrite V with posterior margin simple, weakly emarginate medially. Male genital segment (Fig. 12J) with paired apophyses fused along nearly 1/3 of its length basally; dorsal plate undivided; additional, internal, V-shaped sclerite present.

Aedeagus (Fig. 12K, L) rather long, heavily sclerotized, distinctly curved outwardly near 1/2 of length, and with one branch, rather short and straight, weakly acute apically. Median lobe branched apically, short and straight, flat and widely round apically. Tegmen placed basally, comparatively large, ring-shaped; parameres rather large, fused with tegmen.

Biology and ecology. The adults were collected by hand collected from a large pile of dead bamboos at night (Fig. 13).

Figure 13. Habitats of *B. humeralis* sp. nov. **A** large pile of dead bamboos in Guangxi, China **B** adult of *B. humeralis* sp. nov.

Brachytrycherus conaensis **Chang, Bi & Ren, 2016**
Figs 14, 16D, E, 20–24A

Brachytrycherus conaensis Chang et al., 2016: 139.

Diagnosis. *Brachytrycherus conaensis* is similar to *B. madurensis* in appearance but can be differentiated by each elytron bearing three maculae, anterior two maculae nearly rhomboid in shape, sometimes connected to each other, and the anterior and posterior elytral maculae without dentition.

Length. 8.2–8.3 mm; width: 4.5–4.7 mm.

Type material. Holotype, male, Xizang, Cona, Lexiang, 2500–2600 m, 20-30. VI.2013, Wen-Xuan Bi leg. (MHBU). Paratypes, 1 female, same data as holotype; 2 females, Xizang, Medog, Beibeng, Gelincun, 1700 m, 3.VIII.2014, Wen-Xuan Bi leg. (CBWX); 3 males, 7 females, Xizang, Cuona, Lexiang, 2500 m, 6.VIII.2010, Wen-Xuan Bi leg. (CBWX); 5 males, 6 females, same data except 15.VII.2011 (CBWX); 26 males, 11 females, same data except 29–30.VI.2013 (CBWX); 1 male, 1 female, same data except (MZPW); 18 males, 1 female, same data except 2500–2600 m, 20-30. VI.2013 (CBWX); 1 female, same data except 2700 m, 18.VI.2013 (CBWX).

Type locality. China (Xizang).

Distribution. China (Xizang).

Biology and ecology. Almost all individuals were found active on fence, woodpile or timber piles within the village and its surrounding area at night (Fig.16D, E)). Some larvae and adults were found (sometimes at the same time) feeding on the surface of the perithecia or spores of *Daldinia concentrica* (Xylariaceae) (Fig. 16D), seeming to prefer the asexual phase; however, individuals were also found on mature ascocarps (Chang et al. 2016).

Brachytrycherus curviantennae **Chang, Bi & Ren, 2016**
Figs 15, 16A, C

Brachytrycherus curviantennae Chang et al., 2016: 139.

Diagnosis. *Brachytrycherus curviantennae* is similar to *B. humeralis* and *B. denticulatus* sp. nov. in both bodies being broadly oval, elytral maculae transverse, pronotum sides strongly curved. However, antennomere 3 distinctly curved outwards and elytral maculae nearly cymbiform can distinguish *B. curviantennae* from all its congeners.

Length. 8.5–9.4 mm; width: 5.1–5.2 mm.

Type material. Holotype, male, Xizang, Medog, 1500 m, 20.VIII.2013, Wen-Xuan Bi leg. (SHEM). Paratypes, 1 female, Xizang, Medgo, Beibeng, Gelincun, 3.VIII.2014, Wen-Xuan Bi leg. (MHBU); 1 female, Xizang, Medgo, Beibeng, Gelincun, 3.VIII.2014, Wen-Xuan Bi leg. (CBWX).

Type locality. China (Xizang).

Distribution. China (Xizang).
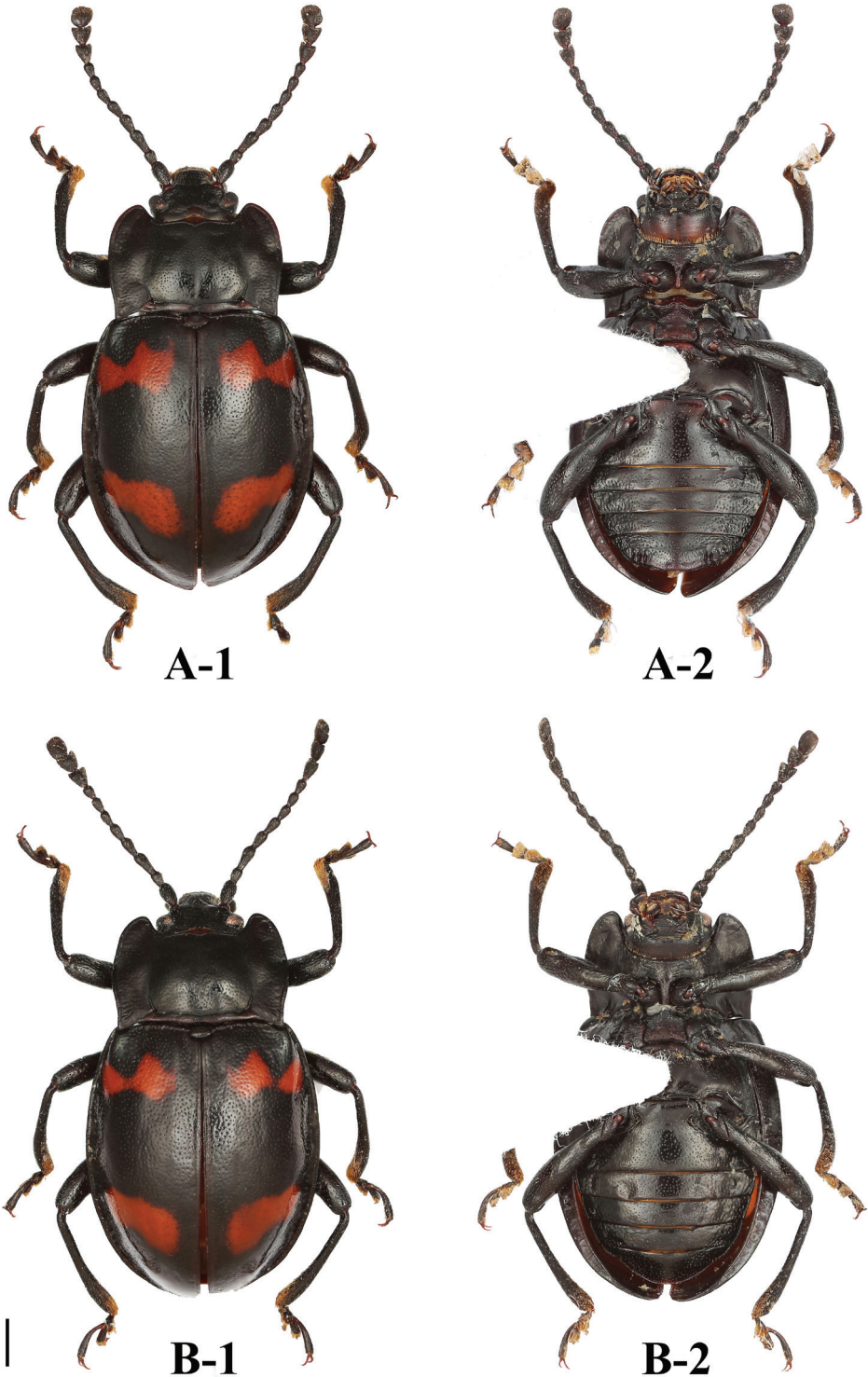
Figure 14. Type specimens of *B. conaensis*. **A** male holotype **B** female paratype **1** dorsal view **2** ventral view. Scale bar: 1 mm.
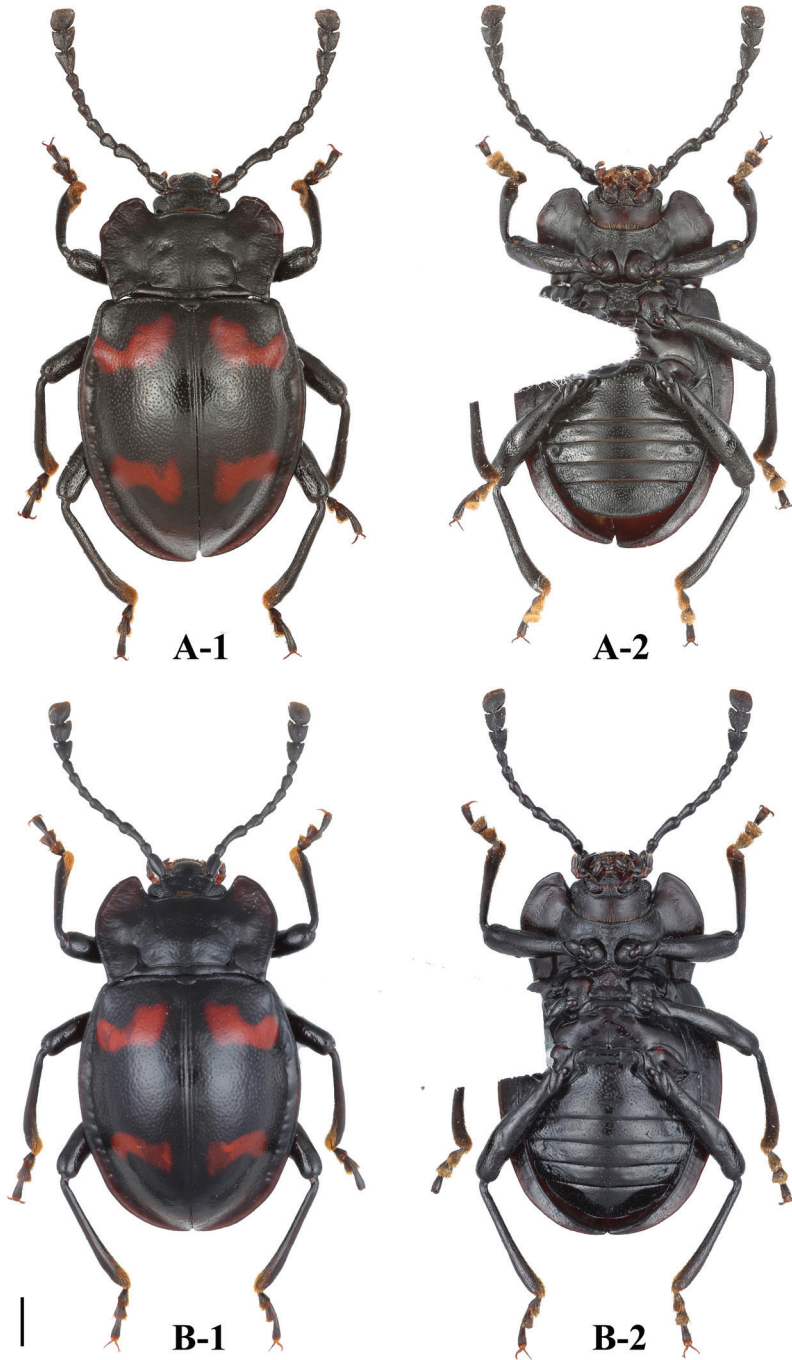
Figure 15. Type specimens of *B. curviantennae*. **A** male holotype **B** female paratype; **1** dorsal view; **2** ventral view. Scale bar: 1 mm.
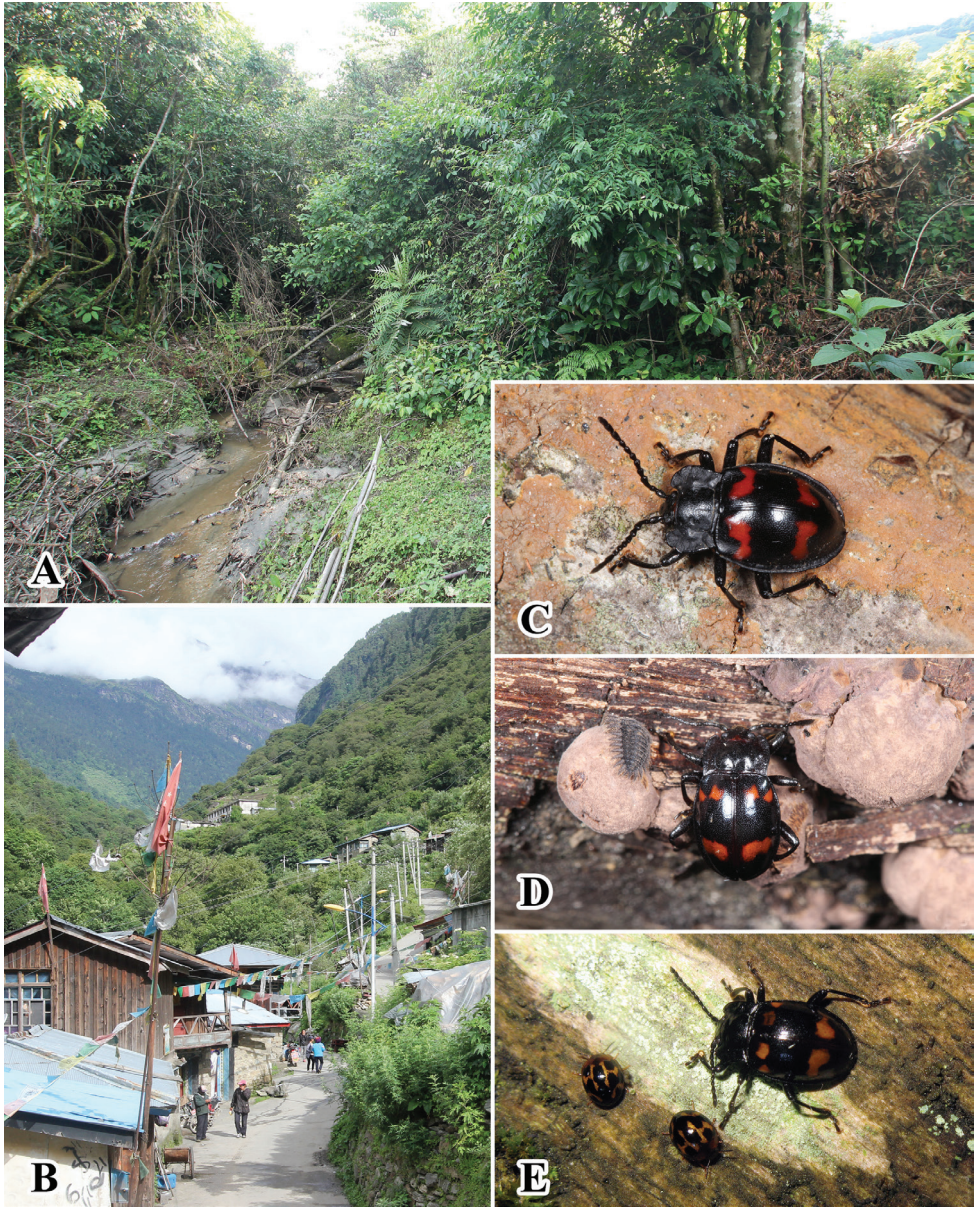
Figure 16. Habitats of *B. conaensis* and *B. curviantennae*. **A** large clump of Fagaceae plants of collecting site in Xizang, China **B** village of collecting site in Xizang, China **C** male of *B. curviantennae* (arranged) **D** male of *B. conaensis* and larva on the wood pile **E** female of *B. conaensis* feeding on the lichen growing on wood.

Biology and ecology. The male was hand collected by simple searching, as it is active on branches at night (Fig. 16C). Two females were collected by shaking the tree from a large clump of dead wood of Fagaceae plants (Fig. 16A) (Chang et al. 2016).

Brachytrycherus femoralis (Arrow, 1928)
Figs 17–19

Engonius femoralis Arrow, 1928: 347.

Diagnosis. *Brachytrycherus femoralis* can be separated from all its congeners by having three elytral maculae; sides of elytra strongly converging from its 1/2 length towards apex, lateral margins moderately widely flattened, not vanishing at apex.

Material examined. China: Guangxi Province: Jinxiu, Yinshan Protection Station, 27.VI.2016, Yu-Yang Lei leg. (1 male, 2 females, CCLX); Huanjiang Yangmeiao Protection Station, 15.VIII.2016, Ling-Xiao Chang leg. (2 males, CCLX); Jinxiu, Dayaoshan, 22–24.IV.2018, Chun-Fu Feng leg. (2 females, CCLX); Jinxiu, Yinshan Protection Station, 1500 m, 12.VIII.2015, Ling-Xiao Chang leg. (2 males, 3 females, MHBU); Jinxiu, Dayaoshan, 17.V.2014, Zhi-Lin Chen leg. (1 female, MHBU); Longsheng, Huaping, 15.X.2005, Ji-Liang Wang & Chao Gao leg. (1 female, MHBU).

Description. Length 9.4–11.2 mm, width 4.3–5.4 mm. *Body* oval, about 2.1–2.3 times as long as wide; moderately convex; shiny. Colour black with purple sheen, three orange-red maculae on each elytron.

Head. Antenna long and rather slender, nearly 1/2 body length, with antennomeres 1–8 distinctly longer than wide; scape approximately 4.0 times as long as pedicel; antennomere 3 as long as 4 and 5 combined; antennomeres 4 nearly as long as 5, antennomeres 5–8 gradually shorter; club composed of three antennomeres, moderately broad, flat, loose. Maxilla with terminal palpomere longer than wide, slightly longer than palpomere 3, tapering anteriorly, truncate apically.

Thorax. Pronotum 2.1–2.2 mm long, 3.5–4.2 mm wide; widest near 1/2 of pronotal length; finely and densely punctate; lateral margins rather narrowly bordered, sides undulate; front angles produced anteriorly, rather acute; disc weakly convex, two small round raised area laterally; transverse wrinkle and inflexed laterally; median furrow shallow, extending to 1/2 length of pronotum; lateral sulci linear, deep, extending to basal 1/3 length of pronotum; basal sulcus weakly undulate, deep. Prosternal process moderately separates procoxae; not extending beyond coxae; sides nearly parallel, expanded apically; posterior margin in male truncate and emarginate in female. Mesoventral process transverse, lateral margins weakly widening apically and overlapping part of mesocoxae; posterior margin nearly straight.

Elytra 6.3–7.3 mm long, 3.0–3.3 times as long as pronotum and 1.2–1.3 times as wide as pronotum, sides curved, widest near 1/2 length of elytron; finely and densely punctate; humeri prominent. Each elytron with three irregular orange-red maculae. Anterior two elytral maculae located near basal 1/4, lateral maculae oval, almost confined to umbo; medial macula nearly round, larger than lateral one, sometimes narrowly connected. Posterior macula located near apical 1/4, weakly transverse, nearly cloud-form, outer sides far from elytral lateral margin, inner margin of macula far from
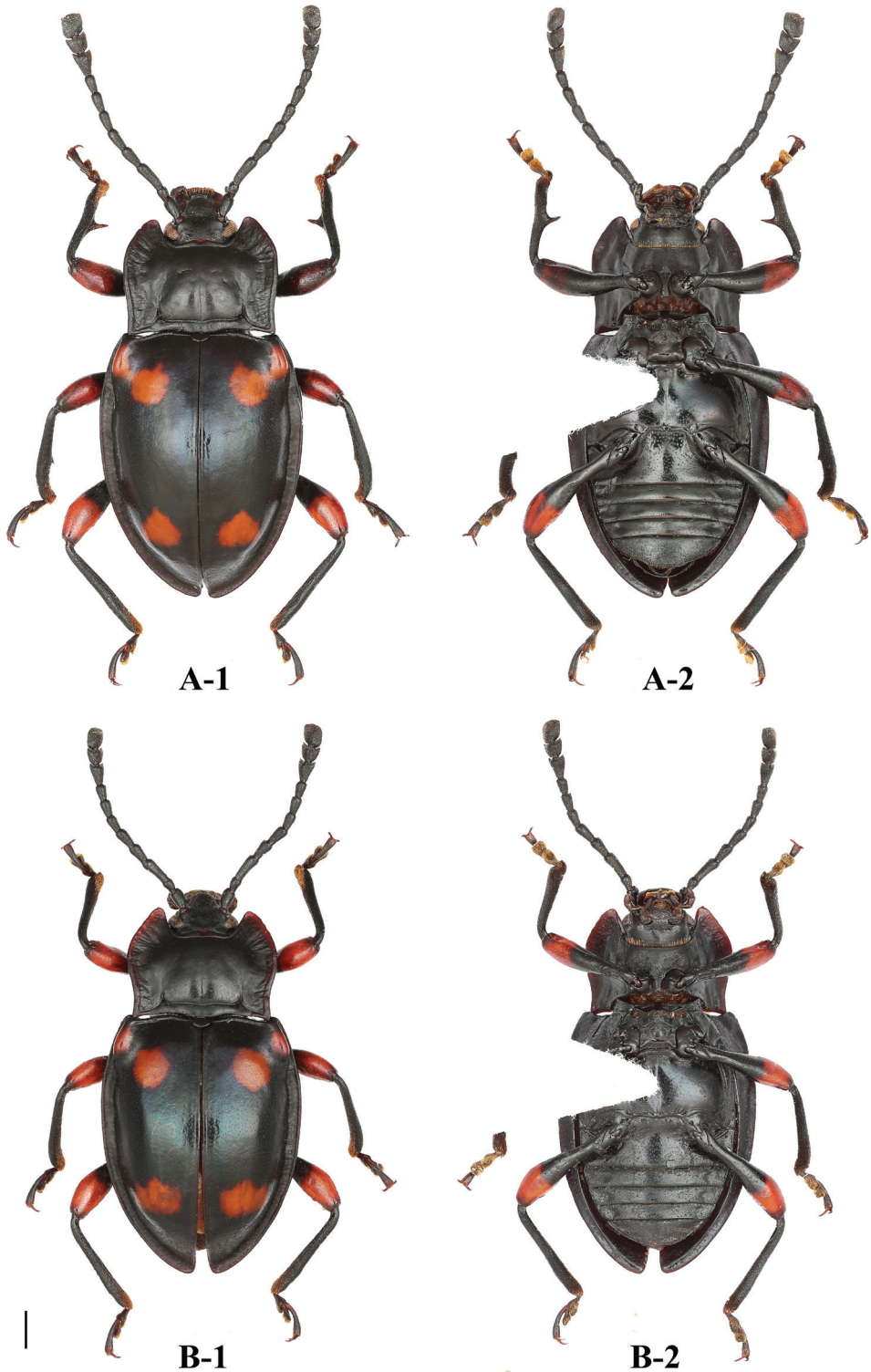
Figure 17. Habitus of *B. femoralis* **A** male **B** female; **1** dorsal view **2** ventral view. Scale bar: 1 mm.

Figure 18. Habitats of *B. femoralis*. **A** large pile of dead bamboos in Guangxi, China **B** adult of *B. femoralis* sp. nov. feeding on the mold growing on dead bamboos.
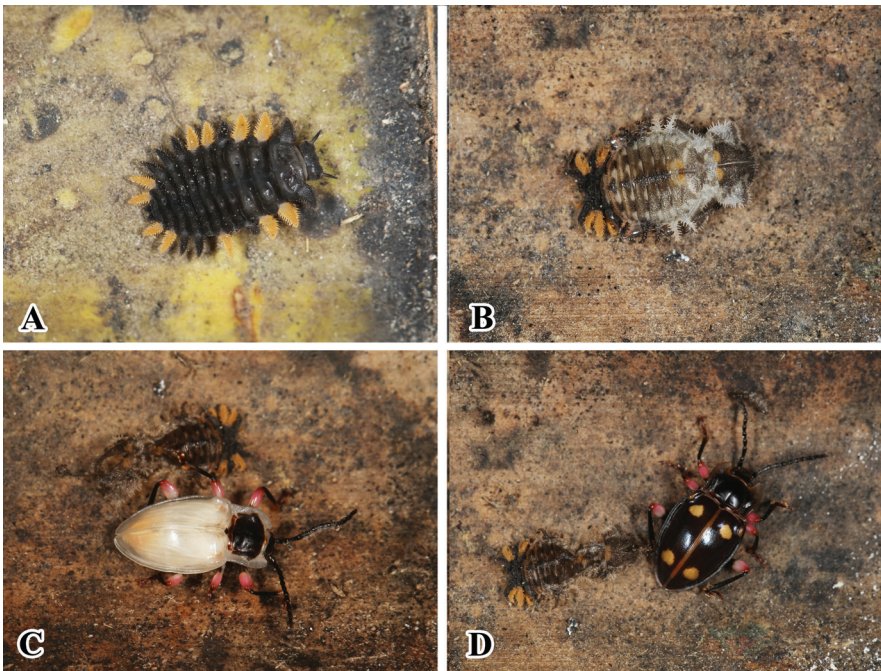
Figure 19. Living adults, larva, and pupae of *B. femoralis* in artificial conditions. **A** last instar larvae **B** pupae **C, D** newly emerged adult.

elytral suture. Protibia in male with rather long sharp tooth near 1/2 length on inner edge, in female without tooth; mesotibia in male with small sharp tooth behind 1/2 length on inner edge, and then abruptly curved to apex, in female without tooth.

Ventrite **V** with lateral margins gently converging posteriorly; posterior margin truncate in male and weakly curved in male medially.

Aedeagus (Fig. 5) rather long, heavily sclerotized, straight. Median lobe one branched apically; branch long and strongly reflexed upwardly, acute apically. Tegmen basal, comparatively large, ring-shaped.

Distribution. China (Guangxi), Laos, Vietnam (Tonkin). First records from China.

Type locality. Lectotype: Laos, 1 male; Syntype: Vietnam (Tonkin), 1 male.

Biology and ecology. The adults were found active and feeding on the mould growing on dead bamboos at night (Fig. 18). The adults and larvae were brought back and placed in artificial conditions to rear. The last instar larvae pupated on surface of dead bamboos, from their pupal stage to matured to adults in approximately seven to nine days (Fig. 19).

Key to the species of *Brachytrycherus* known in mainland China (adapted from Chang et al. 2016)

1	Antennomere 3 distinctly outwardly curved..................... ***B. curviantennae***
–	Antennomere 3 straight **2**
2	Elytron strongly convex, hind wing reduced to narrow straps.................... **3**
–	Elytron moderately convex, hind wing fully developed **4**
3	Elytral humerus distinctly prominent, protibia in male without sharp tooth ....***B. humeralis* sp. nov.**
–	Elytral humerus not prominent, protibia in male with sharp tooth ....***B. denticulatus* sp. nov.**
4	Elytral sides strongly converging from its 1/2 length towards apex, lateral margins moderately widely flattened, not vanishing at apex ......***B. femoralis***
–	Elytral sides gradually converging from its 1/3 length towards apex, lateral margins rather narrowly bordered, vanishing at apex.................................. **5**
5	Elytron with anterior two maculae nearly rhomboid, sometimes connected to each other ....***B. conaensis***
–	Elytron with anterior two maculae nearly oval or round, rather remote from each other .... ***B. bipunctatus* sp. nov.**

Discussion

The genus *Brachytrycherus* belongs to the Amphisternus group of Lycoperdininae; the monophyly of this group was defined by Tomaszewska (2005), based on shared characteristics. However, in some specimens (both new species and *B. femoralis*) the mesoven-

Figure 20. Left antenna of *Brachytrycherus*. **A** *B. conaensis* **B** *B. curviantennae* **C** *B. femoralis*.
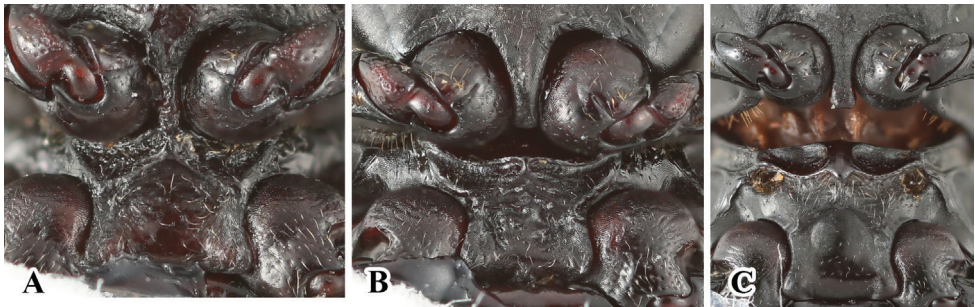
Figure 21. Prosternal and intercoxal processes of males. **A** *B. conaensis* **B** *B. curviantennae* **C** *B. femoralis*.

trite intercoxal process sides are weakly widened apically. The shape of the mesoventrite intercoxal process is not stable; thus, it may not be appropriate as a character used to defined the Amphisternus group.

The unique character for *Brachytrycherus* is a sexual dimorphism in the shape of the prosternal process in some species: for example, the prosternal process in male *B. bipunctatus* sp. nov. is very narrow, the sides are weakly curved outwardly, rounded apically; females are wider than males, the sides are nearly straight, and weakly truncate apically. This character is observed for the first time in the Endomychidae.
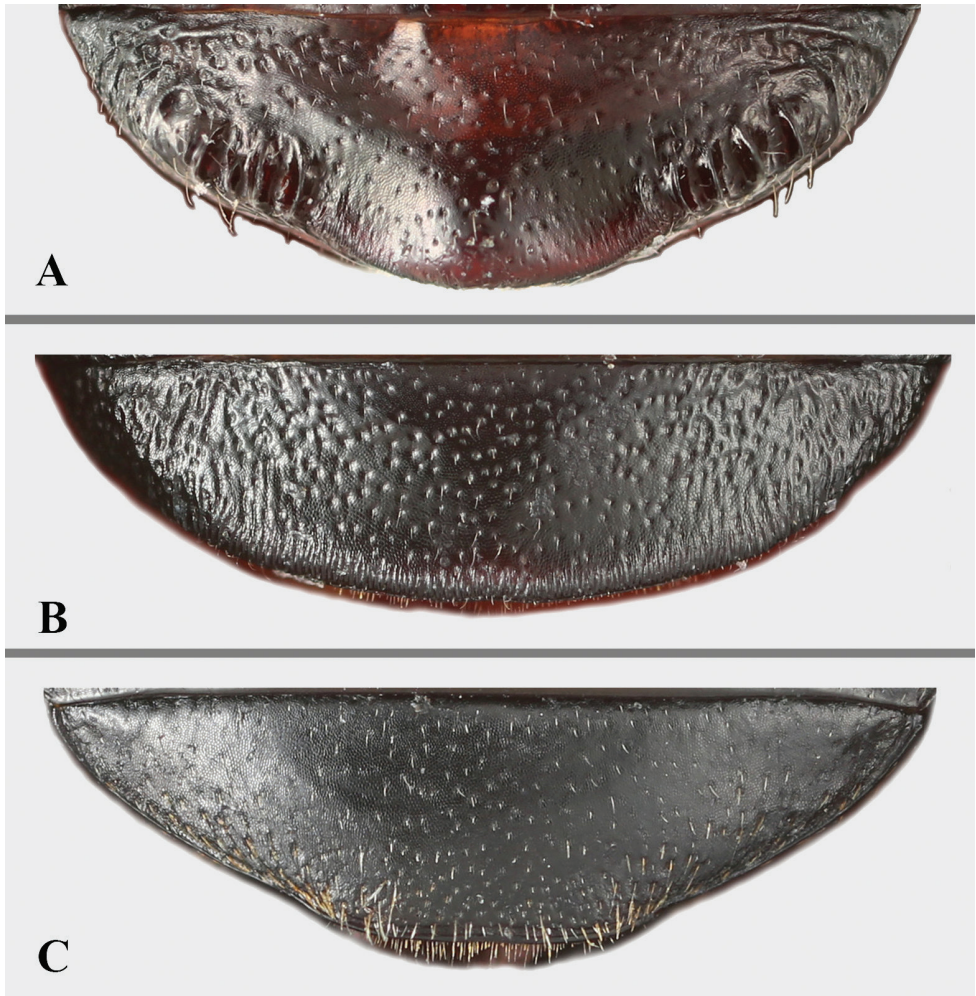
Figure 22. Abdomen with ventrite V of males. **A** *B. conaensis* **B** *B. curviantennae* **C** *B. femoralis.*

Figure 23. Left tibia of *Brachytrycherus* (male). **A** *B. conaensis* **B** *B. curviantennae* **C** *B. femoralis*; 1 protibia; 2 mesotibia; 3 metatibia.
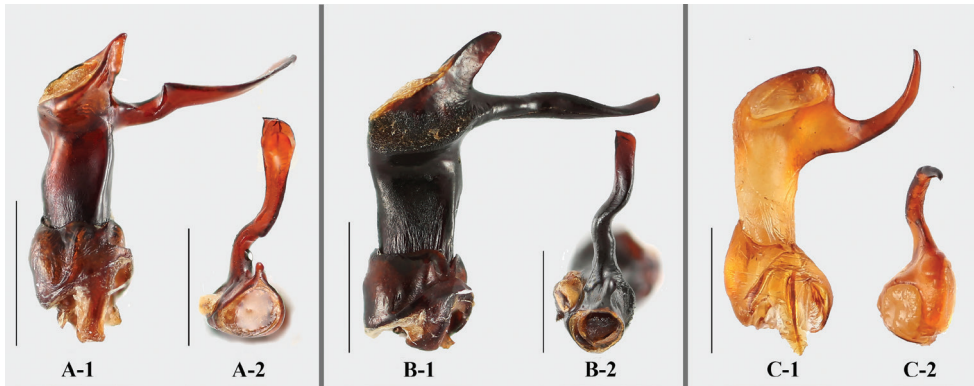
Figure 24. Aedeagus of *Brachytrycherus*. **A** *B. conaensis* **B** *B. curviantennae* **C** *B. femoralis*; **1** lateral view; **2** apical view. Scale bars: 1 mm.

Acknowledgements

References

Arrow GJ (1920) A contribution to the classification of the Coleopterous family Endomychidae. Transactions of the Entomological Society of London [1920]: 1–83. https://doi.org/10.1111/j.1365-2311.1920.tb00205.x

Chang L-X, Bi W-X, Ren G-D (2016) Two new species of *Brachytrycherus* Arrow, 1920 from China (Coleoptera, Endomychidae). ZooKeys 595: 137–146. https://doi.org/10.3897/zookeys.595.7569

Gorham HS (1886) On new Genera and Species of Endomychidae. Proceedings of the Zoological Society [1886]: 154–163.

Shockley FW, Tomaszewska KW, McHugh JV (2009a) An annotated checklist of the handsome fungus beetles of the world (Coleoptera: Cucujoidea: Endomychidae). Zootaxa 1999: 1–113. https://doi.org/10.11646/zootaxa.1999.1.1

Strohecker HF (1964) A synopsis of the Amphisternini (Coleoptera: Endomychidae). Pacific Insects 6(2): 319–357.

Strohecker HF (1971) The genera *Engonius* and *Parindalmus* (Coleoptera: Endomychidae). Pacific Insects 13: 13–25.

Tomaszewska KW (2000) Morphology, phylogeny and classification of adult Endomychidae (Coleoptera: Cucujoidea). Annales Zoologici 50(4): 449–558.

Tomaszewska KW (2005) Phylogeny and generic classification of the subfamily Lycoperdininae with a re-analysis of the family Endomychidae (Coleoptera: Cucujoidea). Annales Zoologici 55(suppl. 1): 1–172.

Tomaszewska KW (2006) *Stroheckeria quadrimaculata*, new genus and new species of Lycoperdininae from Vietnam (Coleoptera: Endomychidae). Annales Zoologici 56: 465–470.

RESEARCH ARTICLE

A new synonym for *Zelia* Robineau-Desvoidy, 1830 (Diptera, Tachinidae), the genus Opsozelia Townsend, 1919, with the description of three new species

Rodrigo de Vilhena Perez Dios[1], Marcelo Domingos de Santis[1]

1 *Department of Zoology, Institute of Biosciences, University of São Paulo, Rua do Matão, Travessa 14, n.101, Cidade Universitária, São Paulo-SP, 05508-900, Brazil*

Corresponding author: *Rodrigo de Vilhena Perez Dios* (rodrigodios@gmail.com)

Abstract

The monotypic tachinid genus *Opsozelia* Townsend, 1919 (Diptera: Tachinidae) is synonymized with *Zelia* Robineau-Desvoidy 1830, **syn. nov**. The single species of *Opsozelia*, *O. discalis* Townsend, 1919, is redescribed as *Zelia discalis*, **comb. nov.**, based on examination of the holotype from Guyana and additional material from Suriname, Brazil and Paraguay. Three new species of *Zelia* similar to *Z. discalis* are described from Brazil: *Z. magna* **sp. nov.**, *Z. guimaraesi* **sp. nov.** and *Z. formosa* **sp. nov**. These four species are treated informally as the *Zelia discalis* species group. An identification key to the species of this species group is provided based on male specimens. Descriptions and illustrations are provided for the male terminalia of all species and for the female terminalia of one species, *Z. guimaraesi*.

Keywords

Introduction

Zelia is a New World genus that was composed, prior to this study, of 19 species (Guimarães 1971, O'Hara and Wood 2004). It was erected by Robineau-Desvoidy (1830) for five species, including *Zelia rostrata* Robineau-Desvoidy, 1830 (= *Dexia vertebrata* Say, 1829) from North America, designated as type species by Coquillett (1910). Of

the other four species, three were left unplaced in the Tachinidae by O'Hara and Wood (2004) (*Z. analis* Robineau-Desvoidy, 1830, *Z. apicalis* Robineau-Desvoidy, 1830, and *Z. veloz* Robineau-Desvoidy, 1830) and the fourth was placed in *Ptilodexia* Brauer & Bergenstamm, 1889 by Guimarães (1971) (*Zelia strenua* Robineau-Desvoidy, 1830).

Zelia was enlarged by subsequent generic synonymies, as follows: Townsend (1919) synonymized *Leptoda* van der Wulp, 1885 with *Zelia*; Aldrich (1929) provided new descriptions for most of the Neotropical species and synonymized *Melaleuca* Wulp, 1891 and *Euzelia* Townsend, 1915 with *Zelia*; and Wood (1987) synonymized *Metadexia* Coquillett, 1899 and *Minthozelia* Townsend, 1919 with *Zelia* (as reviewed by O'Hara and Wood 1998). Earlier, Reinhard (1946) revised a portion of *Zelia*, as *Minthozelia*, including six new species. *Zelia* currently comprises 12 Nearctic and seven Neotropical species. However, the Neotropical species lack a key and are poorly known, being just referenced by lists and catalogues after the original descriptions.

The genus *Opsozelia* was described in the tribe Zeliini by Townsend (1919) for his new species, *O. discalis*, based on a single male from Bartica, Guyana. Later, Townsend (1931a) discovered that his new species was a synonym of *Musca lateralis* Fabricius, 1805, and changed the species name to *Opsozelia lateralis* (Fabricius, 1805). In his catalogue of Neotropical Tachinidae, Guimarães (1971) followed Townsend (1931a) in recognizing *Opsozelia* as a valid genus with the single species, *O. lateralis* (with *discalis* in synonymy). Thompson and Pont (1994) noted that the specific name of Fabricius was preoccupied by *Musca lateralis* Linnaeus, 1758 and the valid name of the species then reverted to Townsend's original one, *Opsozelia discalis*.

The Zeliini were recognized as a tribe of 11 genera in the Americas south of the United States by Guimarães (1971) and a twelfth genus (*Neozelia*) was later described by Guimarães (1975). Tschorsnig (1985) examined one zeliine genus, *Diaugia* Perty, 1833, and placed it in the Dexiini based on male terminalic features. Ziegler (1998) studied the larval cephaloskeleton of third instar larvae, and puparia, of some *Zelia* species and did not find any discernable differences from the Dexiini. O'Hara and Wood (2004) did not recognize Zeliini and incorporated the only North American genus, the type genus *Zelia*, within a more broadly defined Dexiini. This action was recently supported in the recent molecular study of Stireman et al. (2019) in which *Zelia* was nested within Dexiini. We follow the foregoing authors in classifying the Zeliini *sensu* Guimarães (1971) within the Dexiini but note that these *Zelia*-group genera may form a monophyletic clade within Dexiini and some of them (in addition to *Opsozelia*, treated herein) may prove to be congeneric with *Zelia*.

In the present paper, the monotypic genus *Opsozelia* is synonymized with *Zelia*. We also present a small diagnosis for Dexiini and some morphological characters that help identify *Zelia*. We recognize and characterize a group of species within *Zelia* that have at least two discal setae on abdominal tergites III and IV and call this group the *Zelia discalis* species group. This species group is revised and four Neotropical species are recognized: *Z. discalis* (Townsend) from Guyana and three new species from Brazil, namely *Z. formosa* sp. nov., *Z. guimaraesi* sp. nov. and *Z. magna* sp. nov. The new

species are described, *Z. discalis* is redescribed, and an identification key to the males of this species group is provided. Descriptions and illustrations of the male terminalia of all species are presented for the first time. The female of *Z. guimaraesi* sp. nov. is described and illustrated.

Materials and methods

The examined material was deposited at the following institutions: Museu de Zoologia, Universidade de São Paulo, São Paulo, Brazil (**MZSP**), Museu Nacional do Rio de Janeiro, Rio de Janeiro, Brazil (**MNRJ**) and National Museum of Natural History, Smithsonian Institution, Washington, D.C., USA (**USNM**). The labels of type material are represented with quotation marks (") to indicate the same label, a slash (/) for line break, and a semicolon to indicate a new label.

Male terminalia were cleared in a 10% solution of KOH at room temperature for ca. 24 hours, then neutralized with acetic acid (10%) and washed with distilled water and a series of ethanol solutions at increasing concentrations. After examination, the terminalia were placed in plastic microvials filled with glycerin and pinned with their respective specimens. All specimens were measured with the software LEICA LAS version 4.1.0. Photographs were taken using a Leica DFC420 digital camera attached to a Leica MZ16 stereomicroscope, and the software LEICA LAS version 4.1.0. The images were subsequently stacked using Helicon Focus 5.3 and edited in Adobe Photoshop CS6. Illustrations were made using a Leica MZ16 stereomicroscope with camera lucida attached and edited in Adobe Illustrator CS6. Morphological terminology follows Cumming and Wood (2017).

Taxonomic part

Genus *Zelia* Robineau-Desvoidy, 1830

Zelia Robineau-Desvoidy, 1830: 314. Type species: *Zelia rostrata* Robineau-Desvoidy, 1830 (= *Dexia vertebrata* Say, 1829), by subsequent designation of Coquillett, 1910: 621.

Leptoda van der Wulp, 1885: 196. Type species: *Dexia gracilis* Wiedemann, 1830 (= *Dexia vertebrata* Say, 1829), by subsequent designation of van der Wulp, 1891: 250.

Melaleuca van der Wulp, 1891: 213. Type species: *Melaleuca spectabilis* van der Wulp, by subsequent monotypy of van der Wulp, 1891: 247.

Metadexia Coquillett, 1899: 220. Type species: *Metadexia tricolor* Coquillett, 1899, by monotypy.

Euzelia Townsend, 1915: 23. Type species: *Zelia wildermuthii* Walton, 1914, by original designation.

Minthozelia Townsend, 1919: 556. Type species: *Minthozelia montana* Townsend, 1919, by original designation.

Opsozelia Townsend, 1919: 557. Type species: *Opsozelia discalis* Townsend, 1919 (= *Musca lateralis* Fabricius, 1805), by original designation, **syn. nov.**

Notes. The genus *Zelia* is a group with 19 valid species at present. This study began as a revision of the previously valid genus *Opsozelia*, but later it was recognized as a synonym of *Zelia.* Since the original intent of this study was not to revise *Zelia*, we were not able to examine all *Zelia* species. Therefore, we cannot provide a full description for the genus. Instead, we provide a small diagnosis for the genus, as well as some features for the Dexiini, modifying what was stated by Thompson (1963) and Mesnil (1980). The species of *Zelia* with at least two discal setae on abdominal tergites III and IV (i.e., members of the *Z. discalis* species group), are then revised.

Diagnosis. *Zelia* shares with Dexiini the following characters that, simultaneously, differs from other Tachinidae: compound eye bare (except for *Callotroxis* Aldrich, 1929 and *Huascarodexia* Townsend, 1919). Front narrow and without orbital setae in male, broad and with one proclinate orbital seta in female. Lunula bare. Frontal setae, forwardly directed or crossed, anteriorly reaching external angle of lunula, or slightly in front of it, but never descending to parafacial (except in *Psecacera* Bigot, 1880, *Morphodexia* Townsend, 1931 and *Dasyuromyia* Bigot, 1885). Facial carina absent. Antenna short, inserted at level or below half of compound eye height, thickened only at its base, often pubescent or plumose. Thorax with scutellum with decussate (rarely parallel) apical setae, normally without lateral setae. Abdominal sternites usually completely covered by ventrolateral margins of corresponding tergites.

Zelia differs from other Dexiini genera by the following combination of characters: Head silver pruinose (golden pruinose in *Myiomima* Brauer & Bergenstamm, 1889). Pedicel with one long seta and various setulae on its surface (in *Neozelia* Guimarães, 1975 with a tuft of long setulae). Postpedicel long, compressed laterally. Arista long plumose (bare in *Psecacera*). Facial carina absent (e.g., present in *Platyrrhinodexia* Townsend, 1927). Haustellum short, ca. 0.5× the head height (e.g., two or three times in *Prosenoides* Brauer & Bergenstamm, 1891). Thorax with proepisternum and prosternum bare (e.g., setulose in *Tromodesiana* Townsend, 1931). Intrapostalar seta absent. Scutellum with just regular setae (e.g., various upturned setae in *Tropidopsiomorpha* Townsend, 1927). Wing hyaline (smoky in in *Yahuarmayoia* Townsend, 1927; with maculae in *Scotiptera* Macquart, 1835). Costal spine undeveloped. Abdomen strongly pointed apically, especially in male (in *Yahuarmayoia* and *Z. discalis* species group is broad, excluding *Z. formosa* sp. nov.). Male abdomen somewhat elongate (not elongate in *Ophirodexia* Townsend, 1911). Abdominal tergites with just one row of setae (e.g., in *Hystrichodexia* Röder, 1886, two or three rows of discal setae). Tergite IV with three to five discals or without discals (e.g., with discal setae in sytergite I+II to V in *Ptilodexia*).

Justification for the synonymy of *Opsozelia* with *Zelia* and the *Z. discalis* group of species with at least two discal setae on tergites III and IV:

All of the examined species of the *Z. discalis* species group are similar to *Zelia* species, including the terminalia. These species do not present any outstanding morphological features that justify a separate genus. However, considering the difficulty in identifying the Neotropical Dexiini and *Zelia* species, we keep maintain species in their own species group for identification purposes. These species are easily recognized among other *Zelia* by the presence of at least two discal setae on abdominal tergites III and IV (other *Zelia* species without discal setae on these tergites).

Description of the *Zelia discalis* species group. Male holoptic and female dichoptic. Compound eye bare. Frontal vitta and ocellar triangle dark brown. Head light yellow to tawny, covered entirely with silver pruinosity. Minute proclinate setae on fronto-orbital plate. Parafacial bare. Ocellar setae proclinate and well differentiated from the adjacent setae; postocellar setae proclinate. Inner and outer vertical setae subparallel and convergent. No facial carina. Genal dilation with pale pruinosity and covered with black setulae. Facial ridge with small setulae near vibrissal insertion. Antenna inserted below middle of compound eye. Arista densely plumose. Strong and convergent vibrissae; four or five developed subvibrissal setae. Palpus cylindrical and a little clavate. Thorax brown to dark brown with silver or light golden pruinosity. Prescutum with four dark vittae, the two inner vittae thinner than the outer vittae. Prosternum and proepisternum bare. Notopleuron with two equal-sized setae. Two proepimeral setae. Two proepisternal setae. Three katepisternal setae, the lower one weaker. Postalar callus with two large and one smaller setae. Anepimeron with a single long seta. Anatergite bare. Katepimeron with setulae anteriorly. Costal spine absent. Vein M1 ending at wing margin close to tip. Abdomen conical, basally large and rounded, tapering to tip. Mid-dorsal depression on syntergite I+II reaching the posterior margin. Syntergite I+II and tergite III with one pair of median marginal setae. Tergite III and IV with 2–4 pairs of discal setae. Tergite IV with one row of median marginal setae and approximately ten discal seta decreasing in size anteriorly. Tergite V with one row each of marginal and discal setae. Sternites hidden. Male terminalia with cerci separated and pointed, larger basally. Surstylus broad, and usually rounded at tip, sometimes slightly pointed. Pregonite and postgonite fused as curved elongate structure, without a distinct separation; pregonite connected basally to the hypandrium by a membrane (sometimes thin, almost sclerotized). Epiphallus present, fused with basiphallus. Basiphallus varying in size. Distiphallus with extension of dorsal sclerite varying in size; dorsal sclerite ventrally serrulated; granular zone present, varying in size.

Key to species of *Zelia discalis* species group (males).

1   Lower margin of face protruding below vibrissal angle; width of fronto-orbital plate 0.5× or less the height of gena..**2**

–   Lower margin of face not protruding below vibrissal angle; width of fronto-orbital plate 0.8× or more the height of gena **3**

2   Scutum with 4+3 acrostichal setae. Scutellum with two pairs of discal setae. Abdomen pale yellow, with median brown rounded vitta covering syntergite I+II, tergite III with small brownish black spot, at the insertion of the marginal median seta; posterior margin of tergite IV with a triangular spot, covering approx. the posterior ¼; tergite V entirely brownish black, without pruinosity ....**Zelia magna sp. nov.**

–   Scutum with 2+2 acrostichal setae. Scutellum with a single pair of discal setae. Abdomen pale yellow, with median brown longitudinal vitta covering syntergite I+II, continuing along the middle of the abdomen and ending at the middle of tergite V; posterior margin of tergite IV reddish brown; posterolateral margins of syntergite I+II and tergites III and IV with a brown spot; tergite V, reddish brown with silver pruinosity laterally ....
        ....**Zelia discalis (Townsend, 1919), comb. nov.**

3   Thorax with postscutum with pale pruinosity only on the anterior region, not forming vittae; wing dorsally with vein R_{4+5} setulose for 1/4 of distance to crossvein dm-cu; abdominal syntergite I+II with one pair of median marginal setae; syntergite I+II to tergite IV pale yellow, each tergite with a brownish black vitta medially, broadening posteriorly (3× the width of the anterior portion) and with white pruinosity laterally ....**Zelia formosa sp. nov.**

–   Thorax with postscutum brown to dark brown with 4 vittae of silver pruinosity; the inner vittae half the length of the outer ones, neither reaching the scutellum; wing dorsally with setulae only on base of R_{4+5}; abdominal syntergite I+II without median marginal setae; abdomen pale yellow, with median brown longitudinal vitta covering syntergite I+II, continuing along the middle of the abdomen to the end of tergite IV; tergite V entirely reddish black with silver pruinosity laterally ....**Zelia guimaraesi sp. nov.**

Zelia discalis (Townsend, 1919)
Figs 1, 7 A–C

Opsozelia discalis Townsend, 1919: 557. Holotype ♂ (USNM; examined). Type locality: Guyana, Bartica, Kartabo.

Type material examined. Holotype ♂: "Bartica, BG / VII.10.1901" "Type No. / 22237 / U.S.N.M." "Opsozelia / discalis / ♂ T. Det CHTT".
    Additional material examined. Suriname: [unreadable label], 1 ♂, 4.xi.1942 (MZSP); Brasil: *Pará*, Oriximiná, Rio Cumina, Cachoeira da Paciência, 1 ♂, 8.x.1936, Almeida col. (MZSP); *São Paulo*, São Paulo, Alto da Serra, 1 ♂, ii.1926 R. Spitz col. (MZSP); Cantareira, Horto Florestal, 1 ♂, L. Travassos col. (MZSP); *Santa Catarina*, Nova Teutônia, 27 ♂, i.1966, 8 ♂, ii.1966, 3 ♂, iv.1966, 2 ♂, x.1966, 1 ♂, xii.1970, F. Plaumann col. (MZSP); Paraguay: Amambay, Caballera, 1 ♂, 23–25.xi.1971 (MZSP).
    Diagnosis. Frontal vitta width, in the narrowest point, narrower than ocellar triangle; postpedicel entirely yellow to orange; halter entirely pale yellow-tawny.
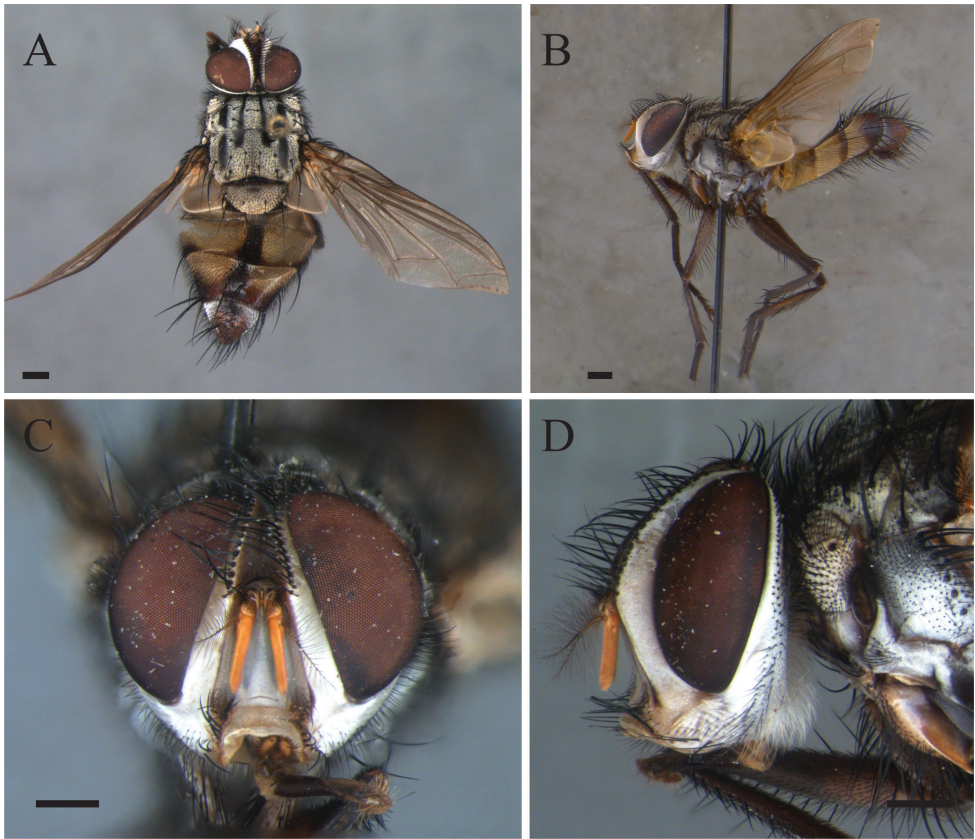
Figure 1. *Zelia discalis*, holotype, male. **A** Dorsal habitus **B** lateral habitus **C** head frontal **D** head lateral. Scale bars: 1 mm.

Description. *Body length*: 12.0 mm.

***Coloration*:** Occiput with long and pale setulae. Antenna yellow to orange. Palpus yellow-orange. Thorax with postscutum with four dark vittae, the inner vittae half the length of the outer, neither reaching the scutellum. Scutellum dark brown, with pale pruinosity posteriorly. Subscutellum with pale pruinosity. Wing hyaline, slightly light brown along the veins. Calypteres white-pale translucent. Halter pale yellow-tawny. Posterior spiracle light brown. Legs brown to tawny with silver pruinosity on coxae and femora; tarsi darker. Claws brown with tip darker. Abdomen pale yellow, with median brown longitudinal vitta covering syntergite I+II, continuing along the middle of the abdomen and ending at the middle of tergite V; posterior margin of tergite IV and tergite V reddish brown; posterolateral margins of tergites III, IV, and V with a brown spot.

***Head*:** Frontal vitta at its widest point approx. as wide as the vertex in dorsal view. Frontal vitta, in the narrowest point, narrower than ocellar triangle. Fronto-orbital plate 17 pairs of proclinate setae minute proclinate setae; narrower than frontal-vitta and parafacial. Ocellar setae proclinate divergent. Orbital plate with three setulae. Post-pedicel slender, 3× the combined length of scape and pedicel; arista plumose with two

or three dorsal and one ventral rows; length of longest cilia ca. 7× basal width of arista. Facial ridge with ten or eleven setulae on lower third. Lower facial margin protruding, and visible in profile. Vibrissa long, inserted above lower facial margin. Prementum as long as palpus. Labella developed, little longer than 0.5× the prementum.

Thorax: Acrostichals 2+2. Dorsocentral 3+3. Intra-alar 1+2, first post-sutural weak; intra-postalar absent. Supra-alar 2+3, first post-sutural weak. Postpronotal lobe with four setae, three forming an anterior row and one posterior. Anepisternum with eight strong setae and two upwardly directed setulae anteriorly. Scutellum with one basal, one lateral, one weak subapical, one apical and one discal pairs of setae.

Wing: Base of R dorsally and ventrally setulose. M vein bent forward to R_{4+5}, forming an angle slightly smaller than 90°, and convex after bend.

Legs: Fore coxa with many setae anteriorly; fore femur with dorsal and posteroventral rows of setae; fore tibia with two posterior setae and row of shorter anterodorsal setae. Mid femur with three posteroventral basal setae, three dorsal to posterodorsal preapical setae; mid tibia with one anteroventral median seta, two anterior median setae and two posterior median setae. Hind femur with three anteroventral setae on basal half and three ventral setae on basal half and with row of anterodorsal setae; one posterodorsal preapical setae; hind tibia with two anterior median, two anteroventral median and two posterodorsal median setae. Claws straight with the tip curved.

Abdomen: Syntergite I+II without pair of median margin setae. Tergite III with three discal setae decreasing in size anteriorly one median marginal seta and one lateral marginal seta. Tergite IV with four discal setae decreasing in size anteriorly a marginal row of median lateral. Ventral borders of tergites with a row of median setae.

Terminalia (Fig. 7A–C): Tergite VI brown and segment VII+VIII brownish black with silver pruinosity. Surstyili in lateral view narrow, less than 2× the maximum cerci width; triangular shaped, narrow at the apex. Surstyli in posterior view without an expansion laterally. Apex of the hypandrium directed backwards. Middle bar subequal to the total length of the granular structure of distiphallus. Apex of distiphallus not curved.

Notes on type. Missing left vibrissa and right one broken in half. Missing right mid femur and so on; missing right trochanter and so on. Abdomen damaged, basally compressed and smashed, and with a rupture on the left side of tergite III.

Variation. Orbital plate with 2–7 setulae. Intra-alar - 2+3. Supra-alar - 2+4.

Distribution. Suriname, Brazil (Pará, São Paulo and Santa Catarina states), and Paraguay (Amambay department).

Zelia magna Dios & de Santis, sp. nov.

http://zoobank.org/7E6A133A-FF41-430E-A2C0-BFA6A9991577
Figs 2, 7 D–F

Type material examined. *Holotype* ♂: BRAZIL: *Rio de Janeiro*, Nova Friburgo, Mury, xii.1980, Gred & Guimarães leg. (MZSP). Labelled as follows: "Mury, Nova Friburgo / Rio de Janeiro – Br. / xii.1980 / Gred & Guimarães col." [printed label]; "Zelia / mag-
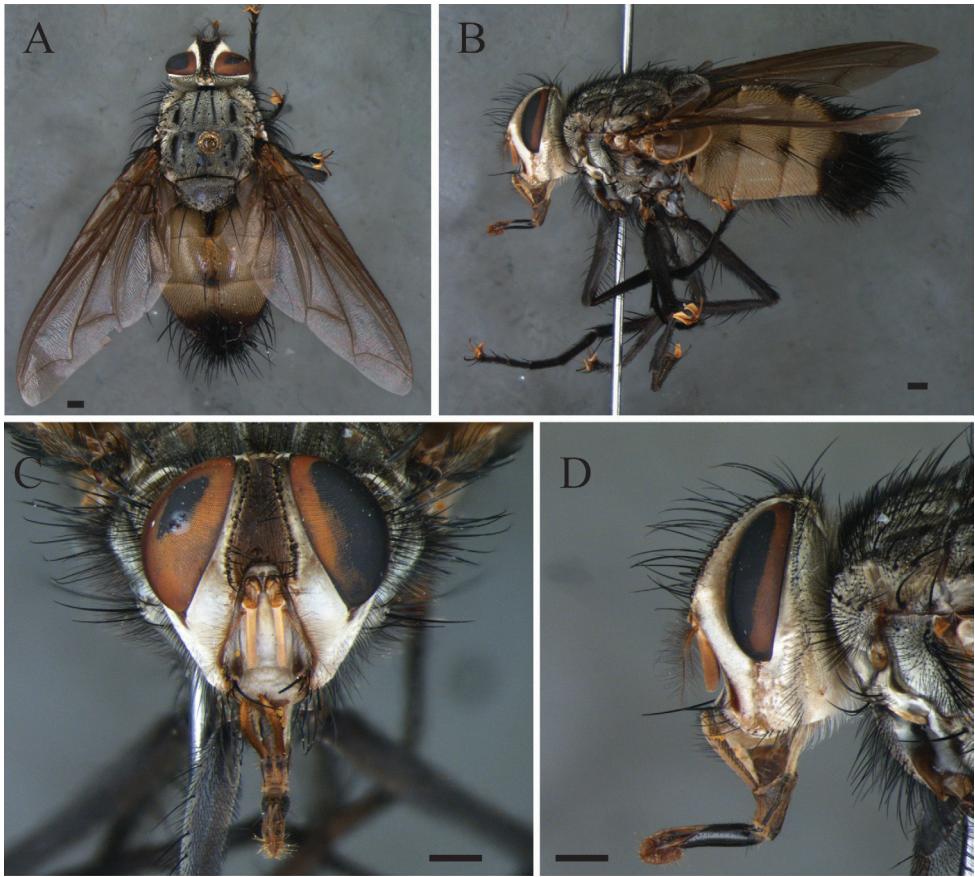
Figure 2. *Zelia magna* sp. nov., holotype, male. **A** Dorsal habitus **B** lateral habitus **C** head frontal **D** head lateral. Scale bars: 1 mm.

na sp. nov. / Dios & Santis det. 2016" [handwriting/printed label]; "Holotipo" [red label]. Paratypes: BRAZIL: *Rio de Janeiro*, Itatiaia (700 m), 1 ♂, 3.iv.1928, J.F. Zikán col. (MZSP); *São Paulo*, São Paulo, Horto Florestal, 1 ♂, 13.ii.1944, Ramalho col. (MZSP).

Diagnosis. Thorax with scutellum with two pairs of discals; abdomen pale yellow, syntergite I+II with median brown rounded vitta; tergite III with small brownish black spot, at the insertion of the marginal median seta; tergite IV posterior margin with a triangular spot, covering approx. the posterior ¼; posterolateral margins of syntergite I+II and tergites III and IV with a brown spot; legs dark brown; light brown claws; tergite V, entirely brownish black, without pruinosity; tergite VI and segment VII+VIII brownish black; largest species of the genus.

Description. *Body length*: 17.8 mm

Coloration: Occiput with long and pale setulae. Antenna yellowish grey-dusted. Palpus yellow-orange. Thorax with postscutum with four dark vittae, the inner vittae half the length of the outer, neither reaching the scutellum. Scutellum dark brown, with pale pruinosity posteriorly. Subscutellum with pale pruinosity. Wing hyaline,

slightly light brown along the veins. Calypteres slightly infuscated. Halter and posterior spiracle light brown. Legs brown with silver pruinosity on coxae and femora; tarsi darker. Claws brown with tip darker. Abdomen pale yellow, with median brown longitudinal vitta covering syntergite I+II, in tergite III a brownish black dot at the insertion of the median marginals, in tergite IV a brownish black triangular spot on the posterior region and in V; and tergite V entirely brownish black without pruinosity; posterolateral margin of tergite IV with a brown spot.

Head: Frontal vitta at its widest point ca. 1.2× as wide as the vertex in dorsal view. Frontal vitta, in the narrowest point, equal to bigger width than ocellar triangle. Fronto-orbital plate with 20 pairs of proclinate setae; broader than frontal-vitta and parafacial. Width of parafacial measured between inner margin of compound eye and antennal insertion is 2× the height of gena. Postpedicel slender, 2× the combined length of scape and pedicel; arista plumose with two to three dorsal and one ventral rows; length of longest cilia ca. 7× basal width of arista. Facial ridge with 16–14 setulae on lower third. Lower facial margin protruding, and visible in profile. Vibrissa long, inserted above lower facial margin. Prementum shorter than palpus. Labella developed, ca. 0.4× the prementum.

Thorax: Acrostichals 4+3. Dorsocentral 4+4. Intra-alar 2+3, first post-sutural weak; intra-postalar present. Supra-alar 2+3. Postpronotal lobe with five setae, four forming an anterior row and one posterior. Anepisternum with nine strong setae and two upward directed setulae anteriorly. Scutellum with one basal, one lateral, one weak subapical, one apical and two discal pairs of setae.

Wing: Base of R dorsally and ventrally setulose. M vein bent forward to R_{4+5}, forming an angle bigger than 90°, and convex after bend.

Legs: Fore coxa with many setae anteriorly; fore femur with dorsal and posteroventral rows of setae; fore tibia with two posterior setae and row of shorter anterodorsal setae. Mid femur with three posteroventral basal setae, three dorsal to posterodorsal preapical setae; mid tibia with one anteroventral median seta, two anterior median setae and two posterior median setae. Hind femur with three anteroventral setae on basal half and three ventral setae on basal half and with row of anterodorsal setae; one posterodorsal preapical seta; hind tibia with two anterior median, two anteroventral median and two posterodorsal median setae. Claws straight with the tip curved.

Abdomen: Syntergite I+II without pair of median margin setae. Tergite III with three discal setae increasing in size anteriorly, one median marginal seta and two lateral marginal setae. Tergite IV with four discal setae increasing in size anteriorly and a marginal row of setae.

Terminalia (Figs 7 D–F): Tergite VI brown and segment VII+VIII brown to tawny with silver pruinosity. Surstyili in lateral view wide, more than 2× the maximum cerci width; triangular shaped, slightly rounded at the apex. Surstyli in posterior view with small expansion laterally. Apex of the hypandrium directed backwards. Middle bar slightly shorter than total length of the granular structure of distiphallus. Apex of distiphallus curved.

Type locality. Brazil, Rio de Janeiro, Nova Friburgo, Mury.

Distribution. Brazil (Rio de Janeiro and São Paulo states).

Etymology. The name refers to the size of this species, being the biggest of the species group. "Magna" (Latin) = large.

Zelia guimaraesi **Dios & de Santis, sp. nov.**
http://zoobank.org/A0CF312A-A8CC-4549-A05F-C955CD868ED1
Figs 3, 4, 7 G–I, 8

Type material examined. *Holotype* ♂: Brazil: *Santa Catarina*, Nova Teutônia, ii.1966, F. Plaumann col. (MZSP). Labelled as follows: "Brasilien / Nova Teutônia / 27°11B 52°23L, 300–500 m / ii.1966 / Fritz Plaumann" "Zelia / guimaraesi sp. nov. / Dios & Santis det. 2016" [handwriting/printed label]; "Holotipo" [red label].

*Paratypes***:** Brazil: *Rio de Janeiro*, Nova Friburgo, "Mury, Nova Friburgo / Rio de Janeiro – Br. / 12.xi.1970 / Gred & Guimarães col." 1 ♂ (MZSP); Petrópolis, Le Vallon, Alt, Mosella, 1 ♀, 1.ii–8–iii.1957, Albuquerque col. (MNRJ); São Paulo, Salesópolis, (Est. Biol. Boracéia / Salesópolis, SP-Br / 22 – 24.x.1982 / EXC. MZUSP col.) 1 ♂, (MZSP); Santa Catarina, Nova Teutônia, 1 ♂, same as holotype, 1 ♀, iv.1967, 1 ♀, xi.1966, 4 ♂, ix.1967, F. Plaumann col. (MZSP); *Rio Grande do Sul*, Santo Augusto, 1 ♂, i–ii, 1962, Roppa col. (MNRJ).

Diagnosis. Parafacial larger or equal to 1/3 of the head width; tergite V entirely reddish brown; facial ridge with only one to two setulae; halter stem dark yellow; wings smokier alongside the veins; frontal vitta larger.

Description. *Body length***:** 12.0 mm.

*Coloration***:** Frontal vitta and ocellar triangle dark brown to black. Head light yellow to tawny covered entirely with silver pruinosity. Occiput with long and black setulae. Postpedicel orange, but distal ¼ brownish orange. Palpus yellow-tawny. Thorax brown to dark brown with silver or light golden pruinosity; scutum with four dark vittae, in prescutum the two inner vittae are thinner than the outer, in postscutum, the inner vittae half the length of the outer, neither reaching the scutellum. Scutellum dark brown, with pale pruinosity posteriorly. Subscutellum with pale pruinosity. Wing hyaline, slightly light brown along the veins. Calypteres slightly infuscated. Halter yellowish to brownish. Posterior spiracle light brown. Legs brown to tawny with silver pruinosity on coxae and femora; tarsi darker. Claws brown, pulvilum yellow. Abdomen pale yellow, with median brown longitudinal vitta covering syntergite I+II, continuing along the middle of the abdomen to the end of tergite IV; tergite V entirely reddish black.

*Head***:** Frontal vitta at its widest point ca. 1.1× as wide as the vertex in dorsal view. Frontal vitta, in the narrowest point, equal to bigger width than ocellar triangle. Fronto-orbital plate with 12–13 pairs of proclinate setae; narrower than frontal vitta and parafacial. Postocellar proclinate. Orbital plate with six setulae. Width of parafacial measured between inner margin of compound eye and antennal insertion is 2× the width of gena. Postpedicel slender, 1.5× the combined length of scape and pedicel; arista plumose with two to three dorsal and one ventral rows; length of the ventral cilia
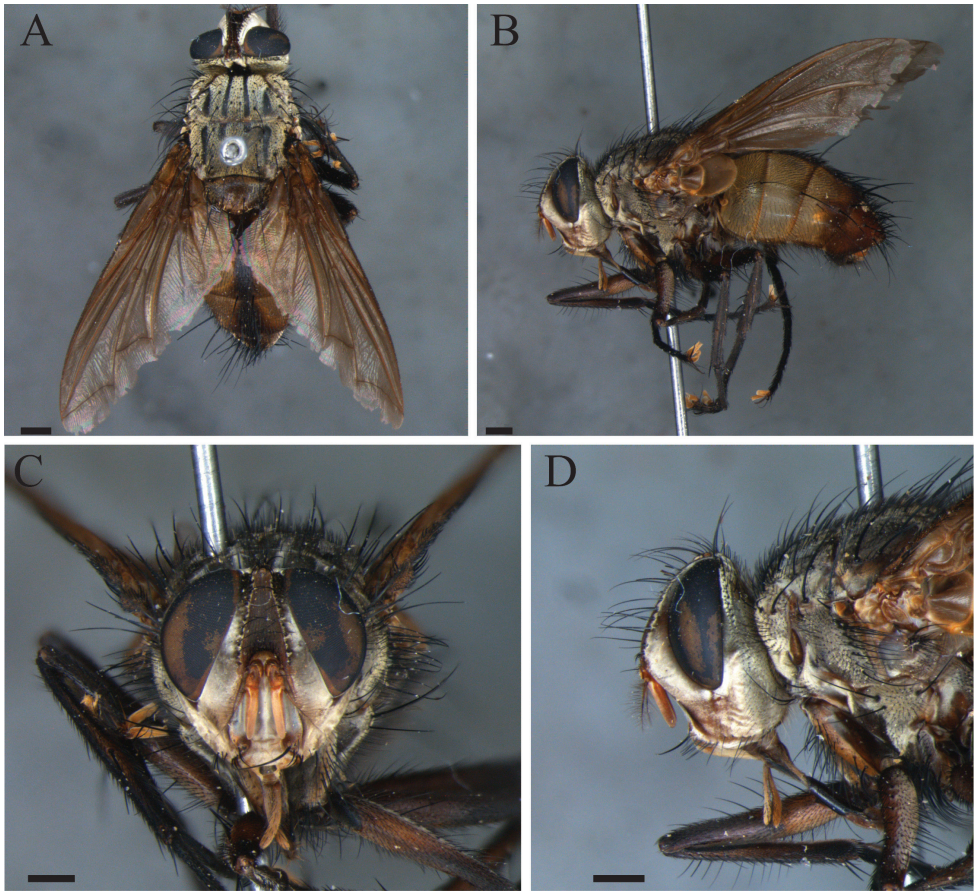
Figure 3. *Zelia guimaraesi* sp. nov., holotype, male. **A** Dorsal habitus **B** lateral habitus **C** head frontal **D** head lateral. Scale bars; 1 mm.

longer than the dorsal, longest cilia ca. 7× basal width of arista. Facial ridge with two to three setulae on lower third. Lower facial margin not protruding, and invisible in profile. Vibrissa long, inserted above lower facial margin. Premuntum as long as palpus. Labella developed, little longer than 0.5× the prementum.

Thorax: Acrostichals 2–3+2. Dorsocentral 3+3–4. Intra-alar 1+2–3, first post-sutural weak; intra-postalar absent. Supra-alar 2+2–3, first post-sutural weak. Postpronotal lobe with four setae, three forming an anterior row and one posterior. Anepisternum with eight strong setae and with one to two upward directed setulae anteriorly. Scutellum with one basal, one apical and one discal pairs of setae.

Wing: Base of R dorsally and ventrally setulose. M vein bent forward to R_{4+5}, forming an angle slightly smaller than 90°, and convex after bend.

Legs: Fore coxa with many setae anteriorly; fore femur with dorsal and posteroventral rows of setae; fore tibia with two posterodorsal setae and row of shorter anterodorsal setae. Mid femur with three anteroventral on apical third, tibia with two pos-
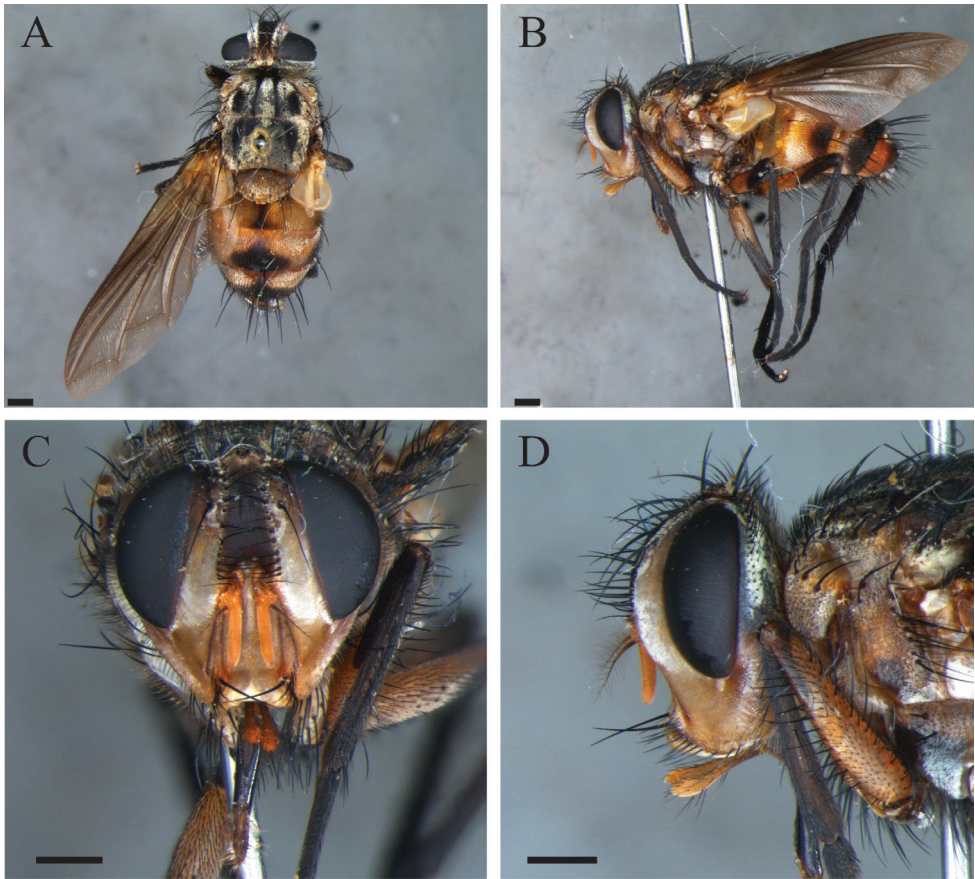
Figure 4. *Zelia guimaraesi* sp. nov., paratype, female. **A** Dorsal habitus **B** lateral habitus **C** head f rontal **D** head lateral. Scale bars: 1 mm.

terodorsal, two anterodorsal and one anteroventral setae, two dorsal, one ventral, one posteroventral and one anteroventral preapical setae; mid tibia with one anteroventral median seta, two anterior median setae and two posterior median setae. Hind femur with three anteroventral setae on basal half and three ventral setae on basal half and with row of anterodorsal setae; one posterodorsal preapical seta; hind tibia with two anterior median, two anteroventral median and two posterodorsal median setae. Claws straight with the tip curved, same length as 5th tarsomere.

Abdomen: Syntergite I+II without pair of median margin setae. Tergite III with two or none discal setae increasing in size anteriorly, one median marginal seta and one lateral marginal seta. Tergite IV with four discal setae increasing in size anteriorly and a marginal row of setae.

Terminalia (Fig. 7 G–I): Tergite VI and segment VII+VIII yellowish tawny with scarce silver pruinosity. Surstyli in lateral view wider, more than 2× the maximum cerci width; triangular shaped, slightly narrowed at the apex. Surstyli in posterior view with an

expansion laterally. Apex of the hypandrium directed upwards. Middle bar longer than the total length of the granular structure of distiphallus. Apex of distiphallus curved.

Female differs from male by the following (Fig. 4): Body length, 12.4 mm. Fronto-orbital plate with two reclinate orbital setae, and one proclinate orbital setae. Inner vertical and outer vertical setae well developed and reclinate. Palpus swollen apically. Postscutum with two black vittae laterally on anterior half. Mid and hind legs yellow, but posteroventrally ¼ brownish black. Pulvillus and claws not elongated. Abdomen yellowish orange, with tergite III with a triangular spot starting posteriorly, and laterally with a brownish black spot at the insertion of lateral margin setae, tergite IV posteriorly with a horizontal brownish black band, laterally and medially almost reaching anterior margin, and tergite V entirely yellowish orange. Tergite III-V with an anteriorly band of pruinosity, in all the tergite.

Terminalia (Fig. 8): Tergite VI and VII complete dorsally, with setae in all tergite VI and with few setae on the posterior margin of tergite VII, 6th spiracle on membrane ventrally, before tergite VI and 7th spiracle ventrally between tergite VI and sternite VIII. Tergite VIII present as thin and incomplete structure, with its apex elongated dorsally; very close to sternite X ventrally. Sternite VI and VII complete ventrally, with few setae in all posterior margin. Sternite VIII subrectangular as a narrow strip with setulae in the entire surface. Sternite X, as a narrow strip, with setula only on the posterior margin. Cerci well developed, sub-circular, with several setae apically with lingulae. Syntergite IX+X absent. Three spermatheca; equal sized; oval with apical portion with a pore and surface entirely rugose.

Type locality. Brazil, Santa Catarina, Nova Teutônia.

Distribution. Brazil (Rio de Janeiro, São Paulo and Santa Catarina states).

Etymology. *Z. guimaraesi* sp. nov. is named in honor of the late Dr. José Henrique Guimarães, the former curator of Diptera at the MZSP, who contributed greatly to the study of Neotropical Tachinidae.

Zelia formosa Dios & de Santis, sp. nov.

http://zoobank.org/102D8C26-F10C-4852-BBC1-AD8C88E13D8F

Figs 5, 6

Type material examined. *Holotype* ♂: Brazil: *Santa Catarina*, Nova Teutônia, 1.ii.1961, F. Plaumann col. (MZSP). Labelled as follows: "Brasilien / Nova Teutônia / 27°11B 52°23L, 300–500 m / 1.ii.1961 / Fritz Plaumann" «Zelia / formosa sp. nov. / Dios & Santis det. 2016» [handwriting/printed label]; «Holotipo» [red label].

Paratype: Brazil: *Santa Catarina*, Nova Teutônia, 1 ♂, i.1940, 1 ♀, 14.v.1963, F. Plaumann col. (MZSP).

Diagnosis. Postpedicel almost entirely brownish black, but 1/6 ventrally yellowish tawny; fronto-orbital plate entirely silvery pruinose; wing with a maculae in its base; R_{4+5} dorsally setulose for 1/4 of distance to cross vein dm-cu; postscutum, with pale pruinosity only on the anterior region, not forming vitta; syntergite I+II, with one pair
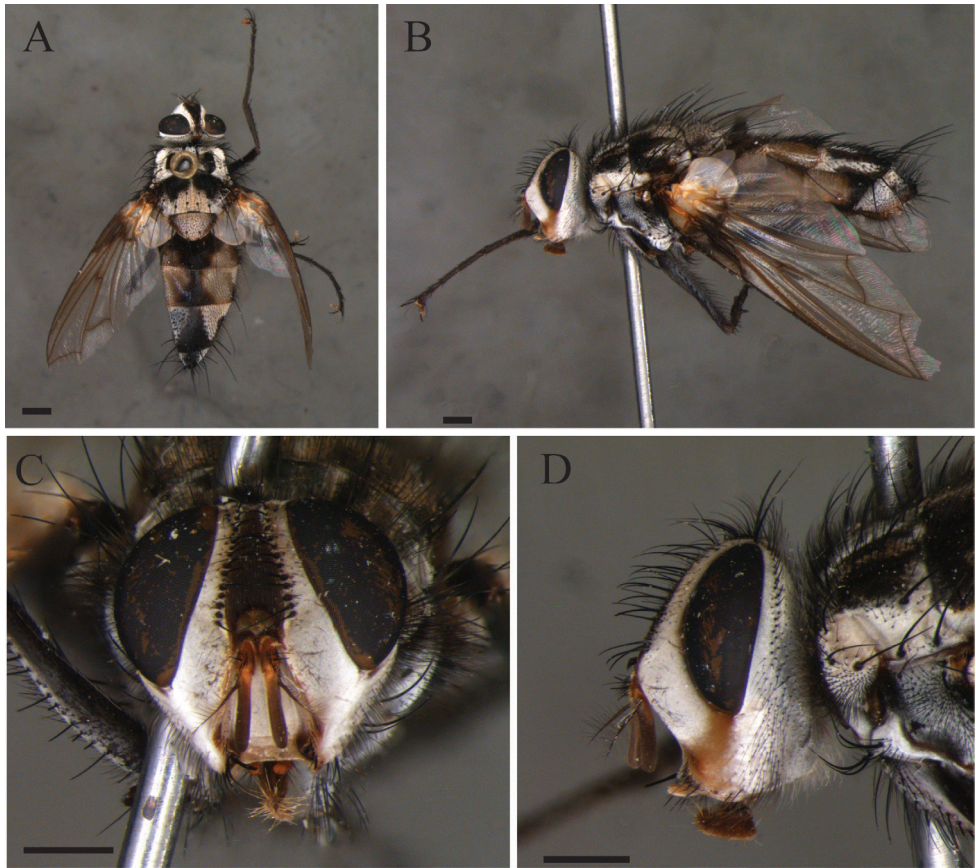
Figure 5. *Zelia formosa* sp. nov., holotype, male. **A** Dorsal habitus **B** lateral habitus **C** head frontal **D** head lateral. Scale bars: 1 mm.

of median marginal setae; abdomen with syntergite I+II to tergite IV pale yellow, with a brownish black vitta on middle, broadening posteriorly (three times the length of the anterior portion) and with white pruinosity on the lateral of each tergite.

Description. *Body length*: 12.4 mm.

Coloration: Occiput with pale setulae. Postpedicel light brown, but proximal ¼ orange. Palpus yellow-orange. Postscutum, with pale pruinosity only on the anterior region, not forming vitta. Scutellum dark brown, with pale pruinosity posteriorly. Subscutellum with pale pruinosity. Wing hyaline, slightly light brown along the veins. Calypteres white-pale translucent. Halter and posterior spiracle light brown. Legs brown with silver pruinosity on coxae and femora; tarsi darker. Claws brown with tip darker. Abdomen pale yellow, with median brown longitudinal vitta covering syntergite I+II, in tergite III a brownish black dot at the insertion of the median marginals, in tergite IV a brownish black triangular spot on the posterior region and in V; and tergite V entirely brownish black without pruinosity; posterolateral margin of tergite IV with a brown spot.
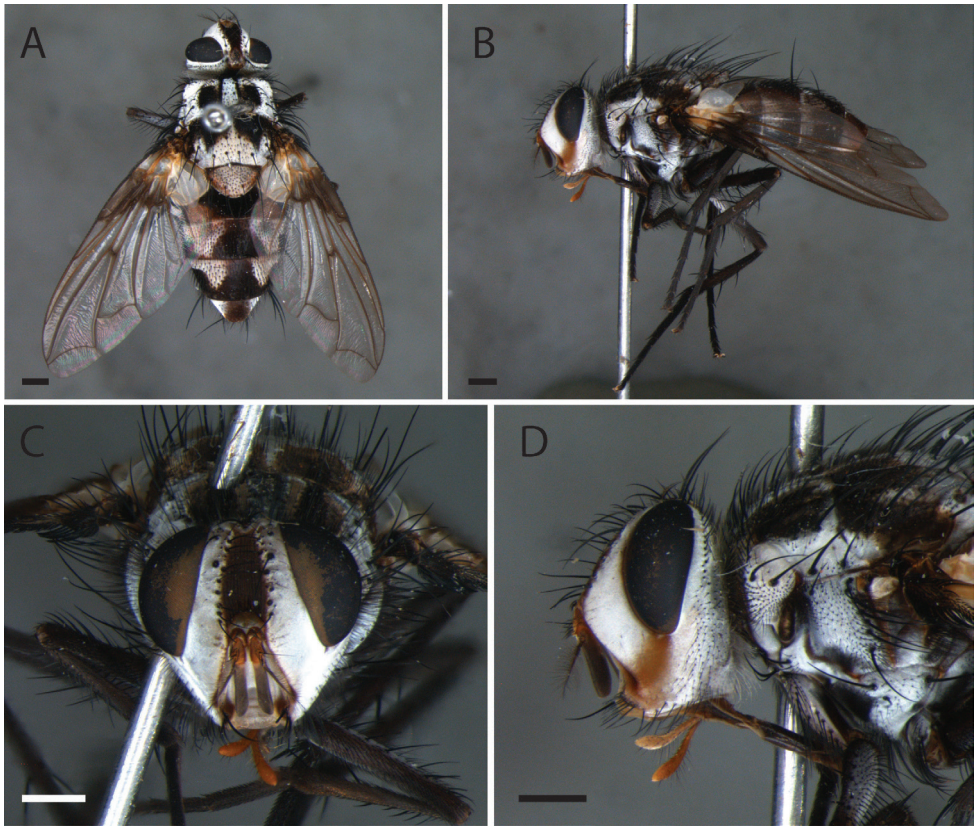
Figure 6. *Zelia formosa* sp. nov., paratype, female. **A** Dorsal habitus **B** lateral habitus **C** head frontal **D** head lateral. Scale bars: 1 mm.

Head: Frontal vitta at its widest point ca. 1.2× as wide as the vertex in dorsal view. Frontal vitta, in the narrowest point, equal to width than ocellar triangle. Fronto-orbital plate with 20 pairs of proclinate setae; broader than frontal-vitta and parafacial. Width of parafacial measured between inner margin of compound eye and antennal insertion is 2.5× the height of gena. Postpedicel slender, 2.2× the combined length of scape and pedicel; arista plumose with two or three dorsal and one ventral rows; length of longest cilia ca. 7× basal width of arista. Facial ridge with 14–16 setulae on lower third. Lower facial margin not protruding, and invisible in profile. Vibrissa long, inserted above lower facial margin. Premuntum shorter than palpus. Labella developed, ca. 0.4× the prementum.

Thorax: Acrostichals 4+3. Dorsocentral 4+4. Intra-alar 2+3, first post-sutural weak; intra-postalar present. Supra-alar 2+3. Postpronotal lobe with five setae, four forming an anterior row and one posteriorly. Anepisternum with nine strong setae and two upwardly directed setulae anteriorly. Scutellum with one basal, one lateral, one weak subapical, one apical, and two discal pairs of setae.

Wing: Base of R dorsally and ventrally setulose. M vein bent forward to R_{4+5}, forming an angle slightly smaller than 90°, and convex after bend.
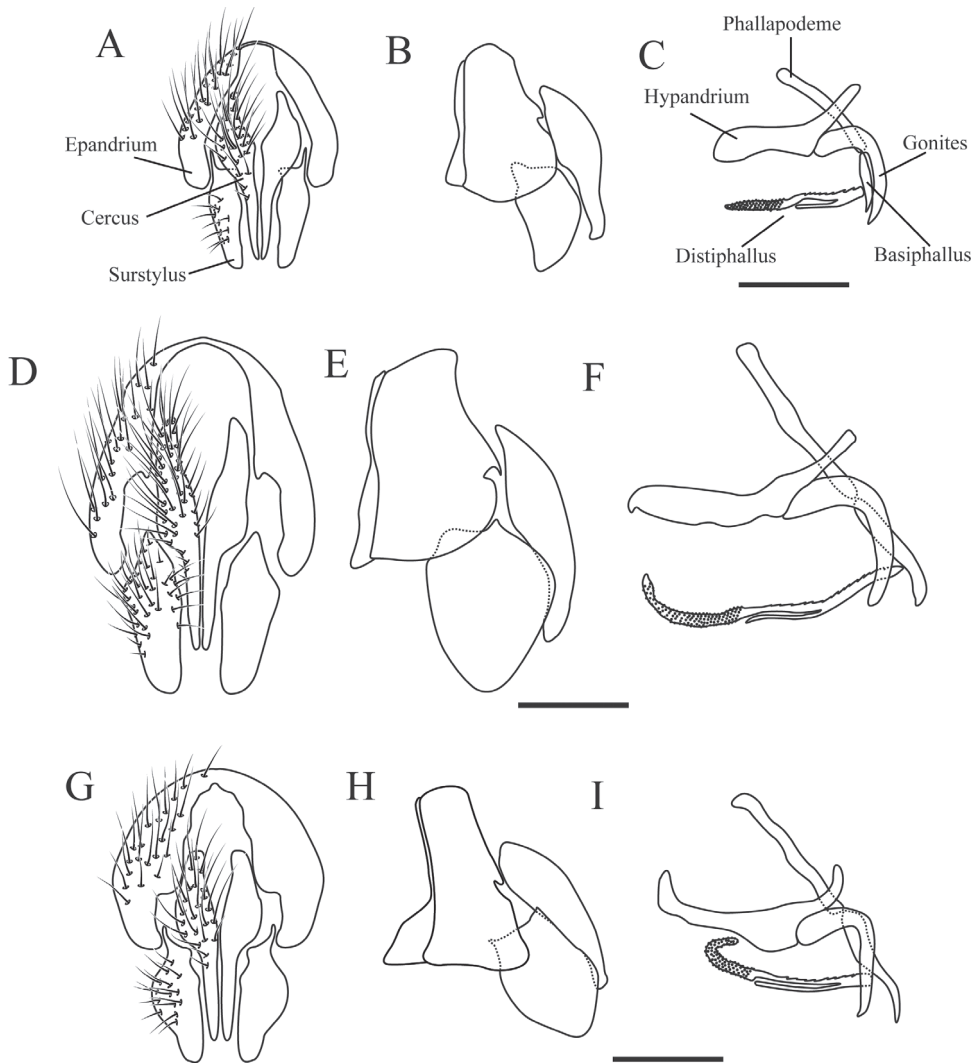
Figure 7. Male terminalia. **A–C** *Zelia discalis* **A** epandrium, cerci and surstylus in posterior view **B** epandrium, cerci and surstylus in lateral view **C** hypandrium, phallapodeme, gonites and aedeagus in lateral view. **D–F** Zelia magna sp. nov. **D** epandrium, cerci and surstylus in posterior view **E** epandrium, cerci and surstylus in lateral view **F** hypandrium, phallapodeme, gonites and aedeagus in lateral view. **G–I** *Zelia guimaraesi* sp. nov. **G** epandrium, cerci and surstylus in posterior view **H** epandrium, cerci and surstylus in lateral view **I** hypandrium, phallapodeme, gonites and aedeagus in lateral view. Scale bars: 0.5 mm.

Legs: Fore coxa with many setae anteriorly; fore femur with dorsal and posteroventral rows of setae; fore tibia with one posterior seta and a row of shorter anterodorsal setae. Mid femur with two anteroventral, three posteroventral basal setae, three dorsal to posterodorsal preapical setae; mid tibia with one anteroventral median seta, two anterior median setae, one posteroventral median seta and four preapicals setae. Hind femur with three anteroventral setae on basal half and three ventral setae on basal half and with row of anterodorsal setae; one posterodorsal preapical setae; hind tibia with
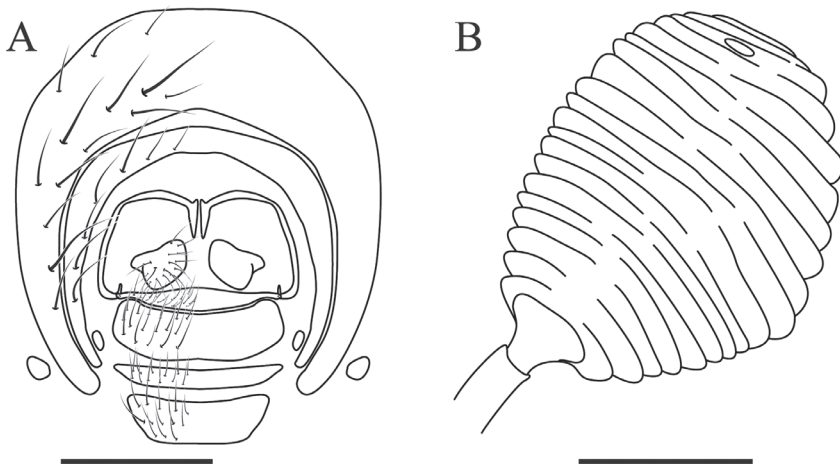
Figure 8. *Zelia guimaraesi* sp. nov. female terminalia. **A** Female terminalia in posterior view **B** spermatheca (only one represented, but three identical present). Scale bars: 0.5 mm (**A**), 0.1 mm (**B**).

one anterior median, two very long anteroventral median and two posterodorsal median setae and one anteroventral and one posteroventral preapical setae. Claws straight with the tip curved.

Abdomen: Syntergites I+II with one pair of median marginal setae. Tergite III with three discal setae increasing in size anteriorly, one median marginal seta and two lateral marginal setae. Tergite IV with four discal setae increasing in size anteriorly and a marginal row of setae.

Terminalia: Tergite VI and segment VII+VIII yellowish tawny with silver pruinosity. The remaining of the terminalia of the only dissected male was lost in the preparation and cannot be described here.

Female differs from male by the following (Fig. 6): Body length, 11.8 mm. Fronto-orbital plate with two reclinate orbital setae, and one proclinate orbital seta. Ocellar setae well developed and decussate. Palpus slightly more robust than in male. Pulvillus and claws not elongated. Abdomen oval. Tergites testaceous laterally white pruinose on syntergite I+II to tergite V; tergite V with row of marginals.

Type locality. Brazil, Santa Catarina, Nova Teutônia.

Distribution. Brazil (Santa Catarina state).

Etymology. The name refers to the unique and abundant pruinosity in the thorax and abdomen. "Formosa" (Latin) = beautiful.

Acknowledgements

References

Aldrich JM (1929) Further studies of types of American muscoid flies in the collection of the Vienna Natural History Museum. Proceedings of the United States National Museum 74 (Art. 19) [= No. 2764]: 1–34. https://doi.org/10.5479/si.00963801.74-2764.1

Coquillett DW (1899) New genera and species of Dexidae. Journal of the New York Entomological Society 7: 218–222.

Coquillett DW (1910) The type-species of the North American genera of Diptera. Proceedings of the United States National Museum 37 [= No. 1719]: 499–647. https://doi.org/10.5479/si.00963801.37-1719.499

Cumming JM, Wood DM (2017) 3. Adult morphology and terminology. In: Kirk-Spriggs AH, Sinclair BJ (Eds) Manual of Afrotropical Diptera. Volume 1. Introductory chapters and keys to Diptera families. Suricata 4. South African National Biodiversity Institute, Pretoria, 89–134.

Fabricius JC (1805) Systema antliatorum secundum ordines, genera, species. C. Reichard, Brunswick, 373 pp. + 30 pp.

Guimarães JH (1971) Family Tachinidae (Larvaevoridae). In: Papavero N (Ed.) A Catalogue of the Diptera of Americas South of the United States. Vol. 104. Departamento de Zoologia, Secretaria da Agricultura, São Paulo, 1–333.

Guimarães JH (1975) *Neozelia alini*, gen et sp. n. (Diptera: Tachinidae), a parasite of cerambycids (Coleoptera), with a listing of Tachinidae parasite of Cerambycidae. Papéis Avulsos de Zoologia 29: 37–44.

Linnaues C (1758) Systema naturae per regna tria naturae, Vol. 1 (10th edn). Stockholm, 824 pp.

Macquart J (1835) Histoire naturelle des Insectes Diptères. Tome deuxième. In: Roret NE (Ed.) Diptera, Vol. 2. Collection des suites à Buffon, Paris, 803 pp. https://doi.org/10.5962/bhl.title.14274

Mesnil LP (1980) 64f. Dexiinae. Die Fliegen der palaearktischen Region 9 (Lieferung 323), 1–52.

O'Hara JE, Wood DM (2004) Catalogue of the Tachinidae (Diptera) of America north of Mexico. Memoirs on Entomology, International 18: 1–410.

Perty M (1833) Insecta brasiliensia. In his Delectus animalium articulatorum quae in itinere per Brasiliam annis MDCCCVII-MDCCCXX jussu et auspiciis Maximiliani Josephi I. Bavariae regis augustissimi peracto collegerunt Dr. J.B. de Spix et Dr. C.F. Ph. De Martius. Monachii, 125–224. https://doi.org/10.5962/bhl.title.102991

Reinhard HJ (1946) The genus *Minthozelia* in the United States (Diptera, Tachinidae). Journal of the Kansas Entomological Society 19: 52–59.

Robineau-Desvoidy JB (1830) Essai sur les myodaires. Mémoires Présentés par divers Savants a l'Académie Royale dês Sciences de l'Institut de France, Paris 2(2): 1–813.

Röder V von (1886) Dipteren von den Cordilleren in Columbien Gesammelt durch Herrn Alphons Stübel. Stettiner Entomologische Zeitung 47: 257–270.

Say T (1829) Descriptions of North American dipterous insects. Proceedings of the Academy of Natural Sciences of Philadelphia 6(1829–1830): 149–178.

Stireman JO, Cerretti P, O'Hara JE, Blaschke JD, Moulton JK (2019) Molecular phylogeny and evolution of world Tachinidae (Diptera). Molecular Phylogenetics and Evolution. https://doi.org/10.1016/j.ympev.2018.12.002

Stuckenberg BR (1999) Antennal evolution in the Brachycera (Diptera), with a reassessment of terminology relating to the flagellum. Studia Dipterologica 6: 33–48.

Thompson WR (1963) The Tachinids of Trinidad. II. Echinomyiines, Dexiines, and allies. Canadian Journal of Zoology 41: 335–576. https://doi.org/10.1139/z63-029

Thompson FC, Pont AC (1994) Systematic database of Musca names (Diptera). A catalog of names associated with the genus-group name Musca Linnaeus, with information on their classification, distribution, and documentation. Theses Zoologicae, 20. Koeltz Scientific Books, Koenigstein, 219 + [2] pp. https://doi.org/10.5962/bhl.title.49060

Townsend CHT (1911) Announcement of further secured results in the study of muscoid flies. Annals of the Entomological Society of America 4: 127–152. https://doi.org/10.1093/aesa/4.2.127

Townsend CHT (1915) Proposal of new muscoid genera for old species. Proceedings of the Biological Society of Washington 28: 19–23.

Townsend CHT (1919) New genera and species of muscoid flies. Proceedings of the United States National Museum [= No. 2301] 56(2301): 541–592. https://doi.org/10.5479/si.00963801.2301.541

Townsend CHT (1927) Synopse dos generos muscoideos da região humida tropical da America, con generos e especies novas. Revista do Museu Paulista 15(1): 203–385. [+ 4 unnumbered pages of errata]

Townsend CHT (1928) New muscoidea from humid tropical South America. Wiener Entomologische Zeitung 44: 143–154.

Townsend CHT (1931a) Notes on American oestromuscoid types. Revista de Entomologia 1: 65–104, 157–183.

Townsend CHT (1931b) New genera and species of American oestromuscoid flies. Revista de Entomologia 1: 313–354, 437–479.

Townsend CHT (1935) New South America oestroidea (Dipt.). Revista de Entomologia 5(2): 216–233.

Tschorsnig HP (1985) Taxonomie forstlich wichtiger Parasiten: Untersuchungen zur Struktur des männlichen Postabdomens der Raupenfliegen (Diptera, Tachinidae). Stuttgarter Beiträge zur Naturkunde, Serie A (Biologie) 383: 1–137.

Walton WR (1914) Report on some parasitic and predaceous Diptera from northeastern New Mexico. Proceedings of the United States National Museum 48[= No. 2070]: 171–186. [pls 6, 7]. https://doi.org/10.5479/si.00963801.48-2070.171

Wiedemann CRW (1830) Aussereuropäische zweiflügelige Insekten. Zweiter Theil. Schulz, Hamm, 684 pp. [5 pls]

Wood DM (1987) Tachinidae. In: McAlpine JF, Peterson BV, Shewell GE, Teskey HJ, Vockeroth JR, Wood DM (Eds) Manual of Nearctic Diptera. Volume 2. Agriculture Canada Research Branch, Ottawa, Monograph 28: 1193–1269.

Wulp FM van der (1885) Langwerpige dexinen-vormen. Tijdschrift voor Entomologie 28: 301–311 (189–200), 1 coloured plate.

Wulp FM van der (1891) Fam. Muscidae [cont.]. In: Godman FD, Salvin O (Eds.), Biologia Centrali-Americana, or, contributions to the knowledge of the fauna and flora of Mexico and Central America. Zoologia-Insecta-Diptera. London, vol. 2, 209–224, 225–248, 249–264. [pls. 5–6]

Ziegler J (1998) Die Morphologie der Puparien und der larvalen Cephalopharyngealskelette der Raupenfliegen (Diptera, Tachinidae) und ihre phylogenetische Bewertung. Studia Dipterologica. Supplement 3: 1–244.